Rita João Pereira Fernandes

Licenciada em Bioquímica

Caged amino acids for controlled release of bioactive compounds with light

Dissertação para obtenção do Grau de Mestre em Bioquímica

Orientador: Dr. Nuno Basílio, Investigador Pos-Doc, FCT-UNL

Co-orientador: Dr. Artur Moro, Investigador Pos-Doc, FCT-UNL

Júri:

Presidente: Dr. José Ricardo Franco Tavares, Professor Auxiliar com Agregação, FCT-UNL

Arguente: Dr. Eurico José da Silva Cabrita, Professor Associado com Agregação, FCT-UNL

Vogal: Dr. Nuno Basílio, Investigador Pos-Doc, FCT-UNL

FACULDADE DE CIÊNCIAS E TECNOLOGIA
UNIVERSIDADE NOVA DE LISBOA

Setembro, 2018

Rita João Pereira Fernandes

Licenciada em Bioquímica

Caged amino acids for controlled release of bioactive compounds with light

Dissertação para obtenção do Grau de Mestre em Bioquímica

Orientador: Dr. Nuno Basílio, Investigador Pos-Doc, FCT-UNL

Co-orientador: Dr. Artur Moro, Investigador Pos-Doc, FCT-UNL

Júri:

Presidente: Dr. José Ricardo Franco Tavares, Professor Auxiliar com Agregação, FCT-UNL

Arguente: Dr. Eurico José da Silva Cabrita, Professor Associado com Agregação, FCT-UNL

Vogal: Dr. Nuno Basílio, Investigador Pos-Doc, FCT-UNL

FACULDADE DE CIÊNCIAS E TECNOLOGIA
UNIVERSIDADE NOVA DE LISBOA

Setembro, 2018

Caged amino acids for controlled release of bioactive compounds with light

Agradecimentos

Quero agradecer aos meus orientadores, Dr. Nuno Basílio e Dr. Artur Moro, por me darem a oportunidade de trabalhar neste projeto e pela disponibilidade, paciência, ensinamentos, dedicação e preocupação ao longo deste ano letivo, sem dúvida que não poderia ter tido mais sorte.

Agradeço também ao grupo de Fotoquímica e Química Supramolecular (atualmente, CHARM) do departamento de química da FCT-UNL por me acolherem e apoiarem o desenvolvimento da minha tese de mestrado.

Quero agradecer à Dr. Sofia Pauleta (UCIBIO@REQUIMTE) pelo acesso ao equipamento de ITC (FCT-ANR/BBB-MET/0023/2012) e à Cecília Bonifácio (UCIBIO@REQUIMTE) pela disponibilidade e assistência técnica.

Um especial obrigado ao Professor Dr. Uwe Pischel (CIQSO – UHU) por me receber e disponibilizar o equipamento de ITC, à Dra. Patricia Ruiz (CISQO - UHU) pela supervisão e assistência enquanto lá estive e ao futuro Dr. Miguel Romero por me integrar no curto espaço de tempo que estive em Huelva, por me (tentar) ensinar espanhol e pelas doses de cafeína.

Obrigada também a todos que me ajudaram e disponibilizaram o seu tempo no meu dia a dia, em particular, ao Johan Mendoza, Alfonso Alejo, Tiago Moreira, João Avó, Noémi Jordão, Ana Lúcia, Andreia Forte, Vânia Pais e Antoine Stopin. Ao Jack Fletcher pela ajuda, discussões científicas e dicas em síntese química. Ao Pedro Ferreira e à Mariana Antunes pelas gargalhadas, desabafos, amizade e excelente companhia ao longo deste ano, sem esquecer os fins de tarde no Teresa.

Quero também agradecer aos meus amigos, Bruno Várzea, Liliana Paulino, Raul Leal e Soraia Correia que apesar da distância a amizade, cumplicidade e apoio estão sempre presentes quando nos encontramos. Aos meus bioquímicos mais loucos (J2J) pelos momentos de diversão e procrastinação que se seguiram por momentos de muito estudo e desespero também.

Obrigada ao Diogo Melo, pelo carinho, apoio, confiança e conselhos neste ano (fora nos outros todos) que não foi nada fácil para nós. Um grande obrigado à minha família, em especial os meus pais, Lucília e João, pelo apoio emocional e financeiro, conselhos, compreensão e dedicação. À minha avó Zéza e ao meu avô Fernando pelas conversas, almoços, boleias e carinho.

Abstract

The use of conditional trigger signals presents advantages such as temporal and spatial control over molecules, which is especially interesting for controlling drug release events. Light is an ideal external trigger signal given the multitude of light sources available to exert that trigger. To make a light-responsive active compound it is usual to use the introduction of a photoremovable protecting group that makes it inactive until light action (caging).

Macrocycles are one of the most well-known systems for carrying and releasing active compounds, mainly due to their increased solubility, bioavailability and stability. The cucurbit[n]uril (CB[n]) family is currently used for this purpose. These synthetic receptors are particularly attractive owing to their high affinity towards positively charged amphiphilic molecules which are the main characteristics of many drugs.

The aim of this work was to develop a series of caged biomolecules as photoresponsive guests for development of supramolecular systems based on CB[7]/[8] capsules. Four amino acids (tryptophan, tyrosine, histidine and phenylalanine) and a tripeptide (FGG) were successfully caged and characterized by NMR spectroscopy. The host-guest interactions between CB[n]s and free/caged biomolecules were studied by techniques such as UV-Vis absorption and emission spectroscopies, NMR and ITC. Photodeprotection of caged compounds was monitored by UV-Vis. The potential of the photocontrolled release supramolecular system was tested by following the displacement of a probe. For CB[7] based system, tyrosine and FGG revealed as potential photoresponsive guests. For CB[8] based system, caged phenylalanine and tryptophan displayed no affinity towards the host cavity, which make them suitable photoresponsive guests for the release system. Lastly, it was found that CB[8]-caged FGG forms 1:1 complex, contrarily to CB[8]-FGG which forms a 1:2 complex, with association constants in the order of magnitude of 10^6 M^{-1} and 10^{11} M^{-2}, respectively. This finding is promising for photocontrolled dimerization applications.

Keywords: Photochemistry, Photocaged biomolecules, Supramolecular chemistry, Host-guest interactions, Photocontrolled release, Spectroscopy

Resumo

O uso de estímulos condicionais apresenta vantagens como o controlo temporal e espacial de moléculas, o que é interessante para controlar a libertação de fármacos. A luz é um estímulo externo ideal dada a multiplicidade de fontes de luz disponíveis para exercê-lo. Para tornar um composto ativo foto-responsivo, é usual introduzir um grupo protetor foto-removível que o torna inativo até ação da luz ("enjaulamento").

Os macrociclos são um dos principais sistemas conhecidos para transportar e libertar compostos ativos devido à sua elevada solubilidade, biodisponibilidade e estabilidade. Os cucurbit[n]uril (CB[n]) são utilizados para esse fim. Estes recetores sintéticos são particularmente atraentes devido à sua alta afinidade para com moléculas anfifílicas e carregadas positivamente, o que são características comuns de muitos fármacos.

O objetivo deste trabalho foi desenvolver biomoléculas "enjauladas" para utilizá-las como hóspedes foto-responsivos num sistema supramolecular à base de CB[7]/[8]. Quatro aminoácidos (triptofano, tirosina, histidina e fenilalanina) e um tripéptido (FGG) foram protegidos com sucesso e caracterizados por espectroscopia RMN. As interações hospedeiro-hóspede entre CB[n]s e biomoléculas livres/"enjauladas" foram estudadas por técnicas como: espectroscopias de absorção UV-Vis e emissão, RMN e ITC. A foto-desproteção dos compostos "enjaulados" foi monitorizada por UV-Vis. O potencial do sistema supramolecular de libertação foto-controlada foi testado seguindo o deslocamento de uma sonda. Para o sistema baseado em CB[7], tirosina e FGG revelaram ser potenciais hóspedes foto-responsivos. Para o sistema baseado em CB[8], fenilalanina e triptofano "enjaulados" não apresentam qualquer afinidade com a cavidade do hospedeiro, o que os torna hóspedes foto-responsivos adequados para aplicar no sistema de libertação foto-controlada. Por fim, verificou-se que CB[8]-FGG "enjaulado" forma um complexo 1:1, ao contrário de CB[8]-FGG que forma um complexo 1:2, com constantes de associação na ordem de grandeza dos 10^6 M^{-1} e 10^{11} M^{-2}, respetivamente. Esta descoberta é promissora para aplicações de dimerização foto-controlada.

Palavras-chave: Fotoquímica, Biomoléculas "enjauladas", Química supramolecular, Interações hospedeiro-hóspede, Libertação foto-controlada, Espectroscopia

Table of contents

Abstract I

Resumo III

Table of figures VII

List of tables XIII

Table of abbreviations XV

1 Introduction 1

1.1 Light: a powerful tool 1

1.2 Photocaging biomolecules 2

1.2.1 State of the art 2

1.2.2 Synthesis of caged biomolecules 3

1.2.3 σ-Nitrobenzyl Protecting Group 3

1.2.4 Applications 5

1.3 Macrocycles in Drug Delivery 6

1.3.1 The CB[n] family 7

1.3.2 Synthesis 7

1.3.3 Structural and chemical properties 8

1.3.4 Host-Guest Chemistry 8

1.3.5 Amino acids and peptides complexes 9

1.3.6 Protein complexes 10

1.3.7 *Trans*-chalcones complexes 10

1.4 Characterization of complexes 11

1.4.1 Absorption and Emission 11

1.4.2 NMR 12

1.4.3 ITC 14

1.5 Aim 15

2 Results and Discussion 17

2.1 Synthesis and Characterization 17

2.1.1 *Trans*-chalcones 17

2.1.2 Caged biomolecules 18

2.2 Determination of association constants 19

2.2.1 Free and caged amino acids · CB[n] 20

2.2.2 Free and caged peptide · CB[n] 22
2.2.3 *Trans*-chalcones · CB[n] 24
2.3 Displacement assays 26
2.3.1 Indicator displacement assays with CB[7] receptor 26
2.3.2 Indicator displacement assays with CB[8] receptor 30
2.4 Photochemical assays 33
2.4.1 Irradiation of caged biomolecules 33
2.4.2 Displacement by photorelease/deprotection 36
2.5 NMR studies 38
2.5.1 Free and caged biomolecules with CB[7] 38
2.5.2 Interaction between $TCDEA_2MeO$ and caged amino acids 42
2.5.3 Free and caged biomolecules with CB[8] 43
2.5.4 DOSY 45
2.6 ITC 46
2.6.1 CB[7] complexes 46
2.6.2 CB[8] complexes 49
3 Conclusions and Future Perspectives 53
4 Materials and Methods 55
4.1 Materials and Reagents 55
4.2 Synthesis and Structural Characterization 55
4.2.1 Trans chalcones 55
4.2.2 Caged amino acids and peptide 57
4.3 Methodologies 59
5 References 65
6 Appendix 69

Table of figures

Figure 1.1 – Controlling proteins in living systems using light. 1

Figure 1.2 – Photodeprotection scheme of caged ATP.[9] 2

Figure 1.3 – Chemical structures of the most commonly used σ-nitrobenzyl-based PPGs. 4

Figure 1.4 – Mechanism of NB photodeprotection.[11] 4

Figure 1.5 – NVOC-Cl molecular structure. 5

Figure 1.6 – Two different applications of photocaging. 5

Figure 1.7 – Representation of the light-induced release principle. 6

Figure 1.8 – Chemical structures of CB[n] on the left and stick representation of CB[7] on the right (side and top view). Adapted from Gibb et al.[38] 7

Figure 1.9 – Scheme of CB[n] synthesis reaction.[39] 7

Figure 1.10– Electrostatic potential map of CB[7]. 8

Figure 1.11 – Different types of CB[n] complexes and their stoichiometries.[43] 9

Figure 1.12 – CB[n] selective recognition of an N-terminal aromatic peptide**.** 9

Figure 1.13 – Illustration of 1D, 2D and 3D cucurbituril-induced protein assemblies. 10

Figure 1.14 – Inclusion complexes formed between TCDMA and TCDEA with CB[7]. 11

Figure 1.15 – Representative NMR spectra of complexes with different exchange rates. 13

Figure 1.16 – Representation of an ITC experiment and data.[59] 14

Figure 1.17 – Representation of the intended release system. 15

Figure 2.1 – Synthesis of *trans*-chalcone by Claisen-Schmidt condensation. 17

Figure 2.2 – Synthesis of compound **1**. 17

Figure 2.3 – Chemical structure of TCDEA (2) and $TCDEA_2MeO$ (3). 18

Figure 2.4 – Synthesis of caged amino acids with the Nvoc protecting group. 18

Figure 2.5 – Spectrophotometric titration of (A) [Trp]= 18 μM and (B) [Tyr]= 184 μM with CB[7]. Experimental data at 280 nm is the black dots and the 1:1 fitting is the red line. 20

Figure 2.6 – (A) TrpNvoc 100 μM without CB[7] (orange) and with CB[7] 1.92 mM (blue), (B) TyrNvoc 100 μM without CB[7] (green) and with CB[7] 2.76 mM (yellow), (C) HisNvoc 90 μM without CB[7] (purple) and with CB[7] 2.75 mM (red). 21

Figure 2.7 – (A) Spectrophotometric titration of HisNvoc with CB[7], (B) Experimental data at 265 nm is the black dots and 1:1 fitting model is the red line. [HisNvoc] = 9.0×10^{-5} M. 21

Figure 2.8 – (A) PheNvoc 40 μM without CB[8] (green) and with CB[8] 0.13 mM (red), (B) TrpNvoc 30 μM without CB[8] (blue) and with CB[8] 0.13 mM (orange). 22

Figure 2.9 – Spectrophotometric spectra of FGGNvoc (orange) and FGGNvoc with CB[7] (green) [FGGNvoc] = 6.0×10^{-5} M, [CB7] = 2.6×10^{-3} M. 23

Figure 2.10 – (A) Spectrophotometric titration of FGGNvoc with CB[8], (B) Experimental data at 350 nm is the black dots and 1:1 fitting model is the red line. [FGGNvoc] = 4.0×10^{-5} M. 23

Figure 2.11 – (A) Spectrophotometric titration of $TCDEA_2MeO$ with CB[7] at pH 7 and (B) experimental data at 420 nm is the black dots and 1:1 fitting model is the red line. [$TCDEA_2MeO$] = 2.3×10^{-5}M. 24

Figure 2.12 – (A) Spectrophotometric titration of TCDPA with CB[7] at pH 9, (B) experimental data at 420 nm is the black dots and 1:1 fitting model is the red line. [TCDPA] = 6.0×10^{-5} M. 24

Figure 2.13 – (A) Spectrophotometric titration of TCDPA with CB[8] at pH 9, (B) experimental data at 420 nm as black dots and 1:1 fitting model as the red line. [TCDPA] = 2.0×10^{-5} M. ... 26

Figure 2.14 – Displacement of $TCDEA_2MeO$ from CB[7] trough competitive titration with (A) Trp, (B) Tyr and (C) His. Experimental data at 511 nm is the black dots, the fitting is the red line and free $TCDEA_2MeO$ 20 µM at 511 nm is the dashed green line. [$TCDEA_2MeO$] = 2.0×10^{-5} M, [CB[7]] = 15×10^{-5} M. 27

Figure 2.15 – Displacement of $TCDEA_2MeO$ from CB[7] trough competitive titration with (A) TrpNvoc, (B) TyrNvoc and (C) HisNvoc. Experimental data at 511 nm is the black dots and the fitting is the green line. [$TCDEA_2MeO$] = 2.0×10^{-5} M, [CB[7]] = 15×10^{-5} M. 27

Figure 2.16 – Displacement with (A) tryptophan (blue) and caged tryptophan (yellow), (B) tyrosine (green) and caged tyrosine (orange), (C) histidine (purple) and caged histidine (pink). The arrows represent the region with higher difference in displacement. 28

Figure 2.17 – Displacement of TCDEA from CB[7] trough competitive titration with (A) FGG and (B) FGGNvoc. Experimental data at 490 nm is the black dots, the fitting is the red line and the free TCDEA 20 µM is the dashed green line. [TCDEA] = 2.0×10^{-5} M, [CB[7]] = 15×10^{-5} M. 29

Figure 2.18 – Displacement of TCDEA from CB[7] with peptide (orange) and caged peptide (blue). The arrow represents the region with greatest difference in displacement. 30

Figure 2.19 – Displacement of TCDPA from CB[8] trough competitive titration with (A) Trp, (B) Phe and (C) FGG. Experimental data at 490 nm is the black dots, the fitting is the red line and the free TCDPA 20 µM is the dashed green line. $[TCDPA]_{(A) \text{ and } (C)} = 1.0 \times 10^{-5}$ M. , $[TCDPA]_{(B)} = 2.0 \times 10^{-5}$ M, [CB[8]] = 9.0×10^{-5} M. 31

Figure 2.20 – Displacement of TCDPA from CB[8] trough competitive titration with (A) TrpNvoc, (B) PheNvoc and (C) FGGNvoc. Experimental data at 490 nm is the black dots and the fitting is the red line. [TCDPA] = 1.0×10^{-5} M, [CB[8]] = 9.0×10^{-5} M. 31

Figure 2.21 – Displacement of TCDPA from CB[8] with peptide (blue) and caged peptide (orange). 32

Figure 2.22 – Illustration of the different types of complexes that caged peptide can make with CB[8]. (I) Loop and (II) supramolecular polymer. 33

Figure 2.23 – UV-vis absorption spectral changes upon irradiation at 366 nm of (A) TrpNvoc 200 µM at pH 7, (B) TyrNvoc 232 µM at pH 7 and (C) HisNvoc 150 µM at pH 8, in aqueous solution. The lower graphs represent the ΔAbs as a function of the irradiation time; the coloured points and their resulted linear equation were used to calculate the quantum yields. 34

Figure 2.24 – UV-vis absorption spectral changes on irradiation at 366 nm of (A) PheNvoc 200 µM and (B) FGGNvoc 120 µM, in aqueous solution at pH 7. In lower graphs is represented the

ΔAbs as a function of irradiation time; the coloured points and their resulted linear equation were used to calculate the quantum yields. 35

Figure 2.25 – UV-vis spectral changes on irradiation at 366 nm of a mixture of (A) CB[7], $TCDEA_2MeO$ and TyrNvoc and (B) CB[7], TCDEA and FGGNvoc. The smaller graphs represent the experimental data at 511 nm in function of irradiation time. [CB[7]](A), (B)= 150 μM, [$TCDEA_2MeO$]= [TCDEA]= 20 μM, [TyrNvoc]= 650 μM, [FGGNvoc]= 200 μM. 36

Figure 2.26 – UV-vis spectral changes on irradiation at 366 nm of a mixture of CB[8], TCDPA, (A) TrpNvoc and (B) PheNvoc. The insets represent the experimental data at 490 nm in function of irradiation time. [CB[8]] = 94 μM, [TCDPA] = 10 μM, [TrpNvoc] = 990 μM, [PheNvoc] = 750 μM. 37

Figure 2.27 – ^{1}H-NMR spectra of tyrosine 2.5 mM (down) and tyrosine 1 mM with CB[7] 1.1 eq. (up) in D_2O, pD 7. 39

Figure 2.28 – ^{1}H-NMR spectra of histidine 32 mM (down) and histidine 1 mM with CB[7] 2.6 eq. (up) in D_2O, pD 7. 39

Figure 2.29 – ^{1}H-NMR spectra of tryptophan 3.1 mM (down) and tryptophan 1 mM with excess of CB[7] (up) in D_2O, pD 7. 40

Figure 2.30 – ^{1}H-NMR spectra of FGG 8.2 mM (bottom) and FGG 1 mM with excess of CB[7] (top) in D_2O, pD 7. 41

Figure 2.31 – ^{1}H-NMR spectra of FGGNvoc 1.2 mM (bottom) and FGGNvoc 0.5 mM with excess of CB[7] (top) in D_2O, pD 7. 42

Figure 2.32 – ^{1}H-NMR spectra of TrpNvoc 0.8 mM (bottom) and TrpNvoc 0.1 mM with excess of CB[8] (top) in D_2O, pD 7. 43

Figure 2.33 – ^{1}H-NMR titration of FGG 0.5 mM with CB[8] (0-0.29 mM) in D_2O, pD 7 44

Figure 2.34 – ^{1}H-NMR titration of FGGNvoc 0.2 mM with CB[8] (0-0.12 mM) in D_2O, pD 7..... 45

Figure 2.35 – DOSY data of CB[8] complex with FGG (left) and FGGNvoc (right). Experimental data is the black dots and the fitting the red line. [FGG] = [FFGNvoc] = 1 mM, CB[8] in excess.. 46

Figure 2.36 – ITC data obtained for the titration of (A) 3 mM CB[7] with 63 mM Trp and (B) 0.09 mM CB[7] with 2.6 mM Tyr. 47

Figure 2.37 – ITC data obtained for the titration of (A) 370 μM TrpNvoc and (B) 300 μM TyrNvoc with 2.95 mM CB[7]. 47

Figure 2.38 – ITC data obtained for the titration of (A) 0.3 mM CB[7] with 5 mM FGG and (B) 0.5 mM FGGNvoc with 3 mM CB[7]. 48

Figure 2.39 – ITC data obtained for the titration of 0.14mM CB[8] with (A) 5mM Trp and (B) 4.5 mM Phe. 49

Figure 2.40 – ITC data obtained for the titration of (A) 0.14 mM CB[8] with 0.82 mM PheNvoc. (B) 0.01 mM CB[8] with 0.75 mM TrpNvoc. 50

Figure 2.41 – ITC data obtained for the titration of (A) 0.14 mM CB[8] with 3.5 mM FGG and (B) 0.09 mM CB[8] with 1.52 mM of FGGNvoc. 51

Figure 6.1 – ^{1}H-NMR spectrum of compound **1** in D_2O. Impurities are assigned with *. 69

Figure 6.2 – ^{1}H-NMR spectrum of TCDEA in D_2O. Signals with * have low resolution but can be assigned from the integration. 70

Figure 6.3 – ^{1}H-NMR spectrum of TCDEA$_2$MeO in D_2O. Signals with * have low resolution but can be assigned from the integration. 70

Figure 6.4 – ^{1}H-NMR spectrum of caged tryptophan in $CO(CD_3)_2$. 71

Figure 6.5 – COSY of caged tryptophan in $CO(CD_3)_2$. 71

Figure 6.6 – ^{1}H-NMR spectrum of caged tyrosine in $SO(CD_3)_2$. * ethyl acetate, **the integration is higher due the proximity to the solvent peak. 72

Figure 6.7 – COSY of caged tyrosine in $SO(CD_3)_2$. 72

Figure 6.8 – ^{1}H-NMR spectrum of caged histidine in $SO(CD_3)_2$. 72

Figure 6.9 – COSY of caged histidine in $SO(CD_3)_2$. 72

Figure 6.10 – ^{1}H-NMR spectrum of caged phenylalanine in $CO(CD_3)^2$. 72

Figure 6.11 – ^{1}H-NMR spectrum of caged FGG in CD_3OD. *it was not possible to assign the type of coupling. 72

Figure 6.12 – Job Plot's of the interaction between TCDPA with CB[8], followed at 450 nm. [total] = 6.0×10^{-5} M. 72

Figure 6.13 – ^{1}H-NMR spectra of TrpNvoc 0.6 mM, before (up) and after irradiation (middle), and tryptophan 3 mM (down) in D_2O. λ_{irr} = 365 nm, t_{irr} = 5h. 72

Figure 6.14 – ^{1}H-NMR spectra of TyrNvoc 0.78 mM, before (up) and after irradiation (middle), and tyrosine 2.6 mM (down) in D_2O. λ_{irr} = 365 nm, t_{irr} = 3h. ……72

Figure 6.15 – ^{1}H NMR spectra of HisNvoc 1 mM, before (up) and after irradiation (middle), and histidine 31.6 mM (down) in D_2O. λ_{irr} = 365 nm, t_{irr} = 5h. 72

Figure 6.16 – ^{1}H NMR spectra of FGGNvoc 1 mM, before (up) and after irradiation (middle), and FGG 0.5 mM (down) in D_2O. λ_{irr} = 365 nm, t_{irr} = 3h. 72

Figure 6.17 – ^{1}H-NMR spectra of TyrNvoc 0.8 mM (bottom) and TyrNvoc 0.5 mM with 3.7 eq. of CB[7] (top) in D_2O, pD 7. 72

Figure 6.18 – ^{1}H-NMR spectra of HisNvoc 1 mM (bottom) and HisNvoc 0.5 mM with 2.4 eq. of CB[7] (top) in D_2O, pD 7. Red dots indicate upfield shifts and the green dots the downfield shifts. 72

Figure 6.19 – ^{1}H-NMR spectra of TrpNvoc (bottom) and TrpNvoc with 1 eq. of CB[7] (top) in D_2O, pD 7. [TrpNvoc]= 0.5 mM 72

Figure 6.20 – ^{1}H-NMR spectra of 1 mM TCDEA$_2$MeO (bottom), 1 mM HisNvoc (top) and 1:1 eq. TCDEA$_2$MeO-HisNvoc (middle), in D_2O. 72

Figure 6.21 – ^{1}H-NMR titration of 0.8 mM TCDEA$_2$MeO with TrpNvoc (0-1 eq.) in D_2O. 72

Figure 6.22 – ^{1}H-NMR spectra of 1 mM mM TCDEA$_2$MeO (top), 0.8 mM TyrNvoc (down) and 1:1 eq. TCDEA$_2$MeO-TyrNvoc (middle), in D_2O. 72

Figure 6.23 – ^{1}H-NMR titration of phenylalanine 0.5 mM (down) with CB[8] (0-0.8 mM) in D_2O, pD 7. 72

Figure 6.24 – DOSY spectra of FGG in D_2O at 298 K. [FGG] = 1 mM.and CB[8] in excess. ….72

Figure 6.25 – DOSY spectra of FGGNvoc in D_2O at 298 K. [FGGNvoc] = 1 mM and CB[8] in excess. 72

Figure 6.26 – Emission titration of 18 µM tryptophan with CB[7] (0 - 4.96 x 10^{-4} M) and data fitting in right upper corner. The black dots correspond to experimental values and the red line to a 1:1 fitting. The resulted association constant was 5.22 x 10^3 M^{-1}. λ_{exc} = 290 nm..... 72

Figure 6.27 – Colour differences between control (left) and irradiated sample (right). Both cells contain 200 µM FGGNvoc, 20 µM TCDEA and 150 µM CB[7]. λ_{irr} = 366 nm, t_{irr} = 100 min. The control cell was left in the dark the same period of time that sample cell was irradiated. ……82

List of tables

Table 1.1 – Structural parameters of CB[n] (n=5-8).[40] 8

Table 2.1 – Yields (%) of each caged biomolecule synthesis. 19

Table 2.2 – Different K_{ass} of *trans*-chalcones with CB[7]. 25

Table 2.3 – K_{ass} of free and caged tryptophan, tyrosine and histidine with CB[7] by UV-Vis displacement assay. 28

Table 2.4 – K_{ass} of free and caged tryptophan, phenylalanine and peptide with CB[8] by UV-Vis displacement assay. 32

Table 2.5 – Quantum yield from each caged biomolecule irradiated at 366 nm. 35

Table 2.6 – ^{1}H chemical shifts (ppm) of caged histidine without and with CB[7] in excess (consult fig. 6.16, appendix). 41

Table 2.7 – Values of D for CB[8] and its complexes with free and caged tripeptide. 46

Table 2.8 – Association constants and thermodynamic parameters of amino acids·CB[7] complexes determined by ITC. 48

Table 2.9 – Association constants and thermodynamic parameters of free/caged peptide·CB[7] complexes determined by ITC. 49

Table 2.10 – Association constants and thermodynamic parameters of amino acids·CB[8] complexes determined by ITC. 50

Table 2.11 – Association constants and thermodynamic parameters of free/caged peptide·CB[8] complexes determined by ITC. 51

Table 2.12 – Association constants of CB[n] (n= 7, 8) with free and caged molecules determined by different techniques. 52

Table 6.1 – Lester rules or Sheehan criteria. 69

Table of abbreviations

2,6 - NP	2, 6-dihydroxynaphtalene
CB[n]	Cucurbit[n]uril
ConA/AzoMan/DDPS/CB[8]	α-Mannopyrasonide Concanavalin A/ azobenzene/ dipyridil salt /CB[8]
COSY	Correlation spectroscopy
DOSY	Diffusion-ordered spectroscopy
FGG	Phenylalanine-Glycine-Glycine
GST	Glutathione S-transferase
ITC	Isothermal titration calorimetry
K_a	Acidity constant
K_{ass}	Association constant
LG	Leaving group
MV	Methyl viologen
NB	Nitrobenzyl
NMR	Nuclear magnetic resonance
Nvoc	Nitroveratryl-oxycarbonyl
ONBY	*σ*-Nitrobenzyl-*O*-tyrosine
PC	Packing coefficient
PPG	Photolabile Protecting Group
TCDEA	*Trans*-chalcone diethylamine
$TCDEA_2MeO$	*Trans*-chalcone diethylamine-2-methoxy
TCDMA	*Trans*-chalcone dimethylamine
TCDPA	*Trans*-chalcone dipropylamine
TCs	*Trans*-chalcones
t_{irr}	Irradiation time
λ_{exc}	Excitation wavelength
λ_{irr}	Irradiation wavelength
λ_{max}	Maximum wavelength

1 Introduction

1.1 Light: a powerful tool

Light interaction with matter is essential for a multitude of biological processes across all kingdoms of life. It can behave as primary energy source in photosynthesis or as regulator of the circadian cycle, phototaxis and in developmental and behavioural responses. [1, 2] A well-known sensory process that requires light as stimulus is the vision, where the conversion of 11-*cis*-retinal into *trans*-retinal triggers a conformational change in rhodopsin protein, which is the first step on visual transduction.[3]

The idea of controlling events with light at the molecular level is inspiring for developing photocontrolled systems for biological applications, since it is an external trigger that is non-invasive, orthogonal, offers spatiotemporal precision, does not cause sample contamination and its properties (intensity, wavelength) can be easily controlled.[4, 5] **Figure 1.1** shows different means to control the levels of active proteins in living systems using light as trigger.

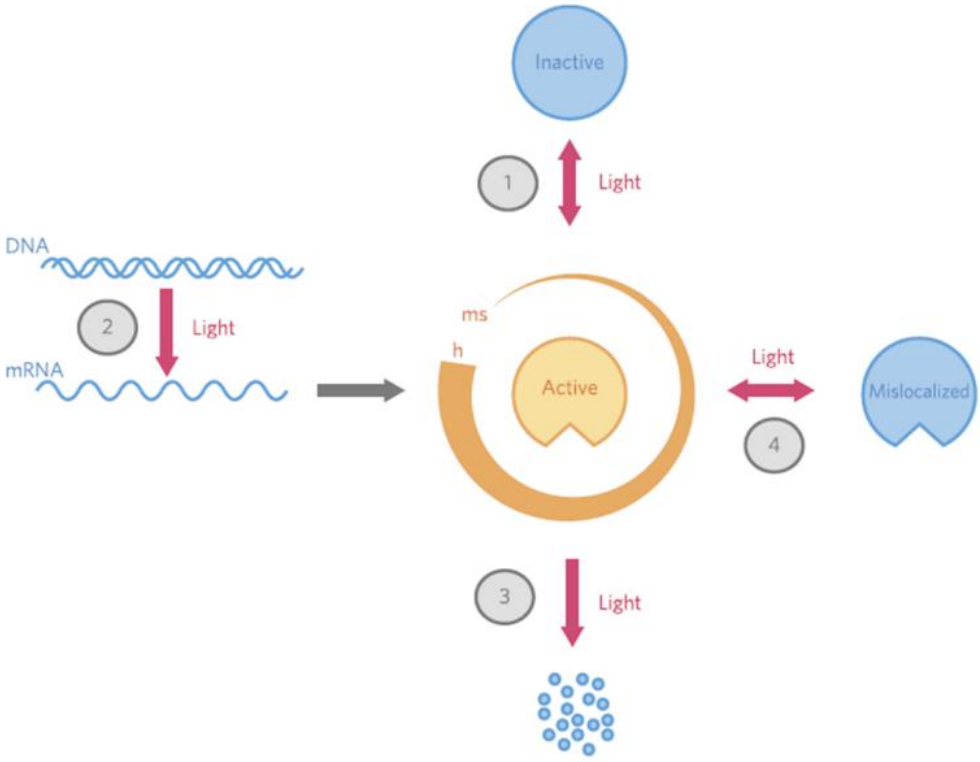

Figure 1.1 – Controlling proteins in living systems using light.
Light allows protein function control by changing its active site (1) or by controlling its synthesis (2), rate of degradation (3) or compartmentalization (4). Reprinted with permission from ref. 6. Copyright 2014 Nature America.

Beside controlling biological events, light also exerts big interest in the pharmacotherapy field (photopharmacology), where many drug related problems are faced, such as poor selectivity

which leads to uncontrolled drug activity in time and space, consequently, the therapeutic window is narrowed, and toxic side effects can occur (e.g. chemotherapy). [7, 8] Therefore, there is the need to develop systems that improve drug selectivity.

To control chemical and biological processes with light, two molecular approaches have been extensively investigated: make use of bistable photoswitches or "caging" the target molecule.[5, 9] Photoswitches are reversible interconverted between inactive and active states, contrarily to caged compounds that upon light irradiation transforms into the active form in an irreversible way. However, structural changes of photoswitches are often insufficient to exert a significant effect on the system under study, therefore, in this situation caging is a reliable choice.[5]

The caging approach relies on a covalent attachment of a photolabile protecting group (PPG) into the desired site of the molecule, which turns the molecule inactive until light activation.[5, 10, 11]

1.2 Photocaging biomolecules

1.2.1 State of the art

The first reported caged molecule was the amino acid glycine with *N*-benzyloxycarbonyl protecting group in 1962 by Barltrop, but was only in 1978, that Hoffman introduced the term "cage" and reported the synthesis of caged ATP and the photorelease/deprotection of the same (**fig. 1.2**).[9,12]

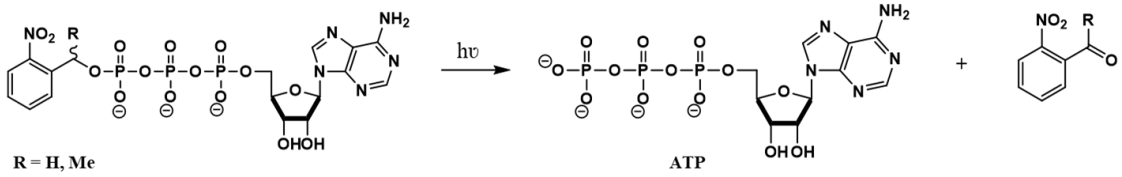

Figure 1.2 – Photodeprotection scheme of caged ATP.[9]

In 1988, Kaplan synthesized novel caged divalent cation chelators when exposed to light resulted in the release of Ca^{2+} and Mg^{2+}.[13] The controlled release of calcium which is a second messenger in various physiologic processes inspired the design of controlling other messengers such as nitric oxide (NO) with light.[14,15] Besides amino acids and second messengers also sugars, steroids and lipids have been caged and used to study biological events.[9]

Peptides and proteins have varied biological functions and are abundant in living systems, therefore are desirable targets for photocaging applications. G-actin protected with 6-Nitroveratryl-oxycarbonyl (Nvoc) was the first caged protein reported in 1994 by Marriot et al.[16] Short et al.[17] reported caged HIV-1 protease that prevented dimerization and its photodeprotection *in vitro* allowed dimer formation. σ-Nitrobenzyl-*O*-tyrosine (ONBY) was incorporated into a mammalian protein by Deiters et al.[18] and it allowed to control phosphorylation

which is an important event in signal transduction. In 2012, a caged amyloidogenic peptide ($A\beta_{16-22}$, a short segment of the amyloid-β peptide associated with Alzheimer's disease) was synthesized. It was shown that it formed amyloid fibrils as the wild type peptide did, but when irradiated disruption of the aggregates was observed. This happened because the deprotection of the peptide resulted in a charged final product that prevented hydrophobic interactions to be established, which are key role interactions in amyloid formation. This discovery helped to elucidate how amyloid fibrils are formed and created a potential mechanism for therapeutic applications.[19]

Controlling genetic function with light was also reported and different photocaged compounds for oligonucleotide modification such as caged carboxylic, phosphate and amino groups are known. Deiters et. al used caged nucleotides to control the formation of antisense agent and the target mRNA duplex and also to regulate gene expression at the transcriptional level.[20]

1.2.2 Synthesis of caged biomolecules

Only approaches used to introduce PPGs in amino acids, peptides and proteins will be focused here. Caging a single amino acid is straightforward since only three targetable sites exist where the introduction of the PPG can be made: amino terminal, carboxyl terminal or side chain.[21] The synthesis of caged peptides and proteins can be more challenging due to the increased size and number of reactivity sites.Two reported approaches to introduce a caged amino acid into a desired position of peptides are: automated solid-phase synthesis or chemically modification of targeted amino acids of an already existing peptide.[22] Chemically modification of targeted amino acids is also used in protein photocaging, but this method is limited to small proteins though. Protein-PPG ratio is an important factor when the aim is to inhibit the protein activity, since low PPG quantity can result in ineffective cage, i.e., do not inhibit at a desirable percentage (> 90%) and high PPG quantity can result in over labeling which causes heterogeneity among cages leading to low photoactivation yields.[23] Other methods such as site-directed mutagenesis using suppressor tRNAs that are able to transport modified amino acids and protein splicing were also reported.[24, 25]

1.2.3 σ-Nitrobenzyl Protecting Group

Choosing the right PPG for protection can be challenging due to the variety of groups available with very different characteristics. PPGs can be organized in classes and several reviews cover in detail each of it.[10, 22] Only the σ-nitrobenzyl-based PPG family will be covered here.

Barltrop et. al[26] was the first to report the use of an σ-nitrobenzyl group to photorelease of benzoic acid. In **fig. 1.3** is represented the chemical structures of common σ-nitrobenzyl-based

1. Introduction

PPGs: nitrobenzyl (**1**), nitrophenethyl (**2**) and their dimethoxy derivatives also known as nitroveratryl (**1.1** and **2.1**).[10]

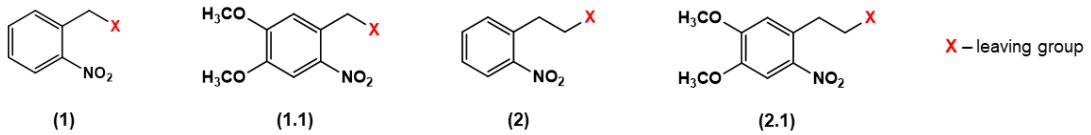

Figure 1.3 – Chemical structures of the most commonly used σ-nitrobenzyl-based PPGs.

Leaving groups (**X**) often used englobe phosphates, carboxylates, carbonates and carbamates, among others. The nature of the leaving group affects the quantum yield and the deprotection rate, also the introduction of substituents in the aromatic ring or in the benzylic carbon is used to improve the photochemical properties and to shift the effective absorbance to less energetic wavelenghts.[11]

Figure 1.4 shows the proposed mechanism for nitrobenzyl (NB) group photodeprotection. The starting NB molecule **1** is promoted to the excited state **1*** upon light absorption. Intramolecular hydrogen abstraction by the nitro group happens forming an *aci*-nitro intermediate **2.** The *aci*-decay rate constants are on the order of 10^2-10^4 s^{-1} and vary strongly with substitution, solvent and pH. Next, an irreversible cyclization (**3**) occurs and it is followed by a subsequent ring-opening reaction to give the hemiacetal **4**, which results in the release of the leaving group (**LG**) and the byproduct **5** (2-nitrosobenzaldehyde).

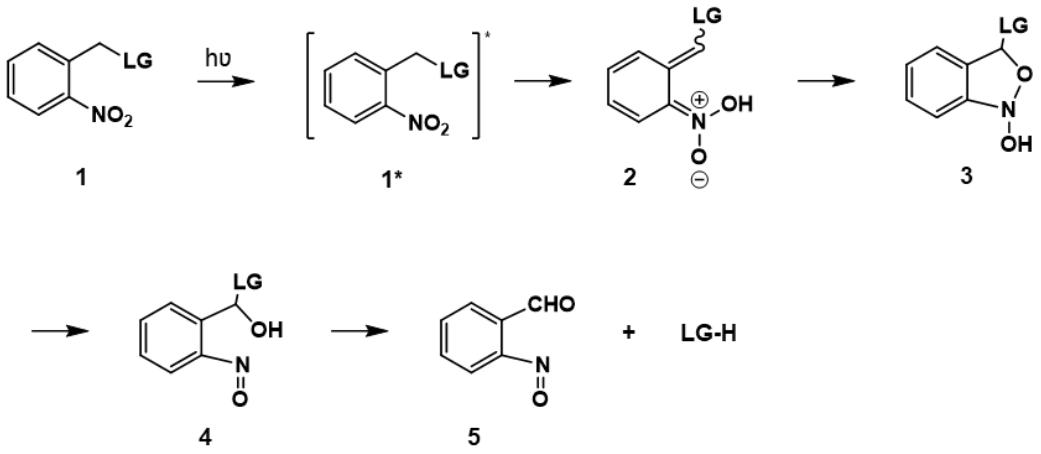

Figure 1.4 – Mechanism of NB photodeprotection.[11]

A set of criteria (Lester rules or Sheehan criteria) to classify the efficiency of a PPG is present in **table 6.1** (appendix), although not all requisites need to be filled to be considerate an efficient PPG since it depends on the type of application pretended. Nvoc protecting group has

been widely used in α-amino protection of amino acids manly due to its easily synthesis procedure.[21, 27, 28] In **fig. 1.5** is represented its structure.

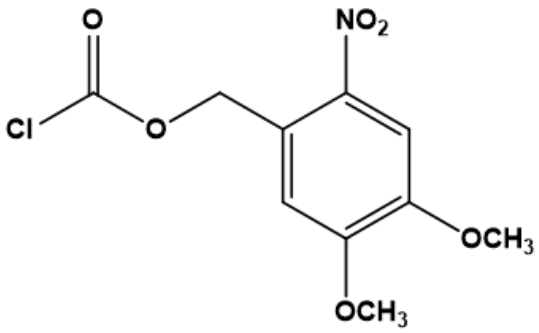

Figure 1.5 – NVOC-Cl molecular structure.

1.2.4 Applications

As said before, photocaging biomolecules allows to control several biological processes (signalling, enzymatic activity, folding, protein-protein interactions, genetic function, etc.), yet other type of caged molecules and applications were reported.

Molecules that yield fluorescence species upon irradiation (photoactivatable fluorophores) can be obtained by coupling a fluorescent compound to a PPG.[22] This coupling usually decreases or quenches the usual fluorescence of the compound. Optical labelling and tracking of living cells, organelles and intramolecular molecules are exciting applications.[29]

In **fig. 1.6** is illustrated two different biological applications of photocaging molecules.

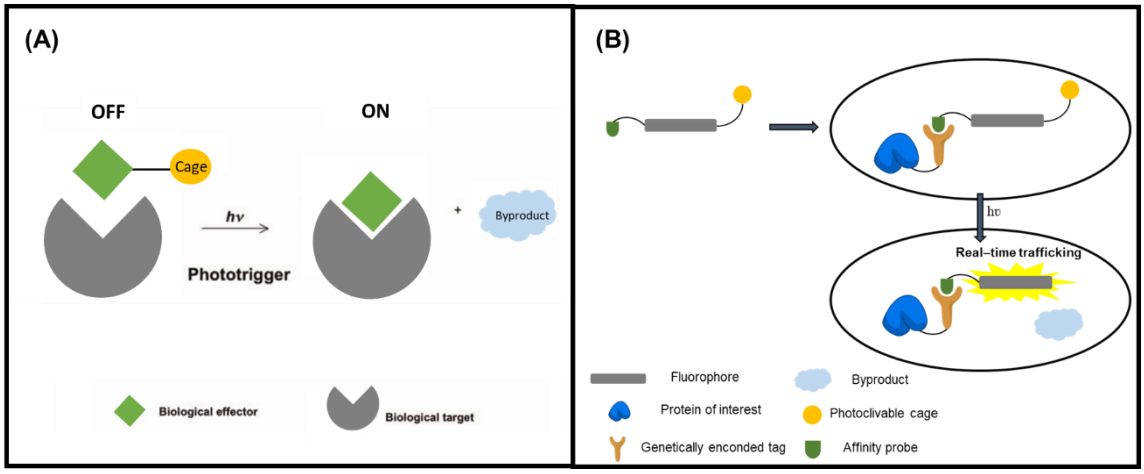

Figure 1.6 – Two different applications of photocaging**.**
(A) Photoregulation of enzymatic activity with a caged binding effector. (B) Cellular protein trafficking studies using photoactivatable fluorophores. Adapted from Specht et al.[29]

1. Introduction

The caging concept has been also employed to aid structural biochemistry techniques such as real time-resolved crystallography, where the most promising and common use is in kinetic studies.[22, 29]

Controlled release applications have also been reported.[30, 31, 32] A recent study, reported by Romero et al.[27], showed that by playing with the binding affinity of caged and free phenylalanine towards the macrocyclic receptor cucurbit[7]uril (CB[7]) it could be possible to control release of functional photoinactive guests with light. The caged compound showed no affinity towards the host cavity (weak competitor) contrary to the free amino acid (strong competitor) – **fig.1.7**. This study was what inspired the present master thesis theme.

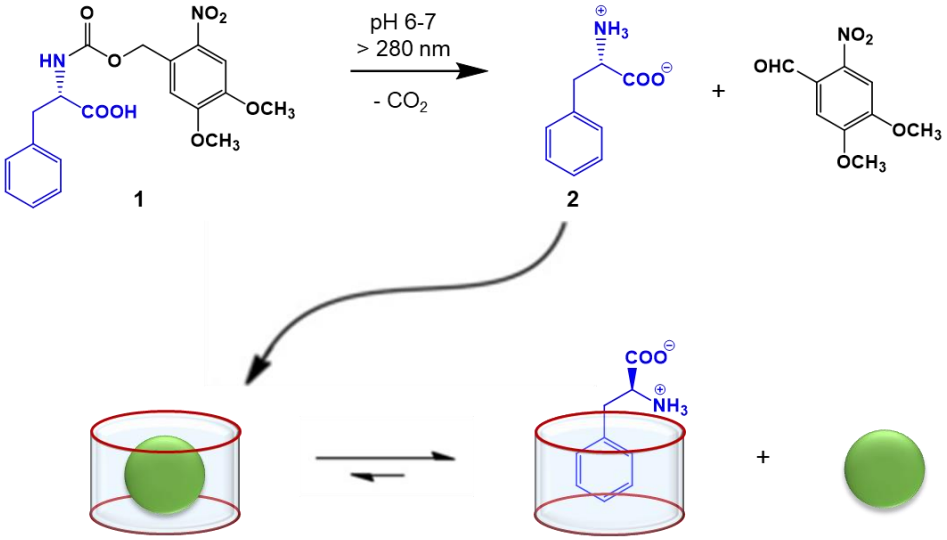

Figure 1.7 – Representation of the light-induced release principle.
The phototrigger **1** is irradiated and liberates the competitor **2**, which contrary to **1** is able to displace a photochemically inactive guest from CB[7]. Adapted from Romero et al.[27]

1.3 Macrocycles in Drug Delivery

Drug delivery englobes the use of formulation strategies, encapsulation technologies, and/or targeted approaches to increase the bioavailability of drugs in the desirable target site. In recent years, this field has expanded due to development of nanomedicine area, where the use of nanoscale carriers, which facilitate drug solubility, protects it from harsh environmental condition and/or enhance drug localization, has been employed.[33]

Polymers are by far the most used nanocarrier in drug delivery systems, but others commonly used are micelles, liposomes, dendrimers, nanoparticles and macrocycles.[34, 35] Macrocycles exhibit great interest due to their unique host-guest chemistry in aqueous medium which provides a tunable molecular recognition and association in a reversible and, in some cases, stimuli-responsive manner.[33, 36] Besides drug carrier role, macrocycles can also be used in drug discovery as an economic and versatile alternative of antibodies in enzyme assays.[37] The most explored and used macrocycles in drug delivery are cyclodextrins, followed by calix[n]arenes, cucurbit[n]urils and pillar[n]arenes.[38]

1.3.1 The CB[n] family

In 1905, Berhend reported the synthesis of the first cucurbit[n]uril (CB[n]) which was CB[6], but its structure was only solved in the 1980s by Mock.[38, 39] The term “cucurbituril” was coined by Mock because of the resemblance of its structure to a pumpkin, which belongs to the botanical family *cucurbitaceae*.[40] The CB[n] (n= 5-8, 10, 13-15) family is composed by macrocyclic compounds that comprises n glycoluril units bridged by 2n methylene units (**fig. 1.8**) [38, 39, 41]

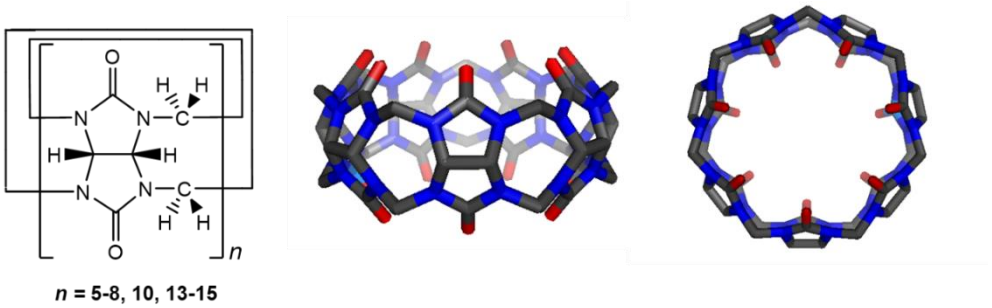

Figure 1.8 – Chemical structures of CB[n] on the left and stick representation of CB[7] on the right (side and top view). Adapted from Gibb et al.[38]

This family of macrocycles shows particular interest because of their high binding affinities towards guests that are complementary. There are binding affinities reported that even surpass the bench-mark high affinity binding pair in nature: biotin-avidin (~ 10^{15} M^{-1}).[42] Also, their solubility in aqueous media and low toxicity are ideal for biological applications.[38, 43] Furthermore, the ability of crossing the cell membrane is reported as well.[42]

1.3.2 Synthesis

CB[n] synthesis is based in acid-catalyzed condensation of glycoluril and formaldehyde (**fig. 1.9**).[38, 39] By controlling the temperature it is possible to obtain different products: at high temperature (110 ºC) the thermodynamic product CB[6] is the major product and at lower temperatures (75-100 ºC) the kinetic products CB[5], CB[7] and CB[8] along with CB[6] are produced.[38] Fractional crystallization and dissolution or chromatography are used to separate the different analogues.[39]

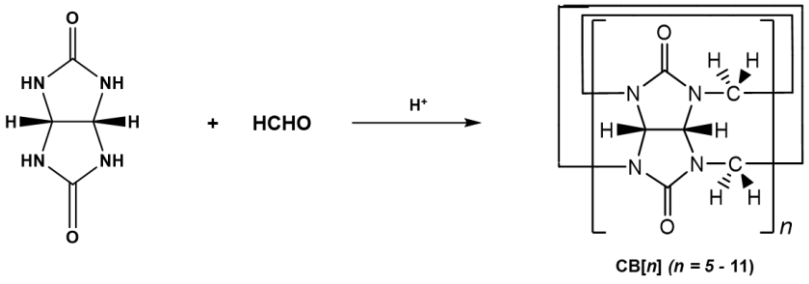

Figure 1.9 – Scheme of CB[n] synthesis reaction.[39]

1.3.3 Structural and chemical properties

CB[n] family have highly symmetric structure with a hydrophobic cavity and two identical ureido carbonyl portals. The electrostatic potential map of CB[7] is represented in **fig. 1.10** where is showed the high electron density at the portals and the lack of it in the cavity.

Figure 1.10 – Electrostatic potential map of CB[7].
The more electronegative areas are in red, which corresponds to the carbonyl portals. Reprinted with permission from ref. 40. Copyright 2015 The Royal Society of Chemistry.

All CB[n]s have the same height but its outer diameter, inner cavity dimensions and volume vary (**Table 1.1**).

Table 1.1 - Structural parameters of CB[n] (n=5-8).[40]

	Outer diameter (Å)	Inner cavity (Å)		Height (Å)	Cavity volume (Å^3)
		a	*b*		
CB[5]	13.1	4.4	2.4	9.1	82
CB[6]	14.4	5.8	3.9	9.1	164
CB[7]	16.0	7.3	5.4	9.1	279
CB[8]	17.5	8.8	6.9	9.1	479

a- inner cavity diameter
b- carbonyl portals diameter

1.3.4 Host-Guest Chemistry

The complexation of guests within CB[n] can be ruled by two effects: ion-dipole and hydrophobic. Therefore, positively charged amphiphilic molecules are excellent guest candidates.[38] A third feature that influences the binding is the size complementary, i.e., the packing coefficient (PC) which is the ratio between guest and host cavity volumes and a value range of 45-65% is connected to higher binding affinities.[40, 42] The lower diameter of carbonyl portal compared to the cavity results in low dissociation rate complexes.[38]

Although hydrophobic, the cavity of CB[n] can accommodate water molecules for entropic reasons.[43] These water molecules are of high energy because of the reduced number of hydrogen bonds compared to the bulk water and due to weak dispersion interactions with the walls of the CB[n] cavity, the release of them upon guest complexation contributes a major part to the overall hydrophobic effect.[40] Moreover, the energy of the system decreases providing an entropic and enthalpic gain in favor of complexation.[43]

Different complex stoichiometries are represented in **fig. 1.11**. Complexation of two guest molecules usually occurs with larger CB[n]s.

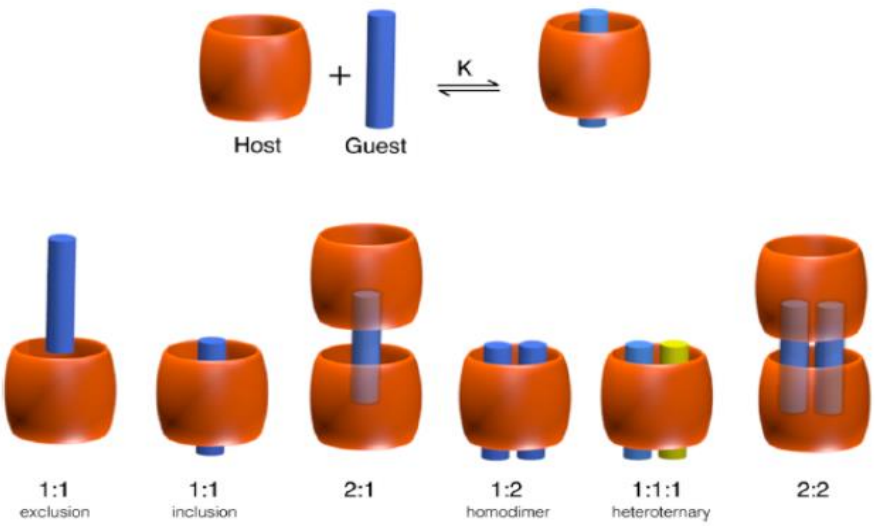

Figure 1.11 – Different types of CB[n] complexes and their stoichiometries.[43]
CB[n] can form two types of complexes: exclusion or inclusion complexes. Inclusion complexes show a variety of stoichiometries. Reprinted with permission from ref. 43. Copyright 2015 American Chemical Society.

1.3.5 Amino acids and peptides complexes

Based on CB[n] characteristics one can tell that amino acids with a hydrophobic side chain are potential guests. Several studies demonstrated that, indeed, complexes of CB[n]·amino acid involve the inclusion of the side chain in the host cavity and that attractive ion-dipole interactions occur between the carbonyl portal and the ammonium group of the amino acid.[44]

Peptides differ from single amino acids in size and possesses an oligoamide backbone with a N-terminal and a C-terminal, plus a variety of sidechains is present, not to forget that the amino acid sequence affects deeply its structure. It was showed that the recognition of peptides is highly dependent on the sequence, therefore the amino acid in N-terminal is extremely important since only in this position the two driving forces mentioned above can take place (**fig. 1.12**).[44, 45]

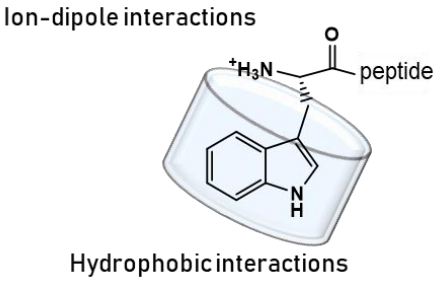

Figure 1.12 – CB[n] selective recognition of an N-terminal aromatic peptide**.**
The N-terminal tryptophan aromatic side chain is included within CB[n] cavity and the ammonium interact with the carbonyl portals. The driving forces involved are hydrophobic interactions and ion-dipole interaction, respectively. Adapted from Urbach et al.[44]

1.3.6 Protein complexes

Proteins are involved in many biological processes which makes them attractive targets for drug design, medical diagnosis and separation.[43, 44] Furthermore, protein assemblies are important in biological context since they have important roles in virus infection, cell skeleton and biological processes.

The CB[n] host-guest chemistry is ideal for the construction of protein assemblies ranging from 1D to 3D. This supramolecular strategy is promising because CB[n]s can recognize N-terminal amino acids with aromatic side chains and when not the case, only requires a small modification at the N-terminal which does not interfere with their active site, maintaining the structural and biological properties of protein assemblies. The modification at N-terminal usually requires the introduction of guest molecules such as FGG peptide, methyl viologen (MV) and 2, 6-dihydroxynaphtalene (2,6-NP) that are connected to the protein with a flexible linker to avoid steric crowding.[36] The cucurbituril-based protein assemblies have several applications ranging from catalysis, biosensing and affinity purification of proteins.[36]

Several examples of cucurbituril-induced protein assemblies are illustrated in **fig. 1.13**.

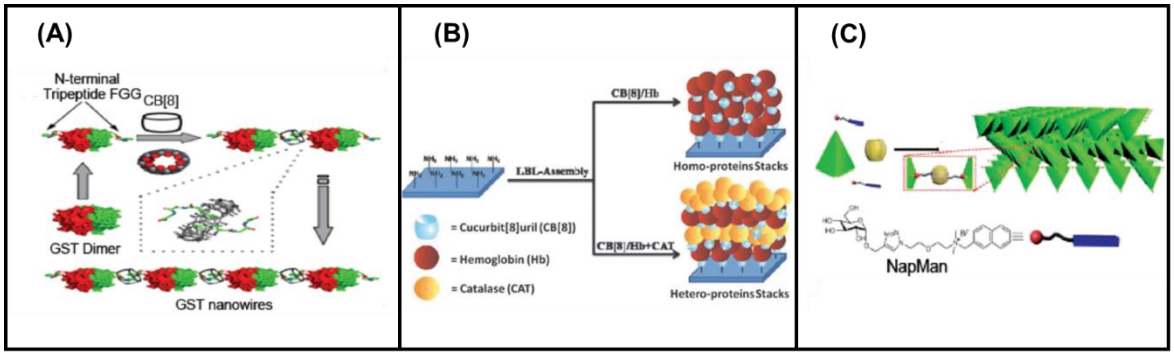

Figure 1.13 – Illustration of 1D, 2D and 3D cucurbituril-induced protein assemblies. **(A)** 1D CB[8] induced GST nanowires. **(B)** 2D layer-by-layer proteins stacks on surfaces using CB[8] as "glue". **(C)** 3D assemblies of ConA/AzoMan/DDPS/CB[8]. Reprinted with permission from ref. 36 and 43. Copyright 2017 The Royal Society of Chemistry. Copyright 2015 American Chemical Society.

1.3.7 *Trans*-chalcones complexes

Chalcone or 1,3-diphenylprop-2-en-1-one, consists in two aromatic rings linked by a three-carbon unsaturated carbonyl system. They are naturally occurring compounds and intermediates in the biosynthesis of flavonoids.[46] The flavylium family of compounds, which include chalcones in their characteristic network of chemical reactions, have been exerted for several applications, such as, food colorants and dye-sensitized solar cells.[47] Chalcones also exhibit antibacterial, antitumor and anti-inflammatory properties.[46, 48] Hence their complexation with CB[n] is of interest in frameworks like drug delivery, indicator displacement assays and dye stabilization.[47]

Currently, the complexation of *trans*-chalcones (TCs) has been studied by Basílio and co-workers.[49, 50] In a recent study [47], they used TCs with amino groups to observe the changes in pKa induced by complex formation (**fig. 1.14**) and showed that it is very sensitive to small structural variations. Briefly, an acid-base titration of the complexes CB[7]·TC was performed and compared to the one performed with only the TC. It was verified an upward pK_a shift for the TCDMA complex which means that the complexation induced protonation. Contrarily, TCDEA had a small decrease in pK_a, therefore the complex is more stable with the TC deprotonated. These results support the hypothesis that the hydrophobic effect contributes more than ion-dipole interactions in the complexation of specific guests in CB[n]s.[47]

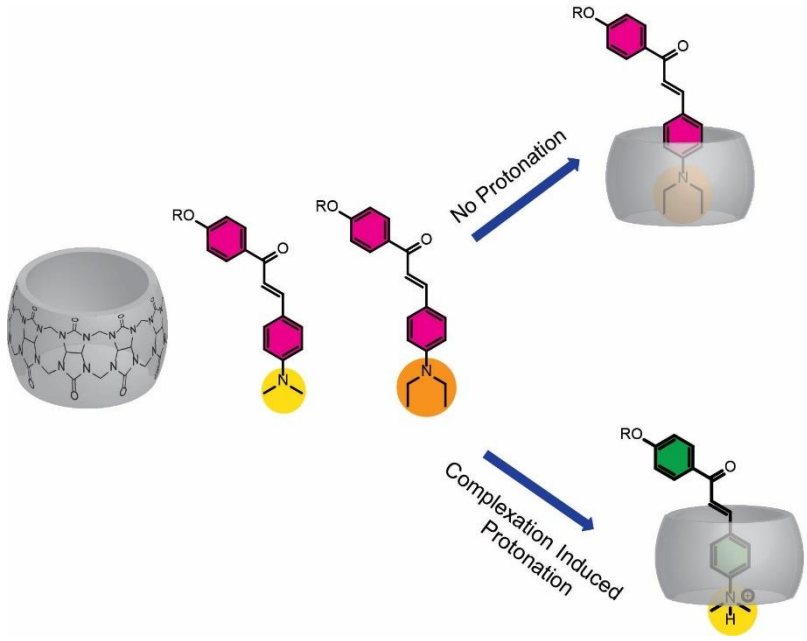

Figure 1.14 – Inclusion complexes formed between TCDMA and TCDEA with CB[7].
The complexation of *trans*-chalcone dimethylamine (TCDMA) induces protonation. In contrast, complexation of *trans*-chalcone diethylamine (TCDEA) does not induce protonation. Adapted from Basílio et al.[47]

1.4 Characterization of complexes

Spectroscopic (absorption, emission and NMR) and calorimetric (ITC) techniques have been frequently used to characterize and understand how complexes are formed. Spectroscopic techniques rely on optical changes that result from the guest inclusion in the host cavity.

1.4.1 Absorption and Emission

When the guest or host has a chromophore is usual to resort to UV-Vis absorption spectroscopy. Therefore, when has a fluorophore, emission spectroscopy can also be used. When it does not possess a chromophore/fluorophore it is usual to rely on dyes as reporters by performing competitive displacement assays. The methodology relies on titrations to determine

the association constant. Usually the reporter molecule is kept constant and the other components vary. Upon several additions of titrant there is a spectral change in the reporter spectra, due to formation of complex or displacement of the dye.[51]

UV-Vis absorption spectroscopy relies on light interaction with the sample, which causes an electron to go from a ground state (lower energy) to an excited state (higher energy). The energy absorbed by this electronic transition is recorded by the spectrophotometer through transmittance measure.[52, 53] The transmittance (T) can be correlated with absorption (A) as demonstrated in equation **1.1**.

$$A = -log_{10}T \quad \textbf{(1.1)}$$

The Lambert-Beer law (eq. **1.2**) correlates the absorbance with parameters such as concentration (c), optical path (l) and the molar extinction factor (ε).

$$A = c.l.\varepsilon \quad \textbf{(1.2)}$$

This technique allows not only a quantitative (through Lambert-Beer law) but also a qualitative analysis comparing the sample spectrum to a pattern compound, also, the maximum absorption (λ_{max}) can be used to identify certain electronic transitions that are characteristic of certain groups.

Emission or fluorescence is the process where an excited electron passes to the ground state with emission of light. The intensity of the radiation emitted (fluorescence intensity) by the sample is recorded by the spectrofluorometer. The detector is placed at 90º of the energy source to register only the radiation emitted by the sample.[52, 53] Intensity of fluorescence (F) and concentration relationship can be obtained through Lambert-Beer law, resulting in the final equation **1.3**, where k is a proportionality constant, I_0 the intensity of the source radiation and c the concentration (this equation only applies to where linearity is verified).

$$F = kI_0c \quad \textbf{(1.3)}$$

1.4.2 NMR

Nuclear Magnetic Resonance (NMR) spectroscopy relies on the magnetic properties of the atoms nucleus. When placed in a strong external magnetic field (B_0) the nucleus tries to align with it. Because the nucleus is spinning and has angular momentum, the torque that B_0 causes results in a circular motion called precession. The precession rate or Larmor frequency (v_0) is given by equation **1.4** where γ is the magnetogyric ratio of the nucleus.[54]

$$vo = \gamma Bo/2\pi \quad \textbf{(1.4)}$$

An important concept is electron shielding that is the effect that electrons create and change how the nucleus feels the B_0. Therefore, the more electrons around a certain nucleus the less B_0 influences the nuclei alignment with it.[54, 55] For spin ½ nuclei are two quantum states: up or down. In a magnetic field, the up state (α) is considered aligned with the magnetic field, while the down state (β) is the opposite. Slightly more than half of nucleus will be in the up state (lower energy). [54, 55] The technique consists in causing perturbations (usually, radio frequency pulses) that will force the nucleus to alter their alignment with B_0 and going from the ground state (α) to an excited state (β). The photon energy must match the energy gap (ΔE, eq. **1.5**) between the two states. [54, 55] When the nuclei are in the same state they are in resonance.

$$\Delta E = h\nu o = h\gamma Bo/2\pi \qquad \textbf{(1.5)}$$

The most used nucleus to characterize a molecule are protons (^{1}H) because they are abundant in chemical structures and produce NMR signal. To characterize and elucidate the formation and structure of complexes is usual to resort to ^{1}H-NMR, where guest protons signal are followed. Hereupon, nuclei inside the host cavity are more shielded and nuclei at the carbonyl portals of CB[n] are more deshielded, resulting in upfield shift and in a downfield shield of the guest signal, respectively. The association constants of complexes can also be determined by NMR titrations. Exchange rate is a relevant property in these experiments, since different rates will influence the final spectrum and how the experimental results are treated. Fast and slow exchanges spectra are illustrated in **fig. 1.15**. Mathematical details are covered in several reviews.[51, 56]

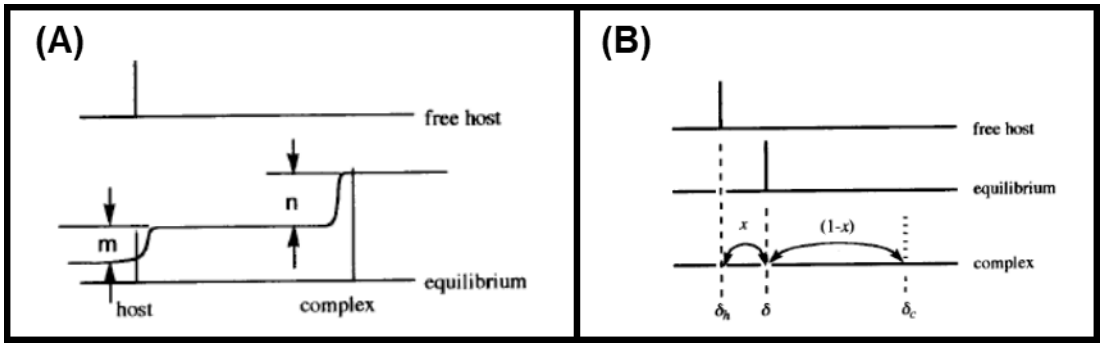

Figure 1.15 – Representative NMR spectra of complexes with different exchange rates. (A) Slow exchange rate complexation has distinguishable peaks for the free and complexed form. (B) Fast exchange rate complexation has fused peaks. Reprinted with permission from ref. 56. Copyright 2001 Kluwer Academic Publishers.

Another NMR experiment that allows us to understand how the complex forms is Diffusion-Ordered SpectroscopY (DOSY). Studying molecular diffusion in solution offers insights of several physical molecular properties (size, shape, aggregation, encapsulation, complexation and hydrogen boding).[55] Random translational (Brownian) motion of molecules driven by the thermal energy of the system can be quantified by the called self-diffusion coefficient D and that is the physical parameter that DOSY experiments aims to determine and it is described in

equation **1.6**, where k_B is the Boltzmann constant, T the absolute temperature and f the frictional factor.[55]

$$D = k_B T/f \qquad \textbf{(1.6)}$$

The frictional factor is related to the hydrodynamic radius of the sphere (r_S) and the solution viscosity (η) as in equation **1.7**.

$$f = 6\pi\eta r_S \qquad \textbf{(1.7)}$$

Combining equations **1.6** and **1.7** gives the known Stokes-Einstein equation:

$$D = k_B T/6\pi\eta r_S \qquad \textbf{(1.8)}$$

Therefore, the diffusion coefficient is inversely related to the size (radius) of the diffusing species, consequently, larger molecules or complexes will tend to exhibit smaller diffusion coefficients.

1.4.3 ITC

Isothermal Titration Calorimetry (ITC) is one of the most common techniques used to determine not only binding constants but also thermodynamic parameters and the stoichiometry of complexes. The ITC apparatus contains two cells (reference and sample cell) within a thermostated environment. The experiment consists in titrating one reactant (usually the guest) into a second one (usually the host). Upon binding, heat can be released or absorbed resulting in a signal that is used to monitor the titration. The ITC machine compensates (and measure) the heat flow to the sample cell so that is maintained at the same temperature as the reference cell.[57, 58] In **fig. 1.16** is represented the typical data obtained in an ITC experiment.

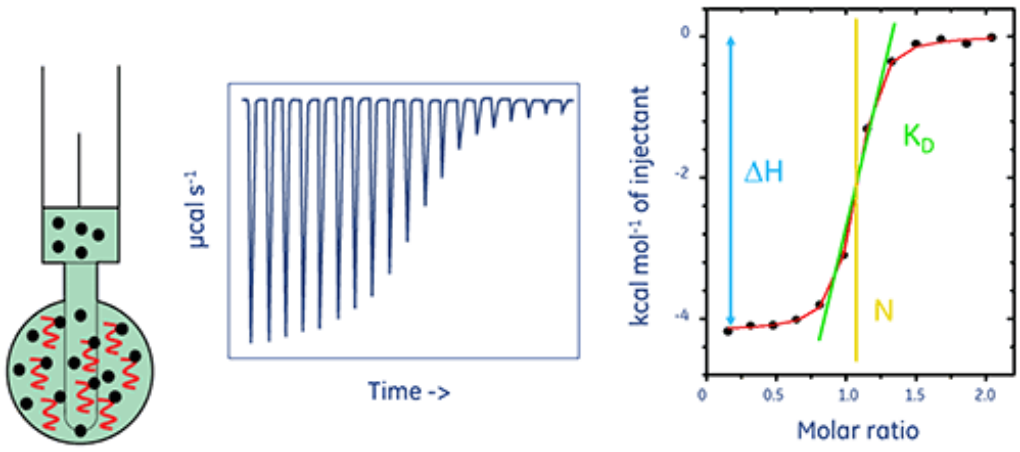

Figure 1.16 – Representation of an ITC experiment and data.[59]
On the left is represented the titration of a reactant (black dots) in the sample cell. In the middle is the resulted thermogram of time in function of raw heat rate. The experimental data fitting and the determined parameters (n, K_D and ΔH) are on the right.

1.5 Aim

The aim of this work was to develop a series of caged amino acids (due to their biocompatibility) as photoresponsive guests for development supramolecular systems based on CB[7] and CB[8] nanocapsules. This was previously proved to work with caged phenylalanine/CB[7] host-guest system and is expanded in this work to other amino acids/peptides and CB[8] to investigate the general scope of the strategy. Due to the higher stability of the complexes formed between peptides and CB[7], an investigation was also carried out to develop phototriggers capable to release cargo that binds stronger to CB[7].

Hence, the system has three components: phototrigger (caged biomolecules), host (CB[7]/[8]) and a probe (*trans*-chalcone). In **fig. 1.17** is represented the intended system where the cage biomolecule behaves as a weak competitor that upon a stimulus (in this case, light) becomes a strong competitor that can displaces probe I.

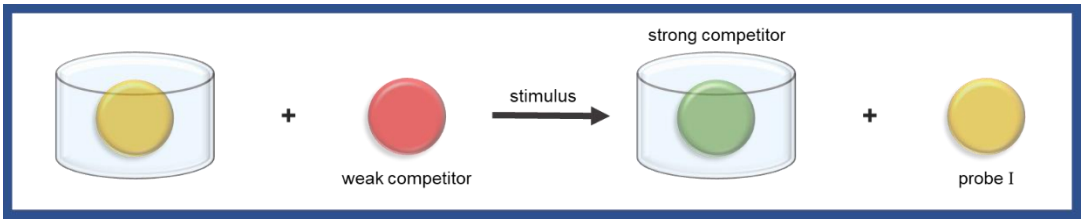

Figure 1.17 – Representation of the intended release system.

The first task of the work was to obtain the caged biomolecules with the Nvoc protecting group, recurring to organic synthesis. The second task consisted in determining association constants between host and guests. Finally, the third task involved the photorelease/deprotection of caged amino acids that was followed by displacement of the probe. Techniques such UV-Vis titrations, displacement assays and ITC were used to determine binding parameters. NMR was used to characterize the synthesized compounds, as well to clarify the intermolecular interactions of complexes.

This system can be applied to solve the drug selectivity problem (**chapter 1.1**) by controlling its release spatial and temporally. Nevertheless, other relevant cargo can be released such as dyes, fragrances or molecules with biological impact. Furthermore, actinometry application can also be achieved using probe I as reporter and caged compounds as actinometer.

2 Results and Discussion

2.1 Synthesis and Characterization

The first aim of the work relied on the synthesis of the compounds required to construct the light-responsive supramolecular systems. It was necessary to synthesize two TCs dyes [TCDEA and *trans*-chalcone diethylamine-2-methoxy (TCDEA$_2$MeO)] and five caged biomolecules. The other TC (*trans*-chalcone dipropylamine - TCDPA) and CB[n] (n=7, 8) were already prepared and characterized from previous studies.[47]

2.1.1 *Trans*-chalcones

To synthesize *trans*-chalcones the Claisen-Schmidt condensation approach was used.[47]

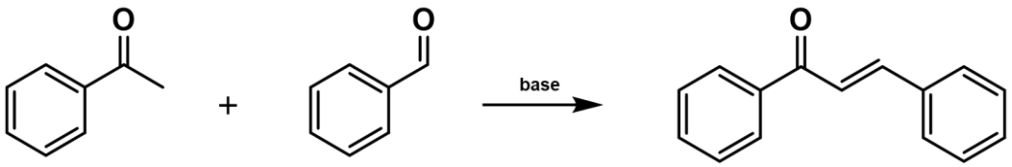

Figure 2.1 – Synthesis of *trans*-chalcone by Claisen-Schmidt condensation**.**

The acetophenone used for the preparation of *trans*-chalcones was the 4'-(1-sulfo-4-butyloxy) acetophenone sodium salt (**1**) due to its increased water solubility owing by the presence of sulfobutyl group. Compound **1** was synthesized according to the reaction showed in **fig. 2.2**, which involves the deprotonation of the hydroxy group of 4-hydroxyacetophenone in presence of a base, followed by a nucleophilic attack in the partial positive carbon **a** of 1,4- butane sultone resulting in the ring-opening to give **1**.

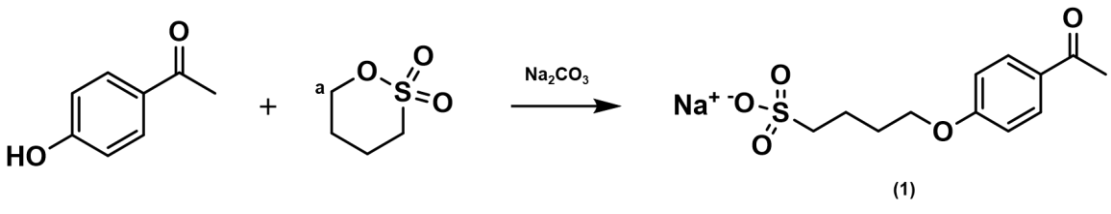

Figure 2.2 – Synthesis of compound **1**.

The product was obtained and isolated with a 40% yield. In its ^{1}H-NMR spectra (**fig. 6.1, appendix**) is visible the presence of an impurity that was confirmed to be acetophenone from the starting material. The product was used without further purification since in the next synthesis it

would be possible to remove any undesired species. The next step was the synthesis of two TCs: TCDEA (**2**) and TCDEA$_2$MeO (**3**) (**fig. 2.3**). Both compounds **2** and **3** were obtained and isolated with a 35.7% and 53.5% yield, respectively. Their structure was confirmed by ^{1}H-NMR (**fig. 6.2 and fig. 6.3, appendix**).

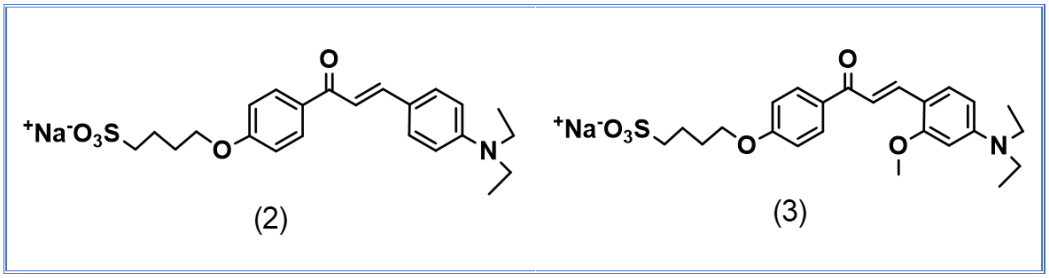

Figure 2.3 - Chemical structure of TCDEA (**2**) and TCDEA$_2$MeO (**3**).

2.1.2 Caged biomolecules

Four amino acids (trp, tyr, his and phe) and one tripeptide (FGG) were successfully protected with a photolabile group (Nvoc). The synthesis was based on a procedure that was already described in literature[28] and involved an amino terminal protection where the amino group attacks the carbonyl of Nvoc-Cl and chloride is liberated (**fig. 2.4**).

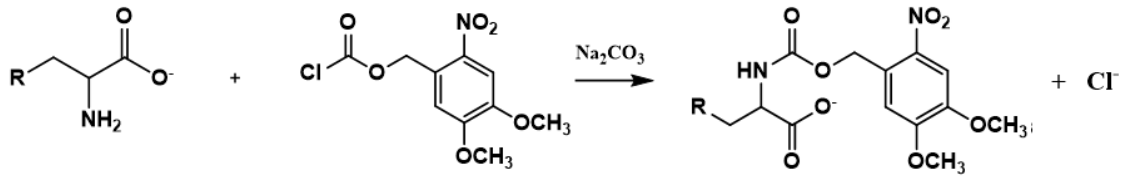

Figure 2.4 – Synthesis of caged amino acids with the Nvoc protecting group.

The identity of the compounds was confirmed by ^{1}H-NMR and ^{1}H -^{1}H COSY (**fig. 6.4 – 6.11, appendix**).

Table 2.1 shows the obtained yields for caged molecules prepared in this work. Tryptophan, tyrosine and phenylalanine present yields above 50% which is expected for this chemical reaction taking in account published results.[60] Histidine and the tripeptide present lower yields (under 50%). It was not found any reports of the photocaging on these two biomolecules with Nvoc-Cl. For all cases the caged compound had affinity for the organic phase at acidic pH when the liquid-liquid extraction was performed, with exception of caged histidine that remained mostly in aqueous phase. At acidic pH (1-2) the terminal carboxylic group is protonated and because of this most of the caged compounds are more soluble in the organic phase than in the aqueous phase. The histidine derivative constitutes an exception, as the imidazole side chain has a pKa of 6 being positively charged at pH 1-2. This increases the water solubility of the caged histidine compared to others caged amino acids. So, liquid-liquid extraction did not work, and

another strategy was needed. It was found that at pH 7, in water, it precipitates. Yet, this event occurred with low yield. Probably, a pH of 6 would have been the better choice since the neutral charge of the imidazole ring would allow pi stacking, decreasing the water solubility. A try-out of different pH could help understand which pH allows the best yield and if the imidazole group is the most influential group in solubility of the caged compound. The peptide lower yield can be due to its increased size or simply because the workup followed was not the more suitable for this case.

Table 2.1 – Yields (%) of each caged biomolecule synthesis.

Compound	Yield (%)
Tryptophan-Nvoc 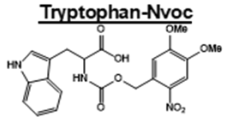	58.0
Tyrosine-Nvoc 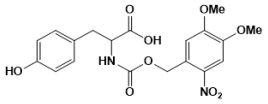	62.0
Histidine-Nvoc 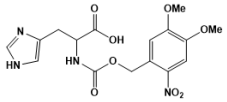	25.8
Phenylalanine-Nvoc 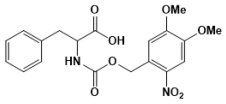	94.5
FGG-Nvoc 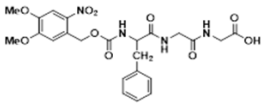	20.0

2.2 Determination of association constants

The second aim of the work consisted in the determination of the association constants (K_{ass}) of free/caged biomolecules (four different amino acids and a tripeptide) towards CB[n] (n=7 ,8) to confirm if the caged analogues would demonstrate lower affinity towards the host compared to the free ones. It was also needed to obtain the K_{ass} of the probes (*trans*-chalcones), in order to choose which one would be a better candidate to be displaced by the competitors.

2. Results and Discussion

2.2.1 Free and caged amino acids · CB[n]

The K_{ass} of free and caged amino acids was determined by titration with CB[n] (n= 7, 8). In **fig. 2.5** is the spectrophotometric data obtained for tryptophan and tyrosine titration with CB[7].

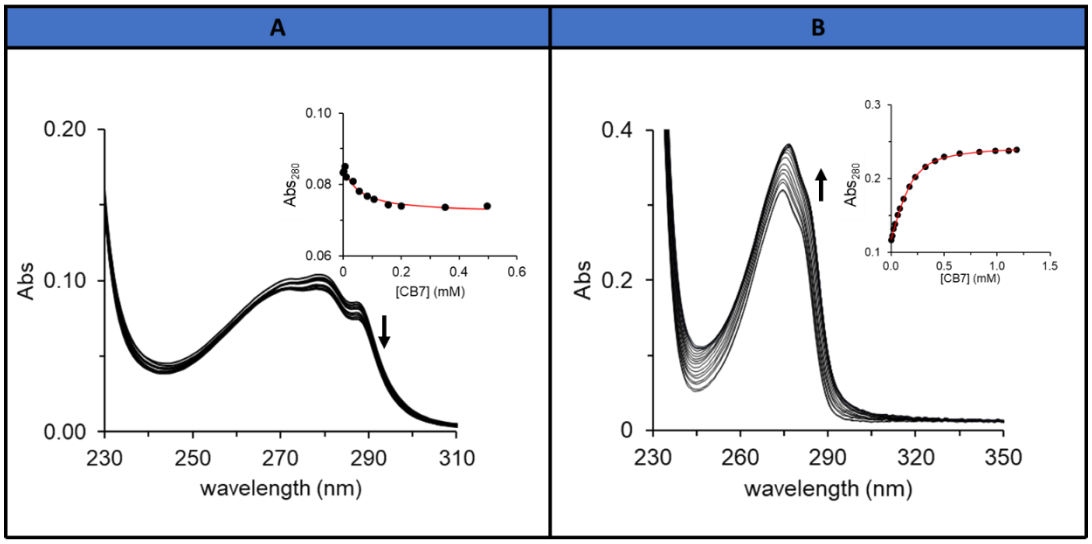

Figure 2.5 – Spectrophotometric titration of (A) [Trp]= 18 µM and (B) [Tyr]= 184 µM with CB[7]. Experimental data at 280 nm is the black dots and the 1:1 fitting is the red line.

Tryptophan and tyrosine showed hypochromic and hyperchromic effects, respectively, upon CB[7] addition. The decrease or increase of absorbance was followed at 280 nm in both cases and it fitted well to a 1:1 host-guest binding model. The best least-squares fit resulted in constants of $2.19 \times 10^4\ M^{-1}$ and $1.88 \times 10^4\ M^{-1}$ for tryptophan and tyrosine, respectively. These results agree with previously published ones determined by ITC, UV titrations and competitive fluorescence titration.[44] The K_{ass} of histidine was not determined by this method since the maximum absorption of CB[7] (λ_{max}= 200 nm) is almost overlapped with the histidine maximum absorption (λ_{max} = 211 nm). The K_{ass} of tryptophan was also determined by emission spectroscopy and the data (area) was fitted with a 1:1 binding model. The best least-squares fit resulted in a constant of 5.22 x $10^3\ M^{-1}$. The experimental data can be consulted in **fig. 6.26** in the appendix.

Next, we aimed to access the K_{ass} of caged amino acids to see if they would be weak binders compared to the free amino acids. For this purpose, the same titration method was performed, and the results are in **fig. 2.6**.

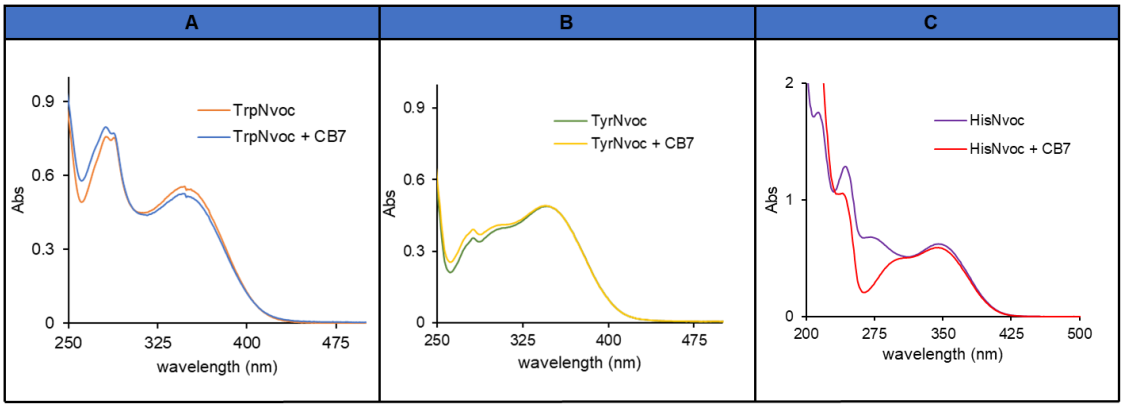

Figure 2.6 – (A) TrpNvoc 100 µM without CB[7] (orange) and with CB[7] 1.92 mM (blue), (B) TyrNvoc 100 µM without CB[7] (green) and with CB[7] 2.76 mM (yellow), (C) HisNvoc 90 µM without CB[7] (purple) and with CB[7] 2.75 mM (red).

In all three cases there were spectral differences upon addition of CB[7]. In the first case (**A, fig. 2.6**), it is observable two different effects: one is a hyperchromic effect in tryptophan maximum absorption (~280 nm) and the other is a hypochromic effect in the Nvoc maximum absorption (~350 nm). In the second case (**B, fig. 2.6**), the signals of tyrosine and Nvoc come together but it is notorious a slight increase in tyrosine maximum absorption (~ 274 nm) and no alterations on the Nvoc signal. In third case (**C, fig. 2.6**), the hypochromic effect is visible until ~ 332 nm. As caged histidine exhibited significative spectral changes between 240-300 nm, a titration was performed. In **fig. 2.7** is represented the titration with CB[7] and the respective 1:1 fitting that resulted in a K_{ass} $< 6.00 \times 10^{2}$ M^{-1}.

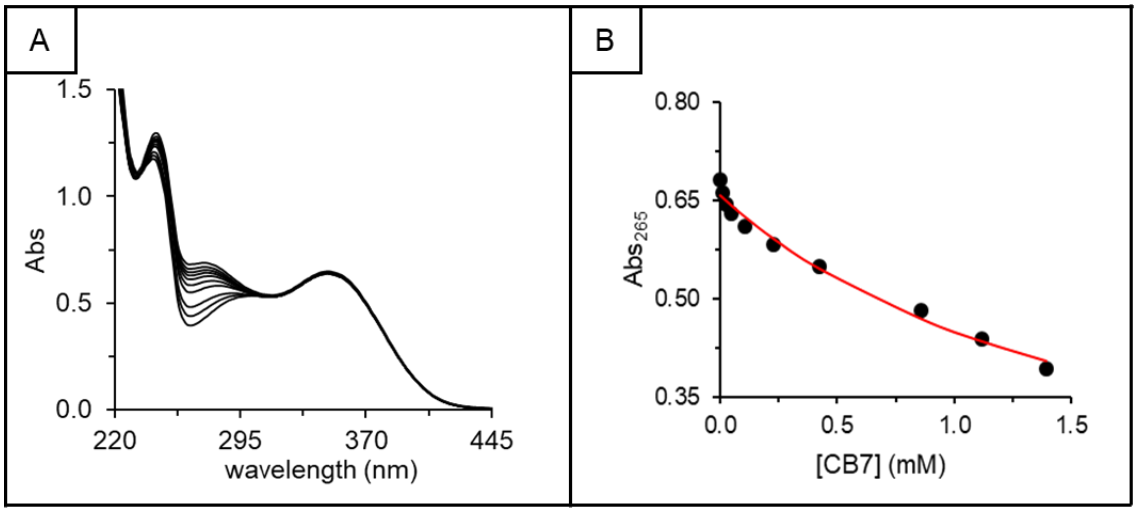

Figure 2.7 – (A) Spectrophotometric titration of HisNvoc with CB[7], (B) Experimental data at 265 nm is the black dots and 1:1 fitting model is the red line. [HisNvoc] = 9.0×10^{-5} M.

The same type of assays was also performed for CB[8], but only with phenylalanine and tryptophan. Phenylalanine has a molar extinction coefficient of 195 M^{-1} cm^{-1} at 257 nm (λ_{max}), which means that millimolar concentrations are required to have signal in UV-Vis spectroscopy

(~ 1 mM to have 0.2 of absorbance). CB[8] has a solubility of ~ 0.1 mM, therefore it was not possible to have a good concentration/signal ratio to perform the assays since we cannot have host in excess to secure that the major percentage of guest is complexed. For tryptophan, it was not possible to determine the K_{ass} towards CB[8] because along the titration the baseline increased and at higher concentrations of CB[8] a precipitate was observed. Therefore, the K_{ass} of phenylalanine and tryptophan was determined by other techniques such as displacement assays and ITC.

Next, was followed the complexation of caged phenylalanine and tryptophan with CB[8] (**fig. 2.8**).

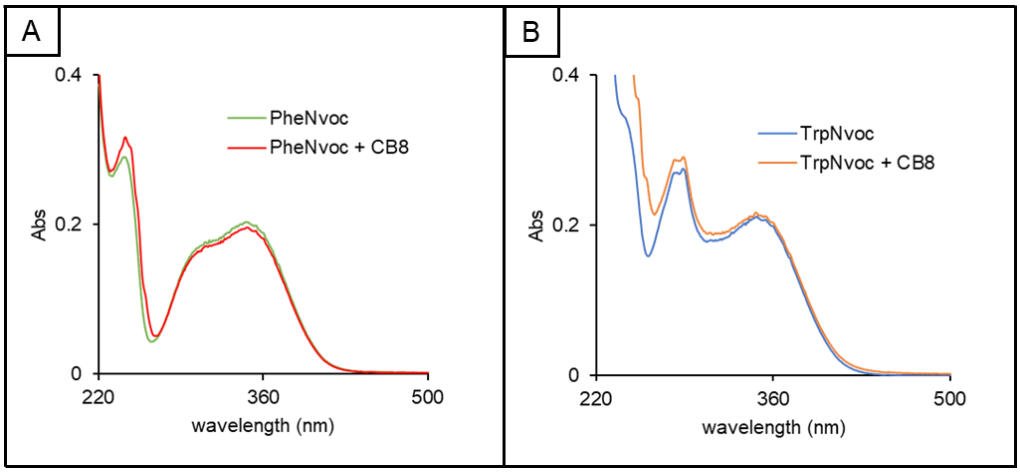

Figure 2.8 – (A) PheNvoc 40 µM without CB[8] (green) and with CB[8] 0.13 mM (red), (B) TrpNvoc 30 µM without CB[8] (blue) and with CB[8] 0.13 mM (orange).

The formation of complexes with CB[8] seems to follow the same behaviour as CB[7] with exception for caged tryptophan where there is a slightly increase in Nvoc maximum. In short, we can say that the caged amino acids tested seems to complex with CB[7] but in much less extent than the free ones, being promising weak competitors for photoresponsive host-guest complexes with exception of caged histidine that has an association constant very close to its free pair. For CB[8] it is necessary to determine the association constants of free phenylalanine and tryptophan by other means, yet the caged analogues also do not reveal strong complexation.

2.2.2 Free and caged peptide · CB[n]

The formation of supramolecular complexes with CB[7] and CB[8] was also studied with the tripeptide (FGG). Since the phenylalanine residue is the only chromophore present in its composition we faced the same problem mentioned above (chapter **2.2.1.**). UV-Vis displacement assays and ITC were performed instead, in which was possible to determine the association constants.

The complexation of caged peptide was accessed by titration with CB[n] (n= 7, 8) and the results are in **fig. 2.9** and **fig. 2.10**. No significant spectral differences were recorded for caged tripeptide upon addition of CB[7]. There was a slight hyperchromic effect in the solution containing the host in excess, but it is more likely to not complex with significant binding affinity. NMR and ITC studies were performed to clarify this result.

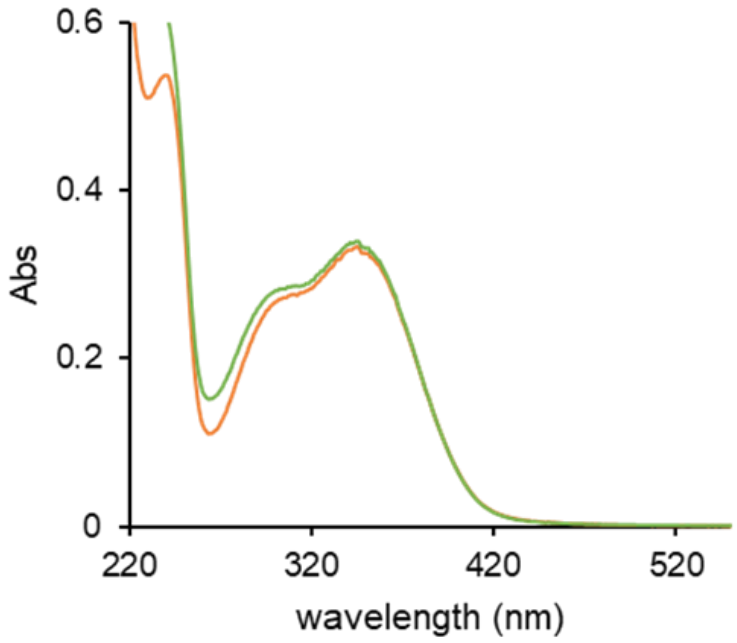

Figure 2.9 – Spectrophotometric spectra of FGGNvoc (orange) and FGGNvoc with CB[7] (green). [FGGNvoc] = $\mathbf{6.0 \times 10^{-5}}$ M, [CB7] = 2.6 × $\mathbf{10^{-3}}$ M.

A hypochromic effect was observed upon addition of CB[8] showing that contrary to CB[7] this species forms stable host-guest complexes. The experimental data fitted well to a 1:1 binding model and the best least of squares fit resulted in a K_{ass} of 2.69×10^6 M^{-1}.

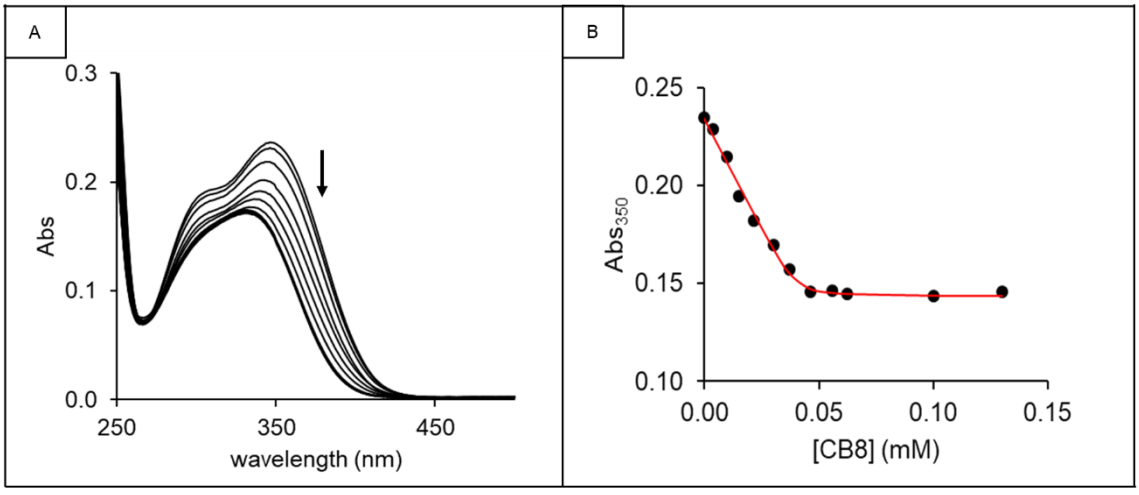

Figure 2.10 – (A) Spectrophotometric titration of FGGNvoc with CB[8], (B) Experimental data at 350 nm is the black dots and 1:1 fitting model is the red line. [FGGNvoc] = 4.0×10^{-5} M.

2.2.3 *Trans*-chalcones · CB[n]

Trans-chalcones dyes were used in indicator displacements assays to investigate the binding of optically silent guests. It was necessary to determine the association constants between the *trans*-chalcones and CB[n] (n=7, 8) to decide which one is a more appropriate probe for displacement assays. The complexation of TCDMA and TCDEA with CB[7] was already studied and characterized as mentioned before (chapter **1.3.7**).[47]

TCDEA$_2$MeO·CB[7]

When not complexed with CB[7] the TCDEA$_2$MeO has an absorbance maximum at 452 nm which decreases upon addition of the host. At higher CB[7] concentrations it is visible the appearance of a new maximum that stops at 490 nm (redshift). The data fitted well to a 1:1 binding model as shown in **fig. 2.11** and the resulted K_{ass} is on **table 2.2.**

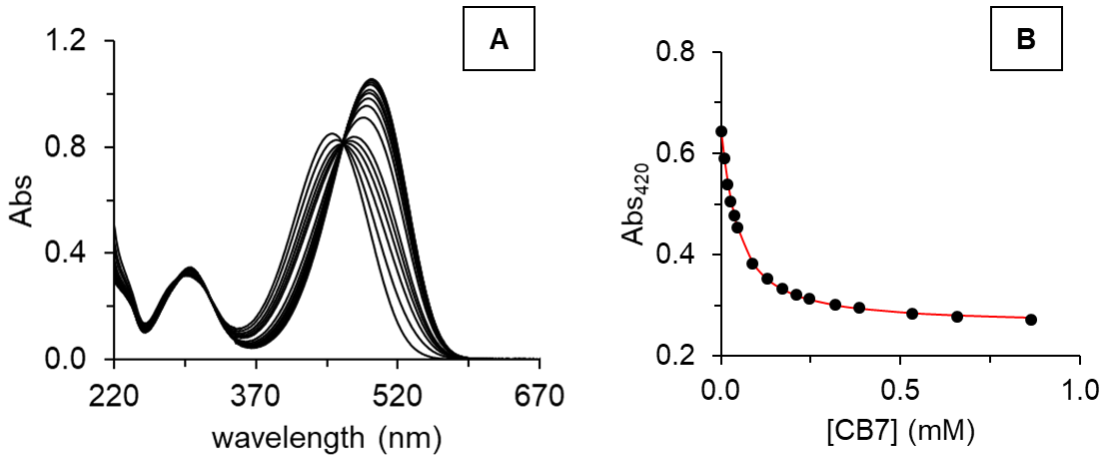

Figure 2.11 – (A) Spectrophotometric titration of TCDEA$_2$MeO with CB[7] at pH 7 and (B) experimental data at 420 nm is the black dots and 1:1 fitting model is the red line. [TCDEA$_2$MeO] = 2.3×10^{-5} M.

TCDPA·CB[7]

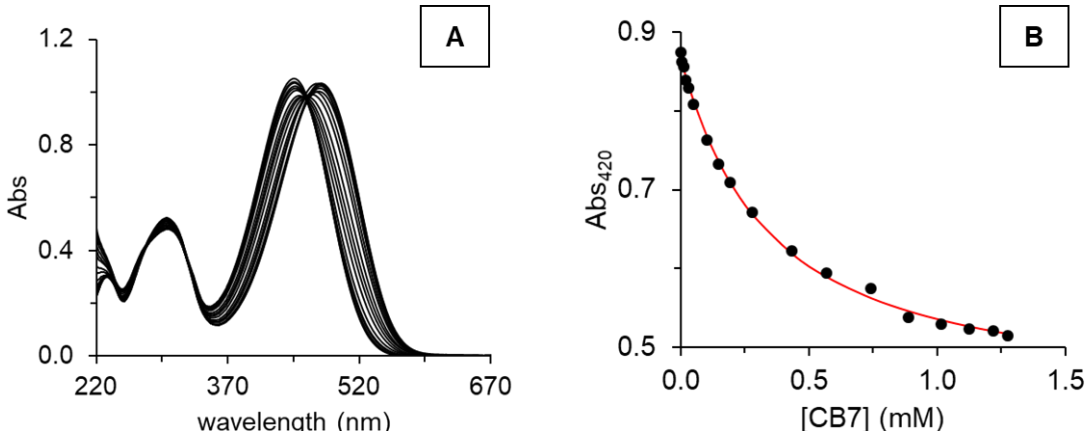

Figure 2.12 – (A) Spectrophotometric titration of TCDPA with CB[7] at pH 9, (B) experimental data at 420 nm is the black dots and 1:1 fitting model is the red line. [TCDPA] = 6.0×10^{-5} M.

As observed for the previous *trans*-chalcone there is a redshift on the λ_{max} (450 nm→ 480 nm) upon CB[7] addition and the experimental data fitted well to a 1:1 stoichiometry (**fig. 2.12**) The resulted K_{ass} is in **table 2.2**.where also is the K_{ass} of other *trans*-chalcones determined by UV-Vis spectroscopy. All the fits were calculated using a 1:1 binding model as mentioned before.

Table 2.2 - Different K_{ass} of *trans*-chalcones with CB[7].

Molecule	K_{ass} (M^{-1})
TCDMA	3.90×10^{4} [a]
TCDEA	2.30×10^{5} [a]
TCDPA	3.29×10^{3}
$TCDEA_2MeO$	2.86×10^{4}

a- In water at pH 9.[47]

$TCDEA_2MeO$ has a lower association constant (2.86 x 10^4 M^{-1}) compared to TCDEA (2.30 x 10^5 M^{-1}). However, its constant has the same order of magnitude as TCDMA. The presence of methoxy group in position two turns the compound bulkier which can represent a drawback in size complementary, nonetheless, as seen before (**chapter 1.3.7**), complexation can induce protonation of TCs. A simple way to prove this is by determining the pK_a of TC in free and complexed form as done in Basilio et al.[47]

TCDPA presents an association constant with two orders of magnitude lower than TCDEA and one lower than $TCDEA_2MeO$ and TCDMA. The dipropylamino group is bulkier than the other tested amino substituents. Once more, size complementary is probably not fulfilled resulting in a less stable complex. Nevertheless, the same tests mentioned above would help clarify the situation.

TCDPA·CB[8]

The different set of *trans*-chalcones was also tested with CB[8], but only TCDPA showed major spectral differences. Therefore, the titration with CB[8] was performed as shown in **fig. 2.13**. It is observable the characteristic redshift and the decrease of the λ_{max} upon addition of CB[8]. The experimental data fitted well with a 1:1 binding model and resulted in an association constant of 4.47×10^5 M^{-1}. To confirm the complex stoichiometry a Job's Plot was also performed (**fig. 6.12, appendix**) and a 1:1 stoichiometry was obtained which agrees with the titration results. The fact that the dipropylamino substituent group is bulkier than the others can explain why CB[8] shows more affinity towards this TC as size complementary is an important factor to stabilize the cucurbituril complexes.

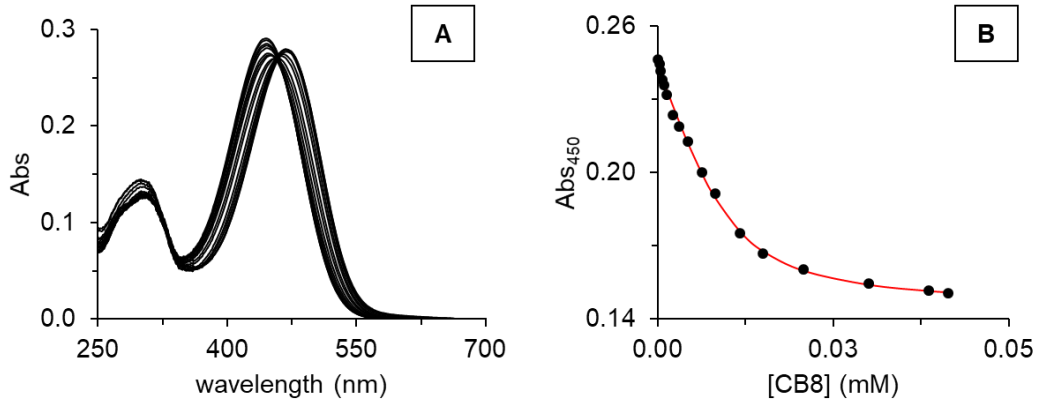

Figure 2.13 – (A) Spectrophotometric titration of TCDPA with CB[8] at pH 9, (B) experimental data at 420 nm as black dots and 1:1 fitting model as the red line. [TCDPA] = 2.0×10^{-5} M.

2.3 Displacement assays

Indicator displacement assays are a reliable alternative to determine association constants of guests that absorb very little or don't absorb at all in the UV-Vis region of the spectrum by using an indicator molecule that absorbs in this region and have significant spectral differences between the free and complexed form. Therefore, *trans*-chalcones were used as indicator molecules which is the same role they have as probes in the photocontrolled release system, being these assays a way of testing the functionality of the system. Since it was not possible to determine the association constant of His and FGG, due to the problems discussed above (chapters **2.2.1**. and **2.2.2.**), this approach was also used to achieve its values.

2.3.1 Indicator displacement assays with CB[7] receptor

For the displacement assays with tryptophan, tyrosine, histidine and their corresponding caged compounds, TCDEA$_2$MeO was chosen as indicator since its constant presents a value within the range of those expected for the amino acids, being ideal for the competitive titration. All the fittings were calculated by the Newton's method.[61] As mentioned above, upon complexation with CB[7], TCDEA$_2$MeO signal undergo a redshift so it was expected that its displacement from CB[7] cavity would lead to a blueshift towards the recovery of the spectra of the free dye. In **fig. 2.14** upper graphs, it can be seen the expected blueshift (490 nm → 452 nm) in all three cases, which means that the *trans*-chalcone is displaced from CB[7] cavity by all three amino acids. In the graphs bellow the fitting of experimental data at 511 nm can be observed. The obtained association constants are listed in **table 2.3**.

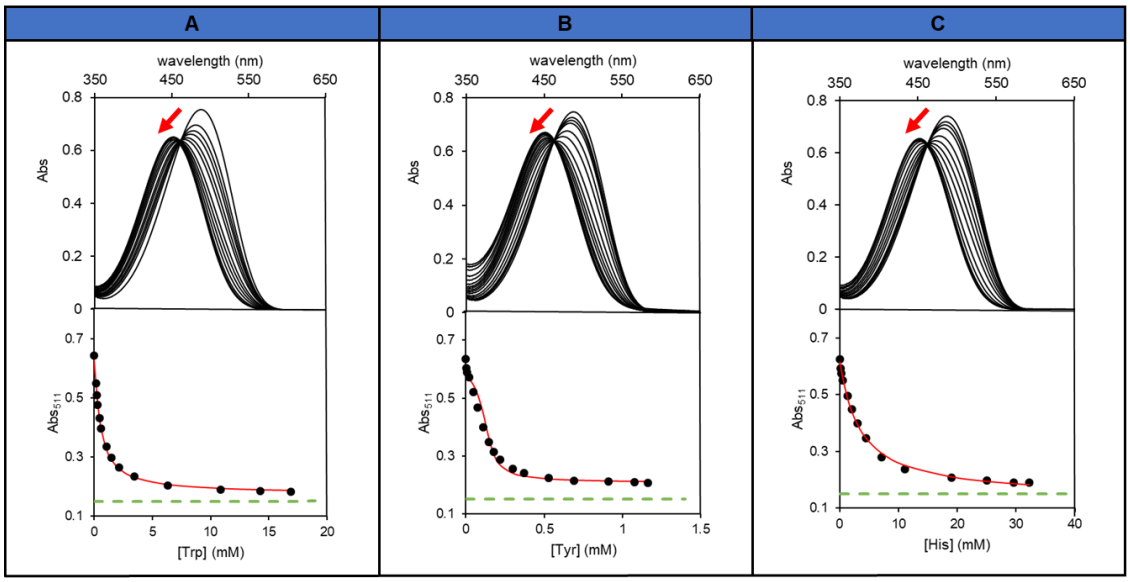

Figure 2.14 – Displacement of TCDEA$_2$MeO from CB[7] trough competitive titration with (A) Trp, (B) Tyr and (C) His. Experimental data at 511 nm is the black dots, the fitting is the red line and free TCDEA$_2$MeO 20 µM at 511 nm is the dashed green line. [TCDEA$_2$MeO] = 2.0 x 10^{-5} M, [CB7] = 15 x 10^{-5} M.

Next, caged tryptophan, tyrosine and histidine were used as competitors. It was expected to observe a weaker or even non-displacement of the *trans*-chalcone since these compounds form less stable complexes with CB[7] as seen before (**chapter 2.2.1**). For all three caged compounds, a blueshift on *trans*-chalcone maximum absorption was verified (**fig. 2.15**). In **fig. 2.15** is the obtained results of this competitive assays where the experimental data was fitted to a 1:1 binding model. The association constants are in **table 2.3**.

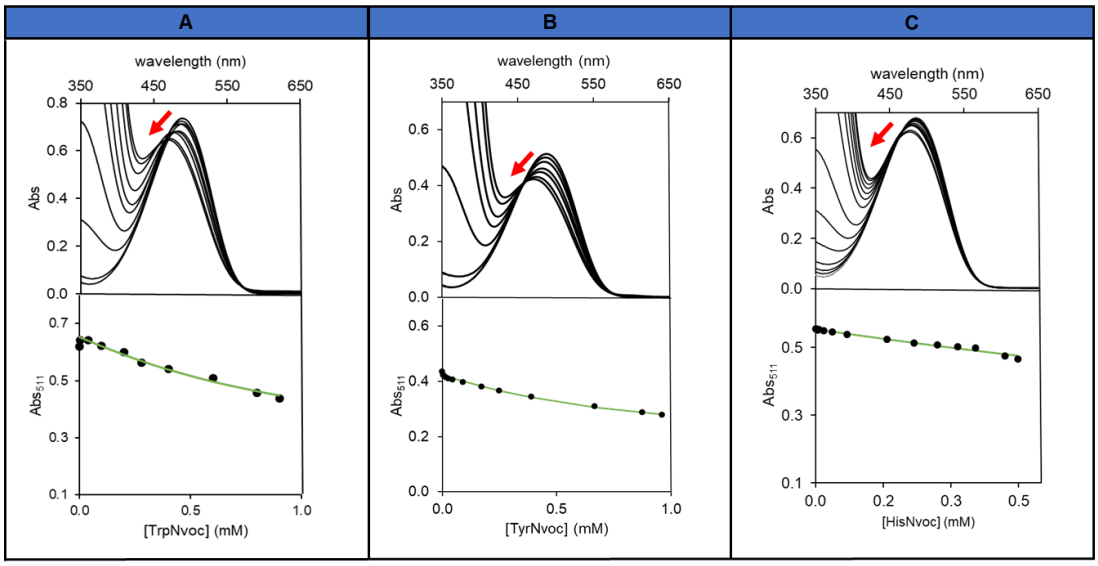

Figure 2.15 – Displacement of TCDEA$_2$MeO from CB[7] trough competitive titration with (A) TrpNvoc, (B) TyrNvoc and (C) HisNvoc. Experimental data at 511 nm is the black dots and the fitting is the green line. [TCDEA$_2$MeO] = $\mathbf{2.0 \times 10^{-5}}$ M, [CB[7]] = $\mathbf{15 \times 10^{-5}}$ M.

However, the resulting fit cannot be used to determine the K_{ass} with accuracy since the *plateau* is not achieved due to the lack of solubility of caged compounds that do not allow to reach higher concentrations for complete displacement. Although, it can be concluded that caged biomolecules have lower affinity towards CB[7] than the free biomolecules. This lower affinity can be explained by the higher contribution of the repulsion effect between C-terminal of amino acids and the carbonyl portal of CB[7], that cannot be compensated by the ion-dipole effect because N-terminal is protected with Nvoc.

Table 2.3 – K_{ass} of free and caged tryptophan, tyrosine and histidine with CB[7] by UV-Vis displacement assay.

Competitor	K_{ass} (M^{-1})
Trp / TrpNvoc	5.46×10^3 / $< 3.00 \times 10^3$
Tyr/ TyrNvoc	1.54×10^5 / $< 4.00 \times 10^3$
His / HisNvoc	1.01×10^3 / $< 1.00 \times 10^3$

The pair free/caged amino acid with greater difference in association constants is Tyr/TyrNvoc, with two orders of magnitude difference. Trp/TrpNvoc pair has association constants of the same order of magnitude and in caged histidine case, the constant is somewhat greater than the one obtained in titration with CB[7] assay ($< 6.00 \times 10^2$ M^{-1}, chapter **2.2.1**) and also than the free histidine constant.

Fig. 2.16 shows the displacement efficiency as a function of the concentrations of caged/ free compounds allowing the identification of the ideal concentrations to perform the light-triggered release of guest molecules from the CB[7] cavity (i.e. where difference in terms of indicator displaced is higher).

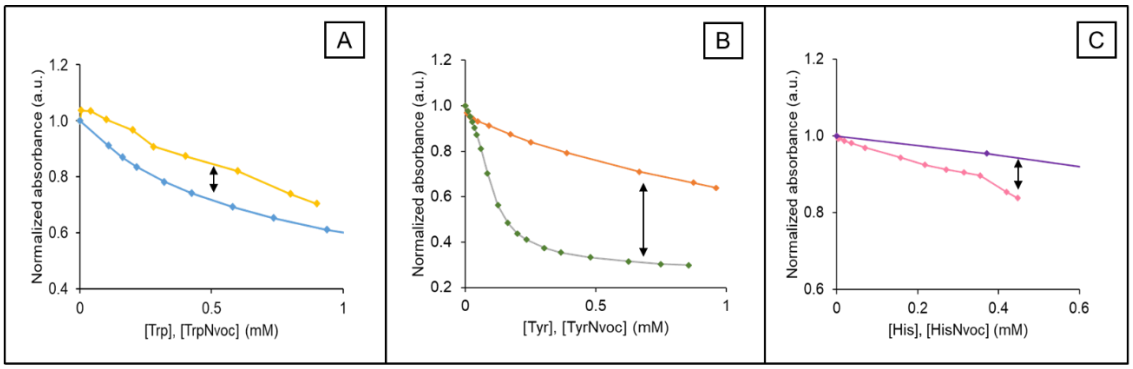

Figure 2.16 – Displacement with (A) tryptophan (blue) and caged tryptophan (yellow), (B) tyrosine (green) and caged tyrosine (orange), (C) histidine (purple) and caged histidine (pink). The arrows represent the region with higher difference in displacement.

For photorelease assays it was necessary to find a significative difference between caged and free complexation. In a perfect scenario the caged compound would not complex with the host and the free compound would complex completely. In case **A** and **C** of **fig. 2.16**, the caged amino acids seem to displace almost the same and even more in histidine case, than the free pairs, therefore this two seem not be good candidates for the photorelease assays. In case **B**, there is a significative difference, where free tyrosine displaces more than caged tyrosine, being this pair a good candidate for the photorelease assays.

Since in a previous published work[27] is proved that caged phenylalanine does not complex with CB[7] and the association constants of the caged amino acids tested here are higher than expected, other hypotheses were considered such as: the caged compounds interacting with the indicator leading to displacement without complexation of the competitor with the host or the formation of ternary complexes (caged compound: indicator: CB[7]). Although the last one is unlikely to be due to the dimensions of CB[7] cavity, that when accommodating both amino acid and TC does not result in a favourable packing coefficient (chapter **1.3.4**). To verify if any of these events were true, NMR studies were performed (chapter **2.5.2**).

The next displacement assay was performed with the peptide and the caged peptide as competitors. The K_{ass} for the dipeptide Phe-Gly (FG) was already reported in literature (K_{ass}= $3.0 \times 10^7\ M^{-1}$)[44], hence it was expected that FGG association constant would be in the same order of magnitude. This time, TCDEA was used as indicator since its constant is higher, being ideal for being displaced by these (stronger) competitors. In **fig. 2.17** is the displacement assay performed with both free and caged FGG as competitors.

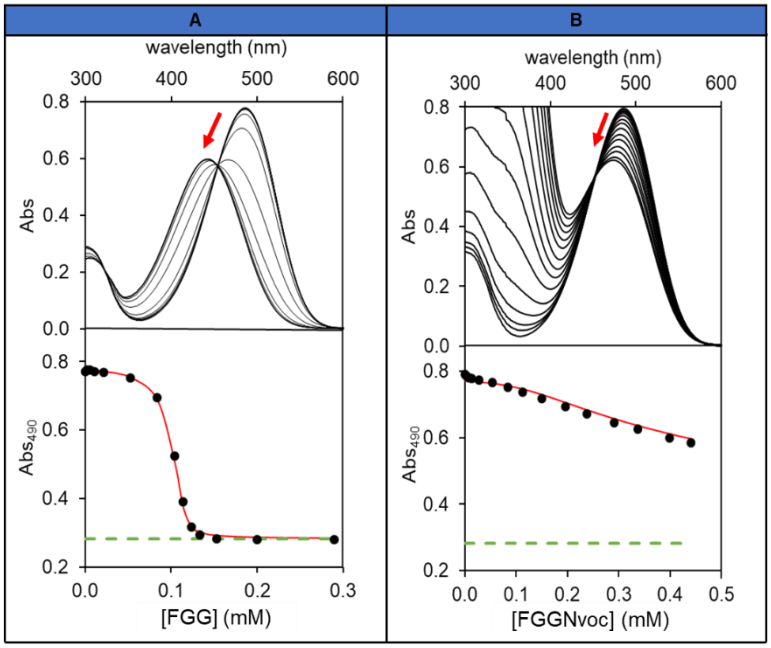

Figure 2.17 – Displacement of TCDEA from CB[7] trough competitive titration with (A) FGG and (B) FGGNvoc. Experimental data at 490 nm is the black dots, the fitting is the red line and the free TCDEA 20 µM is the dashed green line. [TCDEA] = $\mathbf{2.0 \times 10^{-5}}$ M, [CB[7]] = $\mathbf{15 \times 10^{-5}\ M}$.

The association constants obtained were $3.51 \times 10^7\ \mathrm{M}^{-1}$ and $< 6.00 \times 10^4\ \mathrm{M}^{-1}$ for the peptide and caged peptide, respectively. Again, the K_{ass} of caged analogue is not obtained with accuracy. In **fig. 2.18** is represented the gap where the displacement with peptide is greater than with caged peptide. This gap is even bigger than the one observed for the pair Tyr/TyrNvoc.

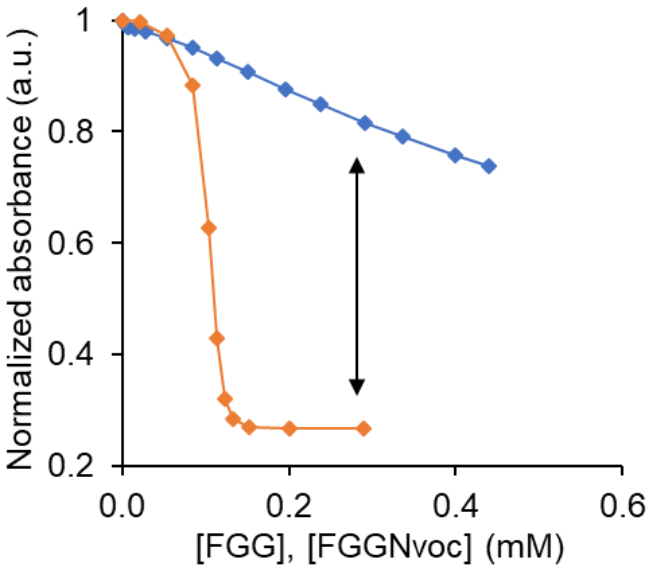

Figure 2.18 – Displacement of TCDEA from CB[7] with peptide (orange) and caged peptide (blue). The arrow represents the region with greatest difference in displacement**.**

Based on these experiments, two pairs of free/caged biocompatible compounds were found to be promisor candidates for the next step: displacement by photorelease (of competitors).

2.3.2 Indicator displacement assays with CB[8] receptor

The same approach was used to determine which free and caged pairs would give promising results. All three amino acids mentioned above, plus phenylalanine and peptide were tested. Only tryptophan, phenylalanine and the tripeptide showed significative spectral differences. From published results it was expected a complexation with a 1:2 host-guest stoichiometry.[44] **Fig. 2.19** shows the displacement of TCDPA from CB[8] with the three compounds that gave the best results. The same pattern of results was obtained, and the experimental data fitted well to a 1:2 host-guest stoichiometry. The association constants obtained are present in **table 2.4**.

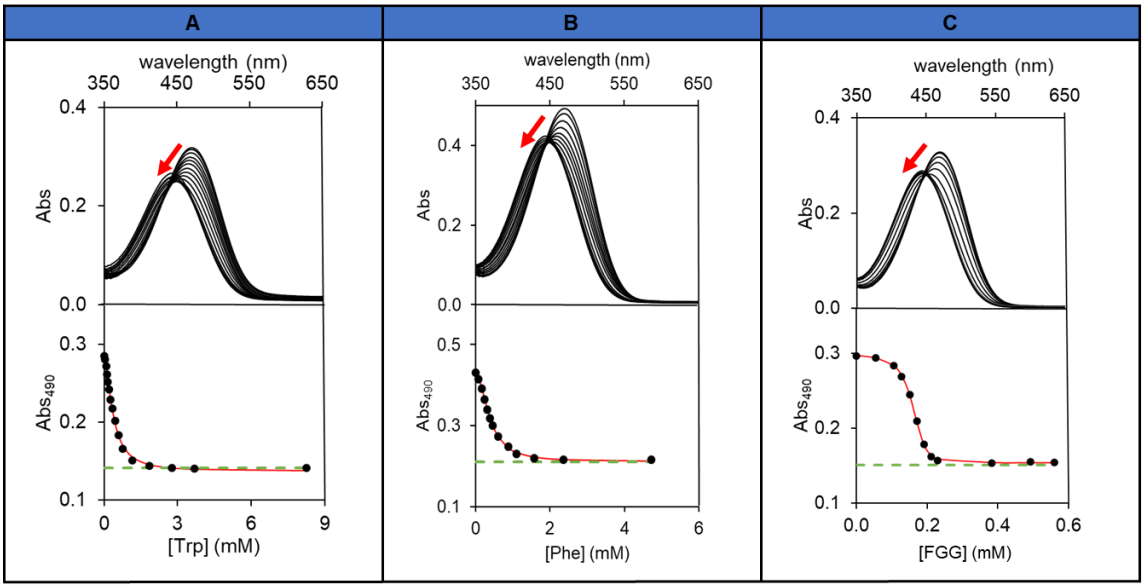

Figure 2.19 – Displacement of TCDPA from CB[8] trough competitive titration with (A) Trp, (B) Phe and (C) FGG. Experimental data at 490 nm is the black dots, the fitting is the red line and the free TCDPA 20 μM is the dashed green line. $[TCDPA]_{(A) \text{ and } (C)} = 1.0 \times 10^{-5}$ M, $[TCDPA]_{(B)} = 2.0 \times 10^{-5}$ M, [CB[8]] = 9.0×10^{-5} M.

As done before, caged compounds were used as competitors (**fig. 2.20**).

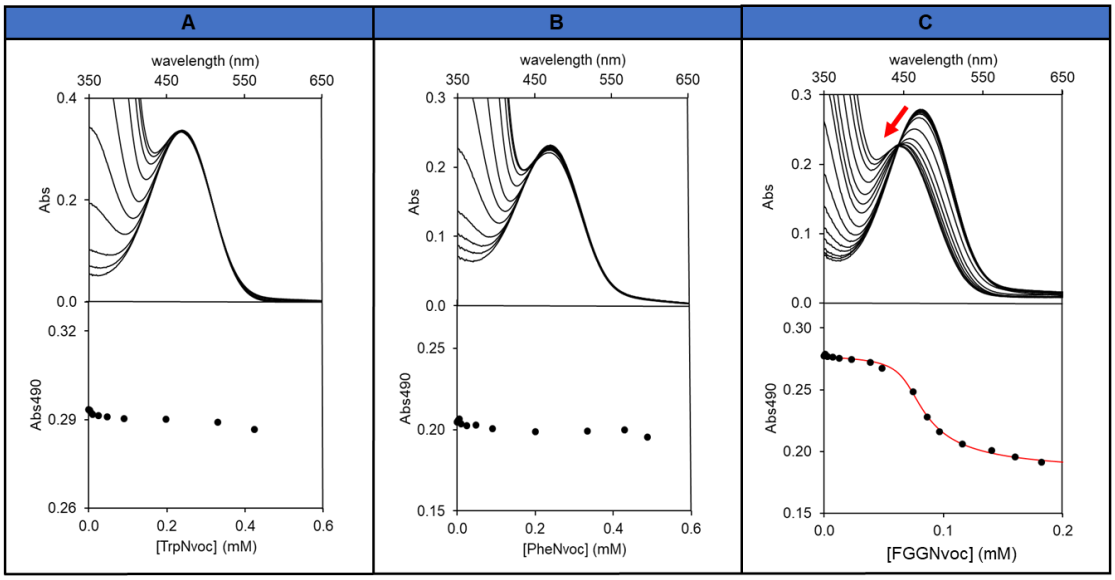

Figure 2.20 – Displacement of TCDPA from CB[8] trough competitive titration with (A) TrpNvoc, (B) PheNvoc and (C) FGGNvoc. Experimental data at 490 nm is the black dots and the fitting is the red line. [TCDPA] = $\mathbf{1.0 \times 10^{-5}}$ **M**, [CB[8]] = $\mathbf{9.0 \times 10^{-5}}$ **M**.

No displacement was observed for caged tryptophan and phenylalanine contrary to caged peptide which displaced the *trans*-chalcone from CB[8] cavity (**fig. 2.20, C**). The data at 490 nm does not fit for case **A** and **B** but in case **C** a 1:1 binding model resulted in the best fit with an association constant of 2.94×10^6 M^{-1}. This last result agrees with the previously obtained

in chapter **2.2.2** by direct UV-Vis titration. **Table 2.4** resumes the association constants of free/caged pairs with CB[8] obtained through displacement assays. The constants obtained for tryptophan, phenylalanine and tripeptide agree with the ones already published in literature.[44]

Table 2.4 – K_{ass} of free and caged tryptophan, phenylalanine and peptide with CB[8] by UV-Vis displacement assay.

Competitor	K_{ass} (M^{-2})
Trp / TrpNvoc	1.78×10^{8} / $n.c.o.$
Phe / PheNvoc	3.29×10^{8} / $n.c.o.$
FGG	3.79×10^{11}
	K_{ass} (M^{-1})
FGGNvoc	2.94×10^{6}

n.c.o. – no complexation observed

Summing up, the pairs free/caged tryptophan and phenylalanine are good candidates to displacement by photorelease since the caged compounds do not complex with CB[8] in the concentrations range used. The caged peptide complexes with CB[8] through 1:1 stoichiometry and the peptide through a 1:2 stoichiometry. In **fig. 2.21** is represented both displacements using free and caged peptide as competitors.

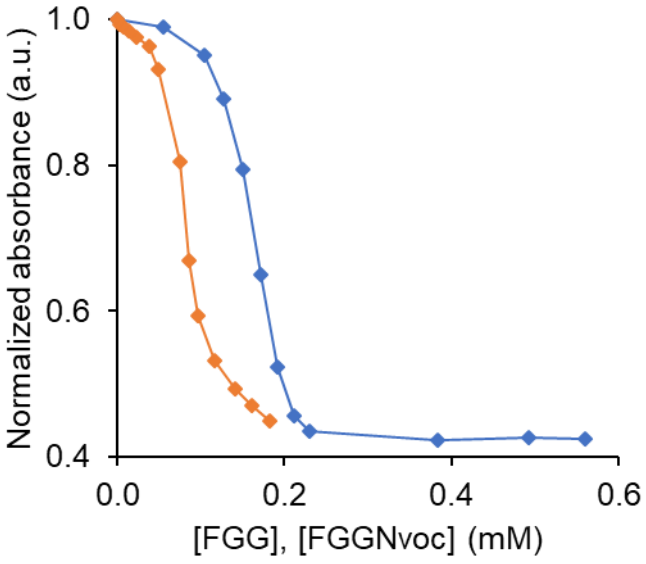

Figure 2.21 – Displacement of TCDPA from CB[8] with peptide (blue) and caged peptide (orange).

There is no range of concentrations where the caged peptide displaces less than the free one, consequently this is not the most promising pair to apply in the photocontrolled release system. Nevertheless, the fact that with light is possible to convert a 1:1 complex into a 1:2 complex turns this discovery much more appealing to other types of applications such as photocontrolled dimerization of biomolecules. With that in mind, it was necessary to understand how the caged peptide complexed with CB[8] since different types of complexes were acceptable as showed in **fig. 2.22**. UV-Vis displacement and ITC cannot distinguish between the formation of complexes of type **I** or **II** (**fig. 2.22**). To clarify which hypotheses were corrected several NMR studies were performed (chapter **2.5.3** and **2.5.4**).

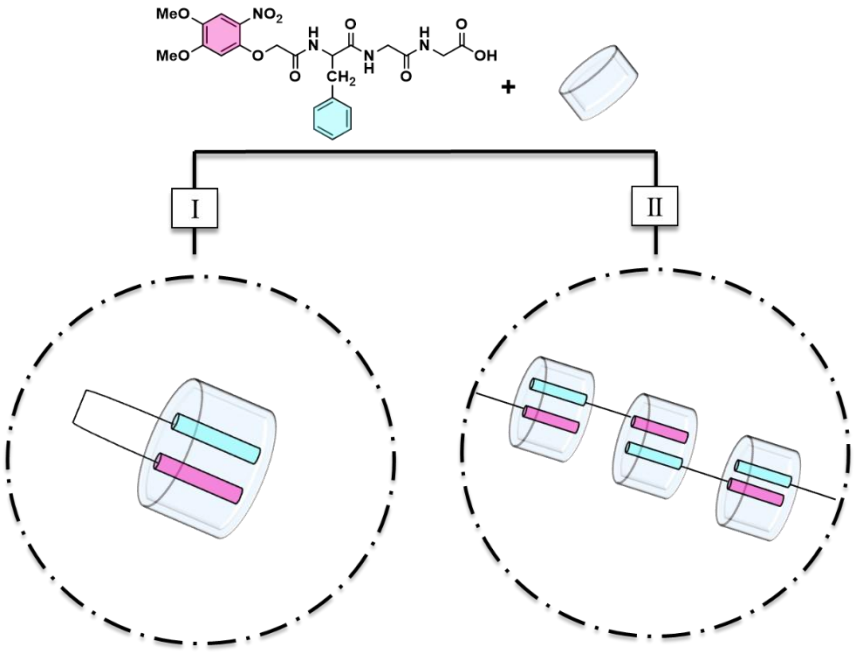

Figure 2.22 – Illustration of the different types of complexes that caged peptide can make with CB[8]. (I) Loop and (II) supramolecular polymer.

2.4 Photochemical assays

Next, studies of light interaction with caged biomolecules in presence and absence of host and probe were performed. With these studies it was possible to access how many free biomolecules are formed using UV light to break the covalent bond between Nvoc and biomolecules.

2.4.1 Irradiation of caged biomolecules

Caged biomolecules were irradiated with UV light (~366 nm) and the liberation of free biomolecules was followed by UV-Vis spectroscopy since the Nvoc maximum absorbance

decreases with the exposure time to light due to the degradation of this photolabile group. The quantum yields (Φ) were determined by the follow equation:

$$\Phi = \frac{moles\ of\ consumed\ reagent}{moles\ of\ absorbed\ fotons} = \frac{\frac{m \times V}{\varepsilon_{365nm}}}{I_0(1 - 10^{-Abs_{365}})}$$

Where *m* is the slope of the line made up of the points where linearity is verified, V the volume, ε_{365nm} is the molar coefficient at 365 nm and I_0 is the number of photons that arrive to the cell per unit of time that was determined by chemical actinometry.

In **fig. 2.23** are the results of caged tryptophan, tyrosine and histidine irradiation. As expected, there was a decrease in the maximum absorption of Nvoc at ~350 nm, which means that photolysis was occurring. The obtained quantum yields are gathered in **table 2.5**.

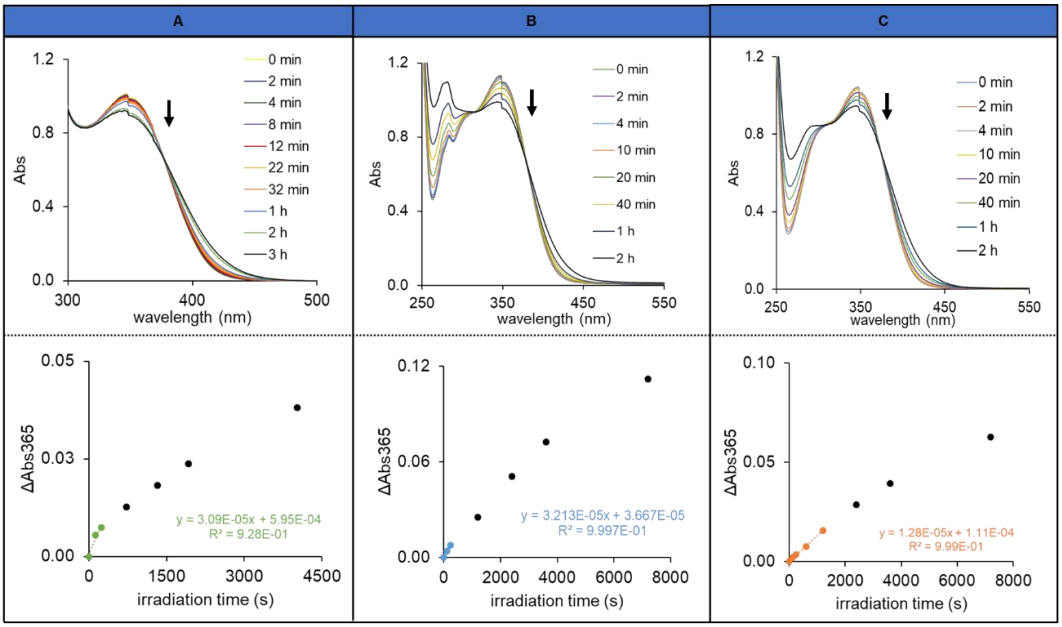

Figure 2.23 – UV-vis absorption spectral changes upon irradiation at 366 nm of (A) TrpNvoc 200 µM at pH 7, (B) TyrNvoc 232 µM at pH 7 and (C) HisNvoc 150 µM at pH 8, in aqueous solution. The lower graphs represent the ΔAbs as a function of the irradiation time; the coloured points and their resulted linear equation were used to calculate the quantum yields.

In **fig. 2.24** are the results of caged phenylalanine and peptide irradiation and it was verified the same pattern of results as expected.

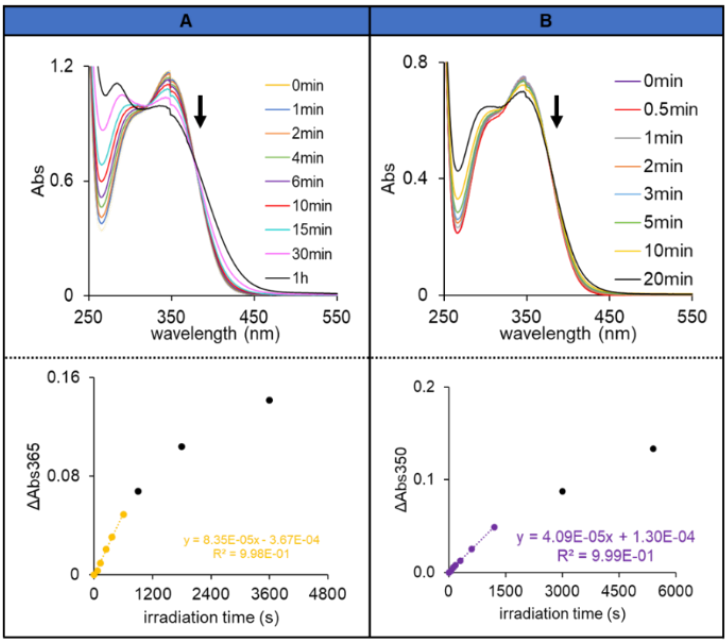

Figure 2.24 – UV-vis absorption spectral changes on irradiation at 366 nm of (A) PheNvoc 200 μM and (B) FGGNvoc 120 μM, in aqueous solution at pH 7. In lower graphs is represented the ΔAbs as a function of irradiation time; the coloured points and their resulted linear equation were used to calculate the quantum yields.

Table 2.5 shows the quantum yields for the photolysis of each caged biomolecule. The results agree with the ones already reported[10] for deprotection of this photolabile group with exception of caged histidine that is 10 times lower than the other obtained results. Since histidine imidazole group has a pKa of 6 and the studies were performed at basic pH the deprotonation of the side-chain can affect photodeprotection quantum yield. More irradiation studies at different pH (from acidic to basic) could help understand if deactivation of the excited state occurs or not.

Table 2.5 – Quantum yield from each caged biomolecule irradiated at 366 nm.

Caged Biomolecule	Φ
TrpNvoc	1.08×10^{-3}
TyrNvoc	1.32×10^{-3}
HisNvoc	3.42×10^{-4}
PheNvoc	2.73×10^{-3}
FGGNvoc	1.40×10^{-3}

The irradiation of caged biomolecules was also followed by ^{1}H-NMR to confirm that the liberation of the biomolecules was really occurring (**fig. 6.13-6.16, appendix**). It was confirmed that the photolysis was occurring and that the resulted products were the free biomolecule and

the Nvoc degradation product. Both these assays allowed to verify that the expected photolysis reaction was occurring and resulting in the desired final products.

2.4.2 Displacement by photorelease/deprotection

By following how many probe molecules were displaced from the host cavity it is possible to determine how many caged biomolecules suffered photolysis. For this purpose, a mixture of caged biomolecule, CB[7] and probe was irradiated at 366 nm and the absorption spectral changes followed by UV-Vis spectroscopy. In this case, the selected wavelength was the probe maximum absorption wavelength since we wanted to follow its displacement (that is proportional to the quantity of photoproduct). A decrease in absorption and a blueshift was expected, as seen previously (**chapter 2.3.1 and 2.3.2**). To clarify what is pretended in this chapter consult **fig. 1.7** from **chapter 1**.

Displacement of the dye from CB[7]

As mentioned before (**chapter 2.3.1**), the pairs caged/free more promising were TyrNvoc/Tyr and FGGNvoc/FGG since the caged molecules displaced in less extent than the free one. **Fig. 2.25** shows the spectral changes observed upon irradiation of these selected pairs and in **fig. 6.27** (appendix) is a real photo where is evident the colour changes upon irradiation due to the photorelease of the stronger competitor (free biomolecule) that displaced the probe. When the probe is complexed the solution is orange and when it is displaced the solution is yellow.

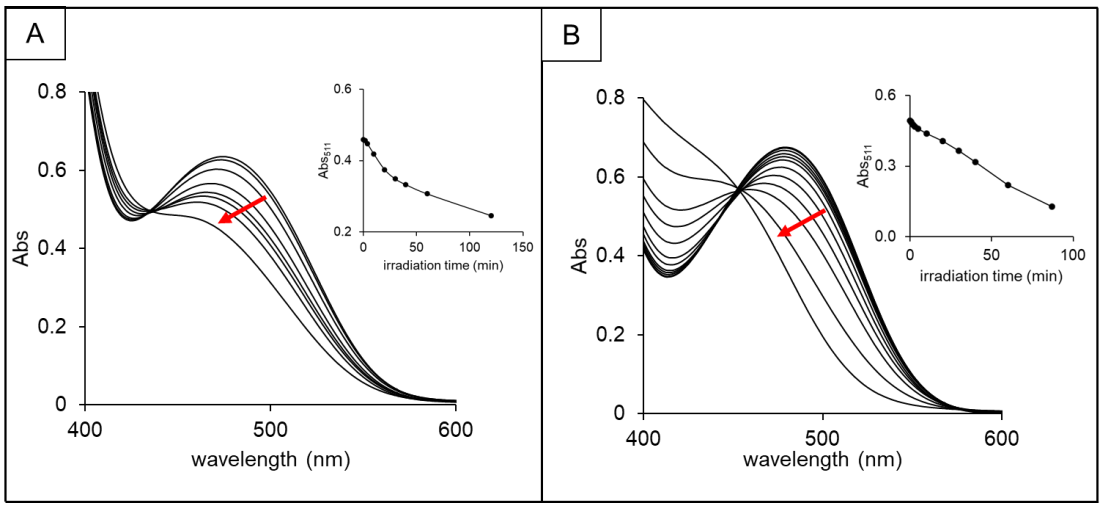

Figure 2.25 – UV-Vis spectral changes on irradiation at 366 nm of a mixture of (A) CB[7], $TCDEA_2MeO$ and TyrNvoc and (B) CB[7], TCDEA and FGGNvoc. The smaller graphs represent the experimental data at 511 nm in function of irradiation time. [CB[7]](A), (B)= 150 µM, [$TCDEA_2MeO$]= [TCDEA]= 20 µM, [TyrNvoc]= 650 µM, [FGGNvoc]= 200 µM.

In both cases it can be observed the expected decrease of the probe maximum absorption followed by a blueshift indicating that it was displaced from the cavity of CB[7]. Plotting the absorption at 511 nm as a function of the irradiation time reveals an exponential behaviour characteristic of displacement events. This is clearer for case **A** than **B**, **fig. 2.25**. Also, an isosbestic point is observable in both cases, which indicates a clean displacement of the probe from the cavity to the bulk without noticeable photodegradation (of the probe).

Comparing to the phenylalanine case reported in literature[27] this two pairs behave as weak competitors when caged and when photoreleased, the free biomolecules turn into a strong competitor just like reported. Yet, contrarily to caged phenylalanine case, the caged tyrosine and caged peptide induces some displacement of the probe prior to the irradiation. This complicates a little bit the calculations since we have two competitors (free and caged biomolecule) that can displace the probe, but it is not impossible to do. By mathematical methods, such as Newton's method and with a little help of coding, a program could be created to solve the problem of extensive deductions and calculus. With this problem solved, we could account how many probe molecules are already displaced in the beginning and discount this event through calculations.

Displacement of the dye from CB[8] cavity

In displacements assays from CB[8] cavity it was not observable displacement of TCDPA using caged tryptophan and phenylalanine (chapter **2.3.2**) making these two cases the most promising to apply as photoresponsive guests. In **fig. 2.26** are the irradiation results of a mixture of CB[8], TCDPA and both caged amino acids mentioned above.

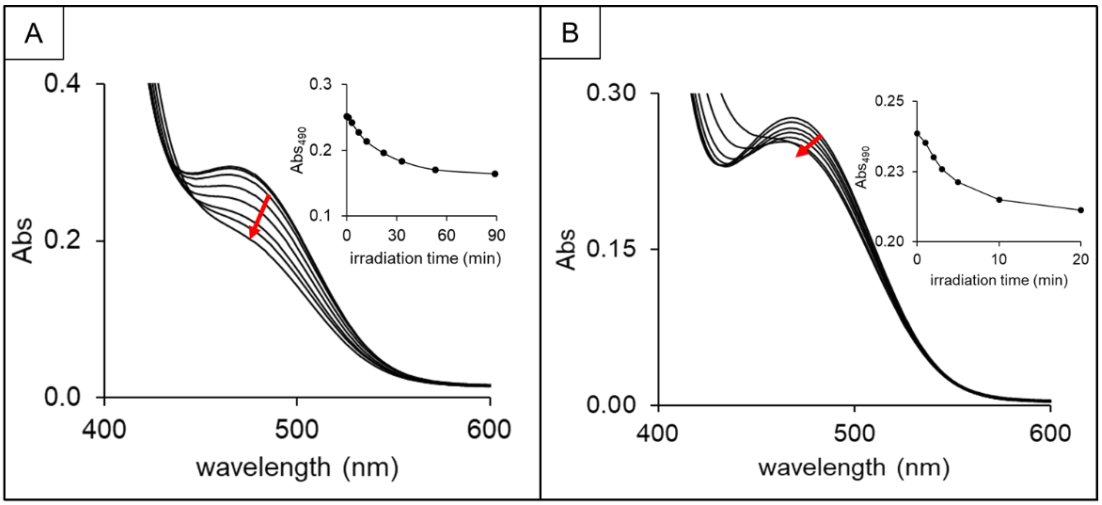

Figure 2.26 – UV-vis spectral changes on irradiation at 366 nm of a mixture of CB[8], TCDPA, (A) TrpNvoc and (B) PheNvoc. The insets represent the experimental data at 490 nm in function of irradiation time. [CB[8]] = 94 µM, [TCDPA] = 10 µM, [TrpNvoc] = 990 µM, [PheNvoc] = 750 µM.

As expected, a decrease in absorbance at 490 nm was observed and a slightly blueshift too. Plotting the experimental data at 490 nm in function of time displayed an exponential behaviour that was already observed in this type of assays. An isosbestic point is noticeable but this is lost with more time of exposure to light. This is due to the decrease of Nvoc maximum absorption (~350 nm) that is close to where the probe absorbs which leads to a lost in the isosbestic point. Since the caged compound do not interact with CB[8] cavity or with the probe the actinometry application reveals to be reliable in these cases in the way that is a simpler system to deal. Also, this system is even more promising for drug release applications since CB[8] can carry more than one drug molecule and the tryptophan and phenylalanine are two biocompatible competitors that can displace up to two drug molecules since they can form 1:2 host-guest complexes with CB[8].

2.5 NMR studies

As mentioned before, the aromatic side chain of amino acids remains in the host cavity and the N-terminal interacts with the carbonyl portals of the CB[n], through hydrophobic and ion-dipole interactions, respectively (chapter **1.3.5**). When the N-terminal is protected with the photolabile group the ion-dipole interactions cannot occur and the caged compound should lose part of his affinity for the host. As seen before, it seems that a slightly interaction with CB[n] host with the tested caged biomolecules can occur (chapter **2.3.1**). To exploit the formation of complexes and to clarify which part of the caged biomolecules interacts with the host cavity several ^{1}H-NMR studies were performed. Also, the possibility of interaction between TCDEA$_2$MeO and caged biomolecules was tested.

2.5.1 Free and caged biomolecules with CB[7]

The interaction of tyrosine, histidine and tryptophan with CB[7] was studied by adding host in excess to guarantee full complexation. The results are shown in **fig. 2.27-2.29** and it was observable the expected upfield deviation of aromatic protons, that is characteristic of the accommodation of the guest inside the host cavity (chapter **1.4.2**).

In **fig. 2.27** a downfield shift seems to occur in the aliphatic protons of tyrosine, which can mean that they are localized at the carbonyl portals of CB[7], but this is not conclusive due to the lack of peak resolution.

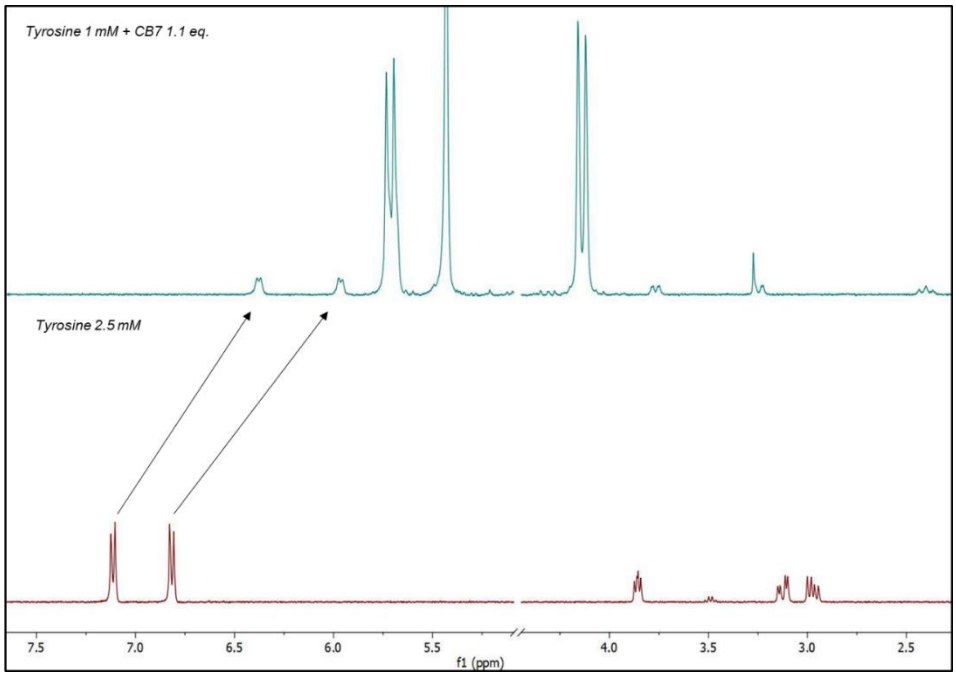

Figure 2.27 – ^{1}H-NMR spectra of tyrosine 2.5 mM (down) and tyrosine 1 mM with CB[7] 1.1 eq. (up) in D_2O, pD 7.

In **fig. 2.28** and **fig. 2.29**, an upfield shift seems to occur in the aliphatic protons of histidine and tryptophan, respectively, which means that they are also localized in CB[7] cavity. Tryptophan results are not conclusive due to the lack of peak resolution.

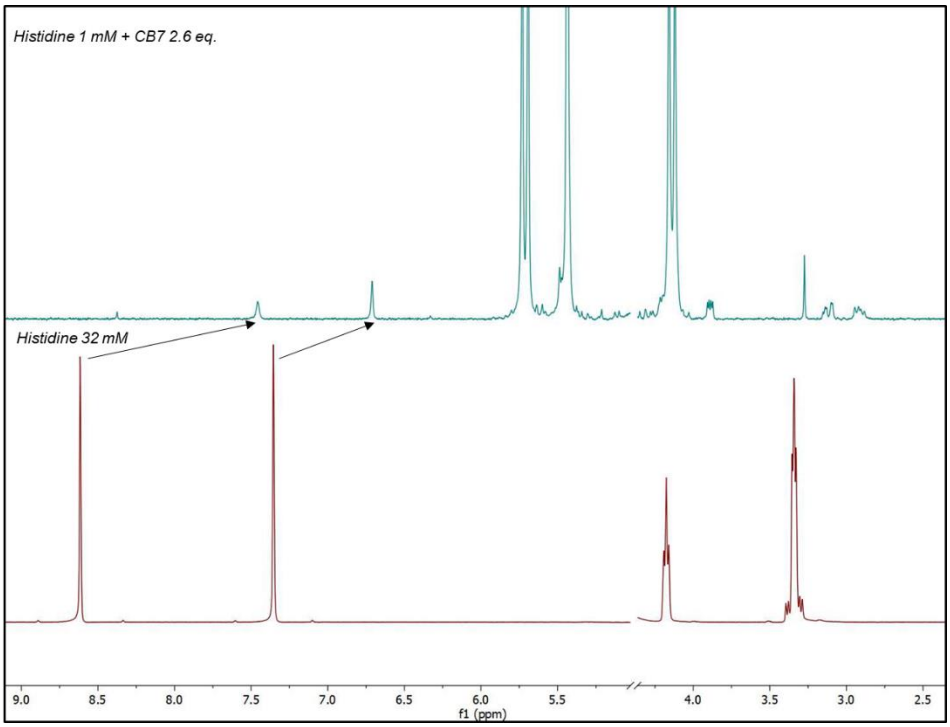

Figure 2.28 – ^{1}H-NMR spectra of histidine 32 mM (down) and histidine 1 mM with CB[7] 2.6 eq. (up) in D_2O, pD 7.

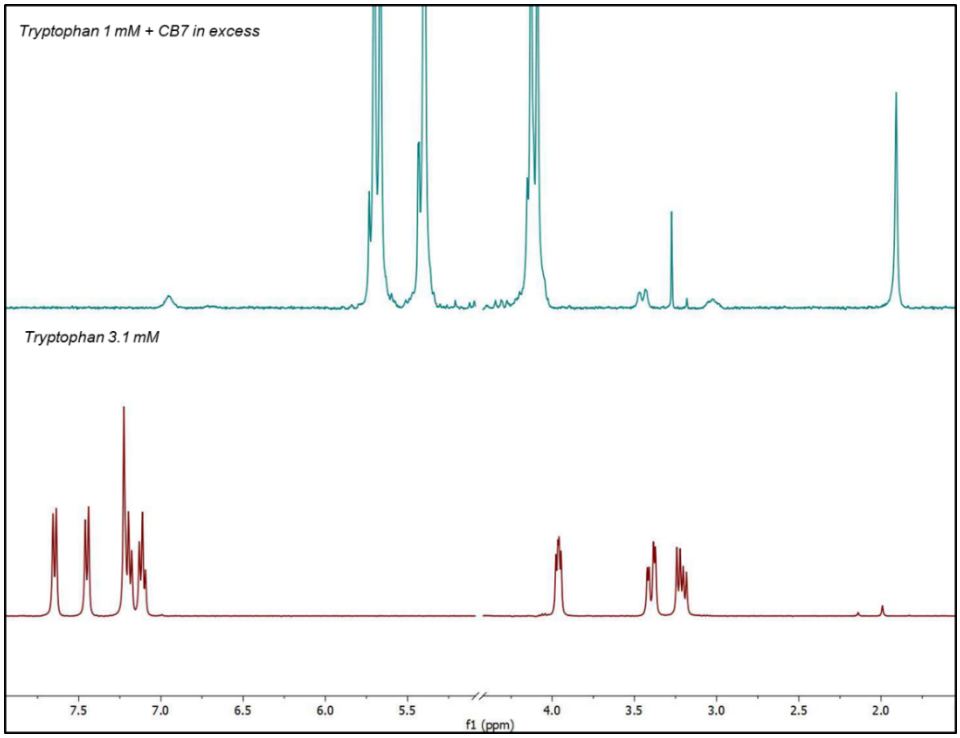

Figure 2.29 – ^{1}H-NMR spectra of tryptophan 3.1 mM (down) and tryptophan 1 mM with excess of CB[7] (up) in D_2O, pD 7.

The same procedure was made for caged analogues and the results are in **fig. 6.17-6.19 (appendix).** No spectral differences were recorded for caged tyrosine or tryptophan (**fig. 6.17, 6.19**) upon addition of CB[7] in excess, which means that complexation does not occur for both compounds which seems to be controversial to the UV-Vis titrations and displacement results (**fig. 2.6,** chapter **2.2.1; fig. 2.15,** chapter **2.3.1**). Yet, the differences observed in UV-Vis titration spectra can be explained by small concentration differences (the solutions were prepared separately) and the fact that CB[7] is highly concentrated, consequently its signal could influence the rest of the absorption spectrum. The results observed in displacement assays can be due to the displacement by interaction of the probe with the caged compound, as hypothesized already.

For the caged histidine, small spectral differences were observed in the aromatic region (**fig. 6.18**) meaning that complexation occurred. This agrees with the result obtained by UV-Vis titration with CB[7] (**fig. 2.7,** chapte**r 2.2.1.**). **Table 2.6** list the chemical shifts of caged histidine before and after CB[7] addition. The signals that suffer an upfield shift belong to the aromatic protons of Nvoc and the ones that suffer a downfield shift correspond to the imidazole protons of histidine side-chain, therefore, it seems that the Nvoc aromatic ring is inside CB[7] cavity and the histidine side-chain at the carbonyl portals. Nevertheless, the formation of the complex is not as favourable when compared to free histidine (**fig. 2.28**).

Table 2.6 – ^{1}H chemical shifts (ppm) of caged histidine without and with CB[7] in excess (consult **fig. 6.16**, appendix).

HisNvoc δ (ppm)	HisNvoc + CB[7] δ (ppm)	Δδ (ppm)
8.51 (·)	8.45	-0.06
7.72 (·)	7.74	+0.02
7.21 (·)	7.18	-0.03
7.02 (·)	7.04	+0.02

To study the complexation of free and caged tripeptide the same method mentioned before was used and the results are in **fig. 2.30** and **fig**. **2.31**.

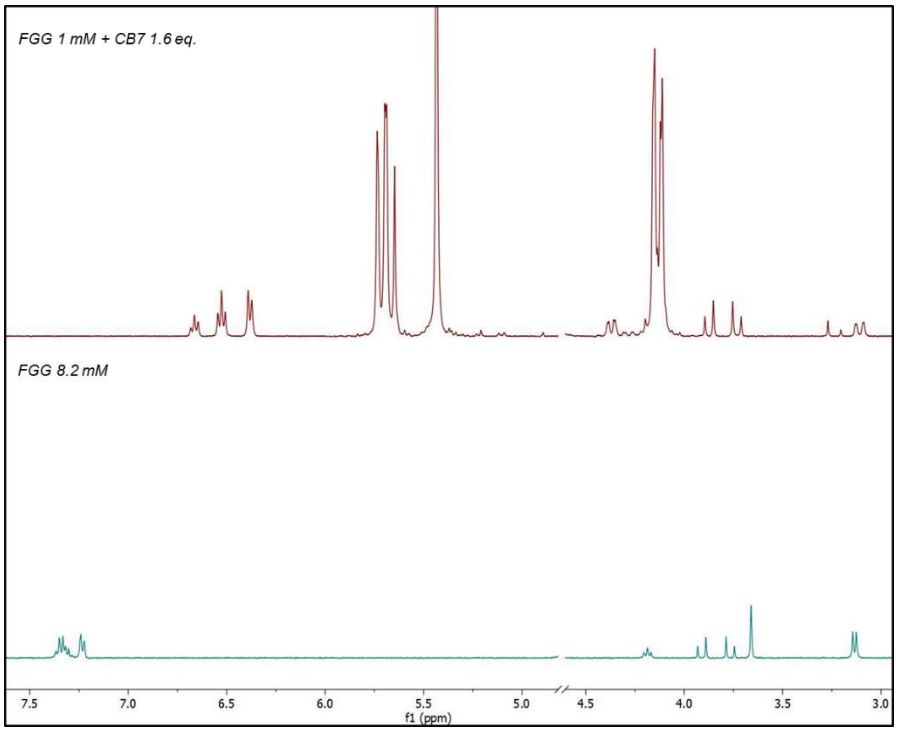

Figure 2.30 – ^{1}H-NMR spectra of FGG 8.2 mM (bottom) and FGG 1 mM with excess of CB[7] (top) in D_2O, pD 7.

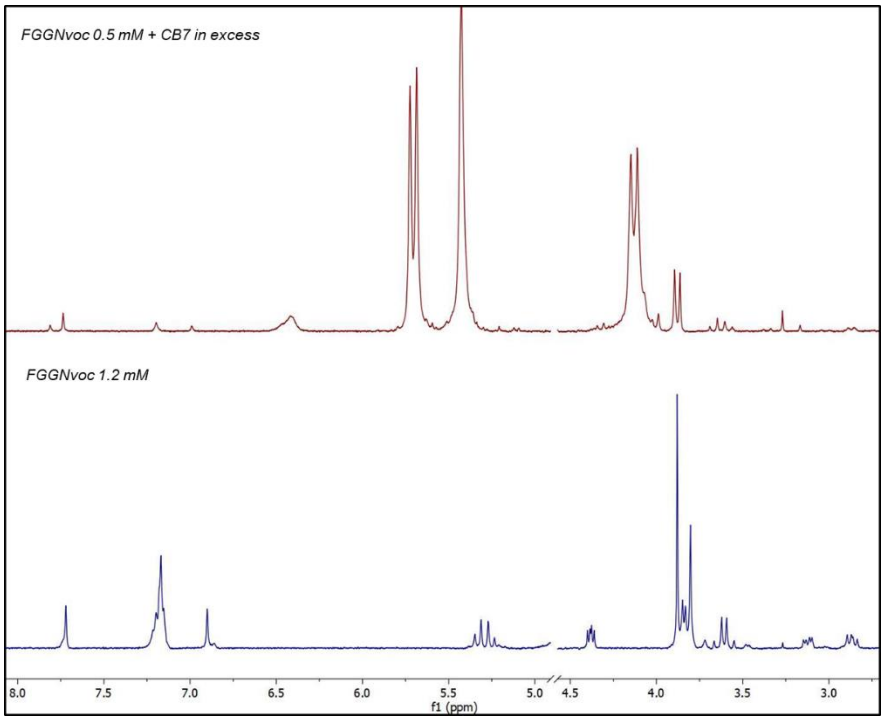

Figure 2.31 – ^{1}H-NMR spectra of FGGNvoc 1.2 mM (bottom) and FGGNvoc 0.5 mM with excess of CB[7] (top) in D_2O, pD 7.

The upfield deviation of the chemical shift of the aromatic protons of phenylalanine (**fig. 2.30**) confirms that the side-chain is within the CB[7] cavity as reported.[27] The caged analogue also exhibits an upfield shift in phenylalanine aromatic protons, therefore, complexation seems to occur which confirms the displacement results previously obtained (**fig. 2.17**, chapter **2.3.1**). The difference between caged FGG and phenylalanine (which does not forms complexes with CB[7]) can be attributed to the fact that in the caged peptide the C-terminal is further away from the N-terminal (two glycine residues away), therefore the repulsive forces between this functional group and the carbonyl portals of CB[7] have lower impact than in caged phenylalanine, resulting in complex formation.

2.5.2 Interaction between TCDEA$_2$MeO and caged amino acids

NMR studies were also performed to verify if the displacement observed in chapter **2.3.1** was owing to the interaction between the probe and caged amino acid. The strategy was to prepare solutions that contained the same equivalents of both molecules and see if any spectral differences were observed. The results are in **fig. 6.20-6.22, appendix**. The results were not conclusive since the alterations did not follow a logical pattern.

2.5.3 Free and caged biomolecules with CB[8]

The inclusion of free and caged tryptophan and phenylalanine within CB[8] was also studied by ^{1}H-NMR. The titration of phenylalanine with CB[8] is in **fig. 6.23** (**appendix**). With higher concentrations of CB[8] there is an upfield shift of the aromatic side-chain of the amino acid, confirming the complex formation as expected. For tryptophan was not possible to make conclusions due to the complete disappearance of its signal upon addition of CB[8].

Fig. 2.32 shows the spectra of caged tryptophan before and after CB[8] addition. In this case it was not possible to obtain the caged phenylalanine spectrum with CB[8] due to solubility problems.

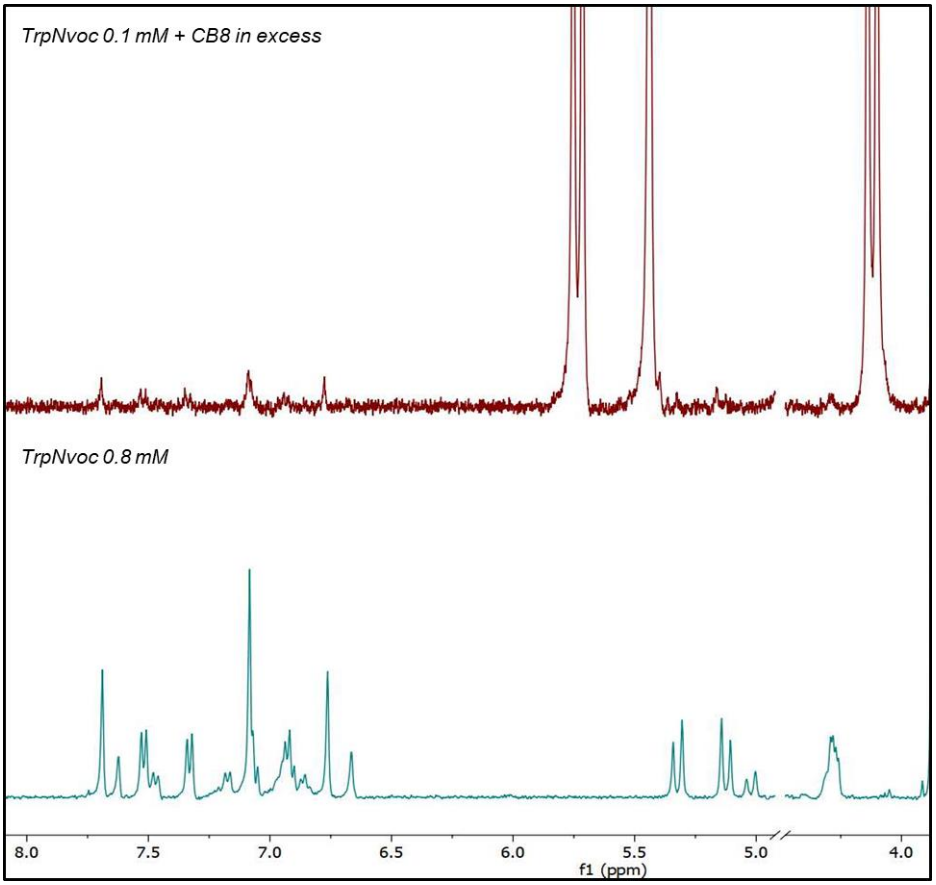

Figure 2.32 – ^{1}H-NMR spectra of TrpNvoc 0.8 mM (bottom) and TrpNvoc 0.1 mM with excess of CB[8] (top) in D_2O, pD 7.

Apparently, there is no change in the chemical shifts of caged tryptophan upon addition of CB[8] what agrees with the previous results of no complex formation in chapter **2.3.2**. By analogy, one can infer the same for caged phenylalanine. ITC assays were also performed to confirm these results.

Next, the complexation of free and caged tripeptide was followed by performing a titration. The results are in **fig. 2.33** and **2.34**.

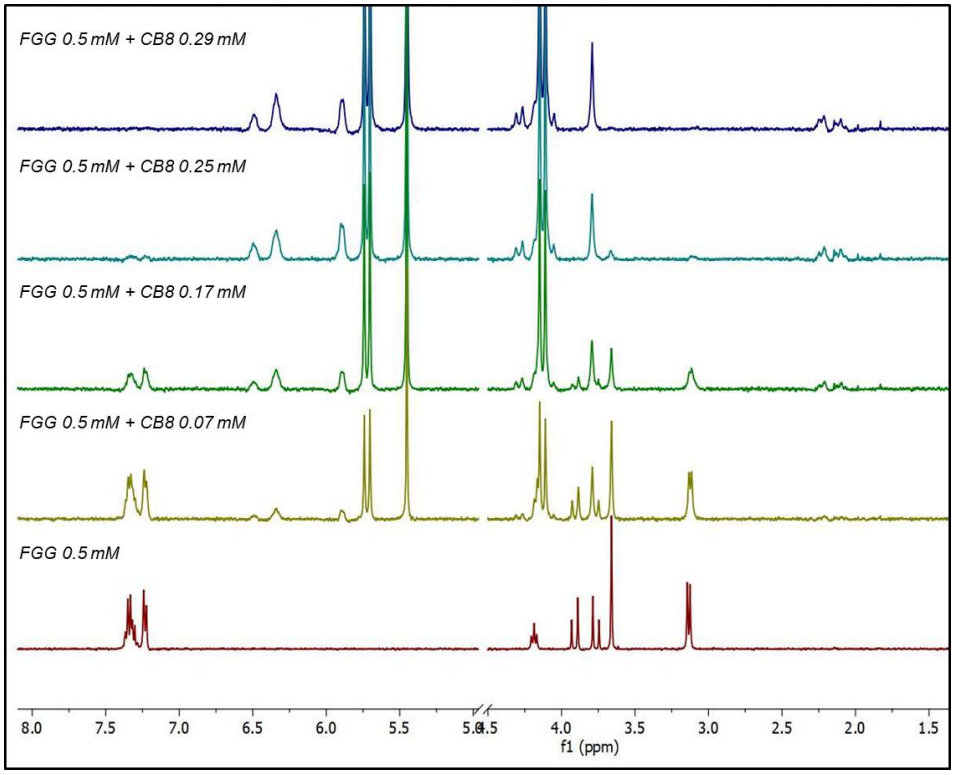

Figure 2.33 – ^{1}H-NMR titration of FGG 0.5 mM with CB[8] (0-0.29 mM) in D_2O, pD 7

As in CB[7] complexation (chapter **2.5.1**), the aromatic protons of phenylalanine suffer an upfield shift and along titration is observable signals from both free and complex amino acid due to the slow exchange on the NMR time scale. Since a titration was performed, information about the stoichiometry can be obtained. All the peptide molecules are complexed around 0.5 equivalents of titrated host, hence, the complex formed must have a 1:2 host-guest stoichiometry. These results corroborate the ones obtained by displacement assays in chapter **2.3.2**.

In **fig. 2.34** is the titration of caged peptide with CB[8]. The characteristic upfield shift of aromatic protons is also observable which means that complex is formed, as expected from previous results (chapter **2.3.2**, **table 2.4**). Phenylalanine protons suffer an upfield shift, as expected. Furthermore, protons from the Nvoc aromatic ring also suffer an upfield shift which indicates that they are within CB[8] cavity. Yet, no conclusions about the type of structure of the complex can be made. Contrarily, to the free peptide not all the caged analogue is complexed when 0.5 equivalents of host are titrated. Therefore, this must be a 1:1 host-guest complex as hypothesized before.

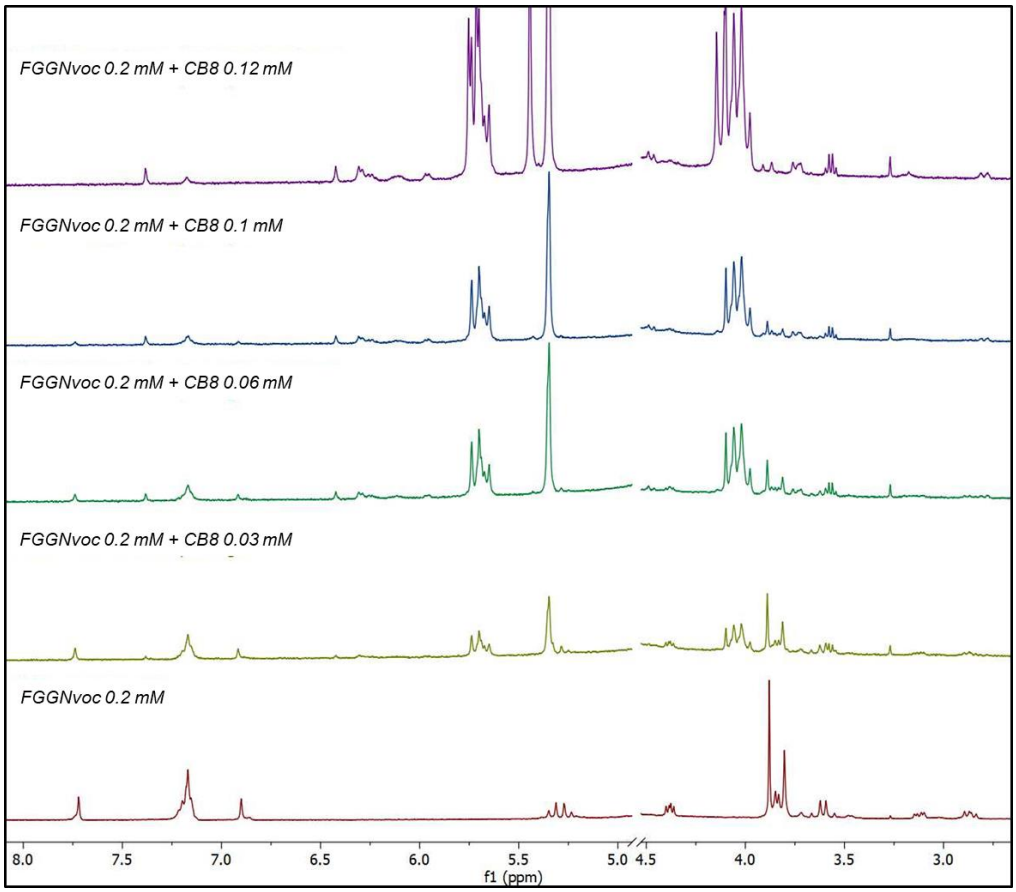

Figure 2.34 – ^{1}H-NMR titration of FGGNvoc 0.2 mM with CB[8] (0-0.12 mM) in D_2O, pD 7.

Previously, was hypothesized that two types of complex structures could take place (**fig. 2.22**). To clarify which type of complex is formed, diffusion-ordered spectroscopy (DOSY) experiments were performed.

2.5.4 DOSY

The aim of DOSY experiments is to determine the diffusion coefficient (D). Larger molecules/complexes have smaller values of D; hence, complexes of type II (**fig. 2.22**) should have a significant difference on D value compared to type I, being the first smaller. To achieve the value of D, equation **2.1** was used. The I correspond to the experimental intensity, I_0 the reference intensity, D the diffusion coefficient, Υ the gyromagnetic ratio of the nucleus, g the gradient strength, δ the duration of the gradient and Δ the diffusion time.

$$I = I_0 e^{-D\Upsilon^2 g^2 \delta^2 (\Delta - \delta/3)} \quad \text{or} \quad I = I_0 e^{-DQ} \qquad \textbf{(2.1)}$$

The values of D were calculated for CB[8] and for the complexes with free and caged tripeptide (**table 2.7**). The D value for both complexes is lower than CB[8] D value which was

expected once the complex is larger than the cucurbituril itself. Comparing the values between the complex with the tripeptide and its caged analogue it is observable no significant difference. From these results we can conclude that complex type II (supramolecular complex) do not occur, supporting the hypothesis of complex type I (loop).

Table 2.7 - Values of D for CB[8] and its complexes with free and caged tripeptide.

molecule / complex	D ($cm^2\ s^{-1}$)
CB[8]	3.15×10^{-6}
CB[8]·FGG	2.89×10^{-6}
CB[8]·FGGNvoc	2.91×10^{-6}

In the figure below (**fig. 2.35**) are the fittings of experimental data of the molecules that gave the D values of the complexes with CB[8].

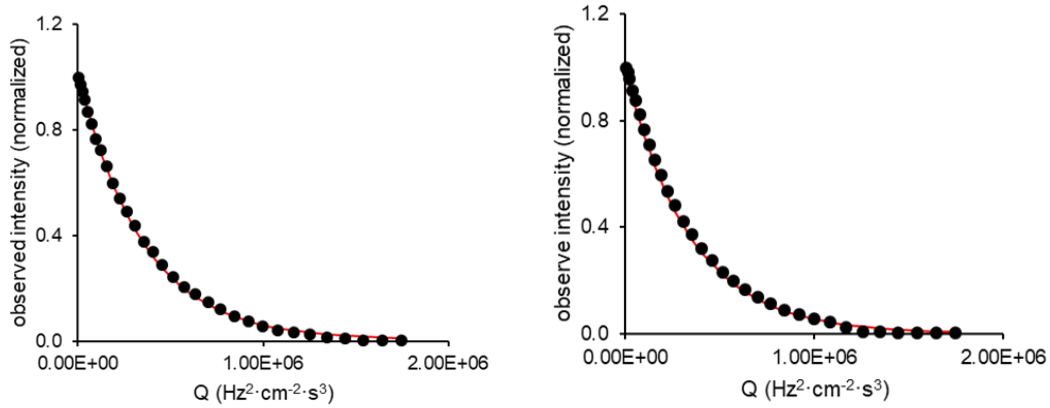

Figure 2.35 – DOSY data of CB[8] complex with FGG (left) and FGGNvoc (right). Experimental data is the black dots and the fitting the red line. [FGG] = [FFGNvoc] = 1 mM, CB[8] in excess.

2.6 ITC

Lastly, isothermal titration calorimetry (ITC) was performed to confirm and clarify the association constants, as well the stoichiometries of the complexes. Further, thermodynamic parameters were also determined.

2.6.1 CB[7] complexes

The ITC experiments of free biomolecules were carried out by injecting the biomolecule into the sample cell containing CB[7]. Contrarily, caged biomolecules were in the sample cell and were titrated with CB[7], due to their poor water solubility.

ITC results for tryptophan and tyrosine are in **fig. 2.36** and the results for the caged analogues in **fig. 2.37**. The titration data of CB[7] with amino acids (**fig.2.36**) fitted well to a 1:1 binding model and the resulting association constant and thermodynamic parameters are in **table 2.8**. It was not possible to test free/caged histidine due to equipment unavailability.

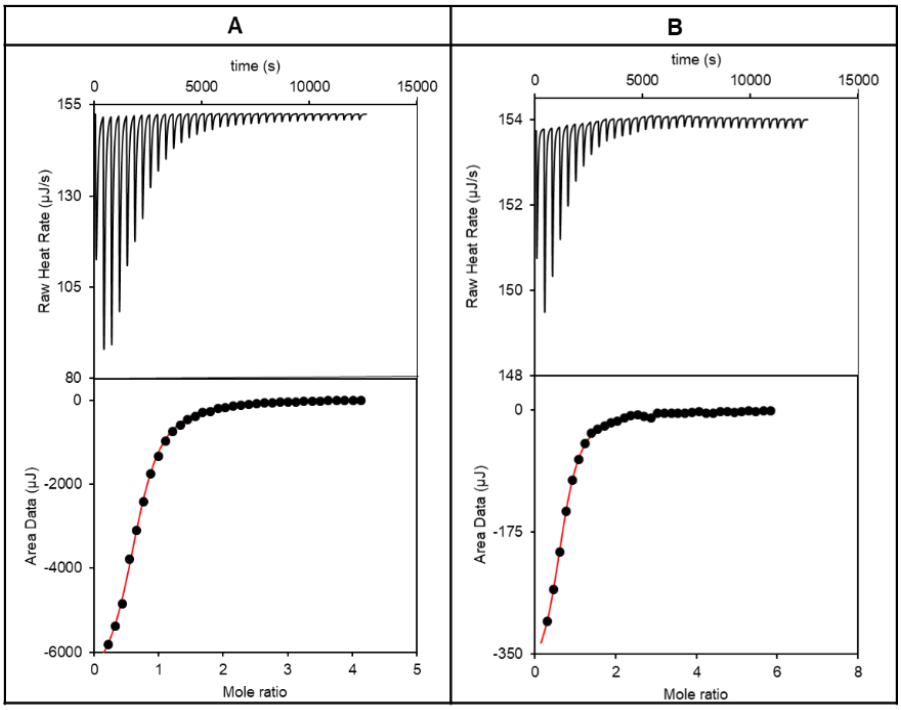

Figure 2.36 – ITC data obtained for the titration of (A) 3 mM CB[7] with 63 mM Trp and (B) 0.09 mM CB[7] with 2.6 mM Tyr.

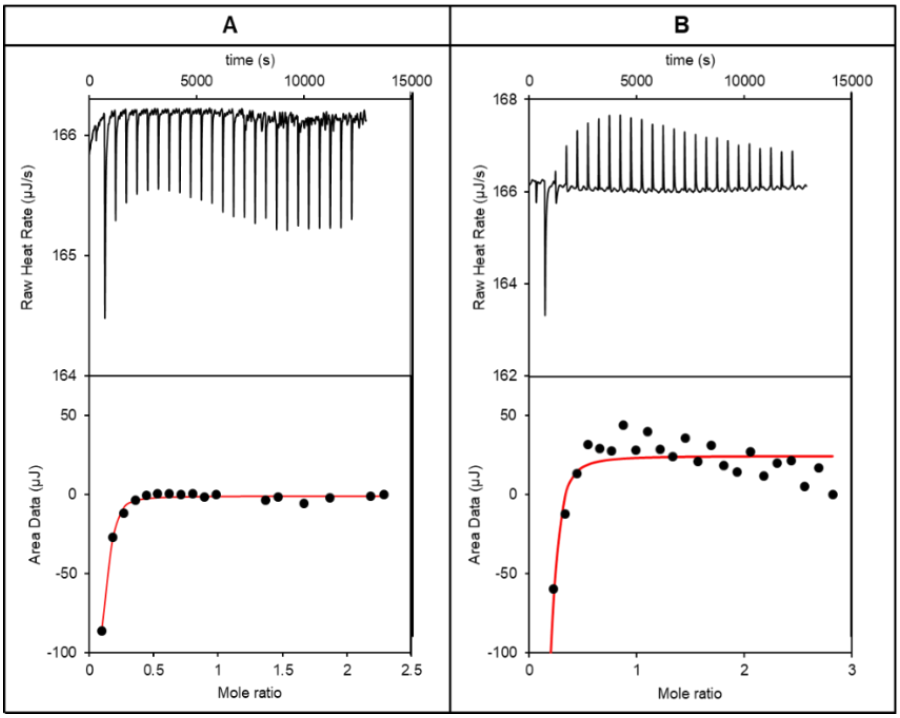

Figure 2.37 – ITC data obtained for the titration of (A) 370 µM TrpNvoc and (B) 300 µM TyrNvoc with 2.95 mM CB[7].

2. Results and Discussion

The titration data for caged tyrosine does not fit to 1:1 binding model, but caged tryptophan does (**fig. 2.37**). However, the *n* (number of molecules that complex) parameter given by the fit is 0.1 which is not an acceptable value. When this parameter is restricted to a minimum of 0.5, the data don't fit well. Therefore, one must conclude that no complex is formed for these two caged amino acids. Furthermore, dilution heat, aggregation or non-specific interaction can also occur which would result in non-fit of data.

The obtained association constants are in agreement with the previous obtained results.The binding of amino acids is an exothermic process and it is enthalpically favourable and entropically unfavourable (**table 2.8**).

Table 2.8 – Association constants and thermodynamic parameters of amino acids·CB[7] complexes determined by ITC.

guest	K_{ass} (M^{-1})	ΔG (kJ/mol)	ΔH (kJ/mol)	-TΔS (kJ/mol)
Trp	4.00×10^3	-20.6	-23.0	2.40
Tyr	1.03×10^5	-28.61	-31.0	2.43

The complex formation with free and caged peptide was also acessed by ITC and the experimental results are in **fig. 2.38**. In both cases, the experimental data fitted well to a 1:1 binding model and the resulted parameters are gathered in **table 2.9**.

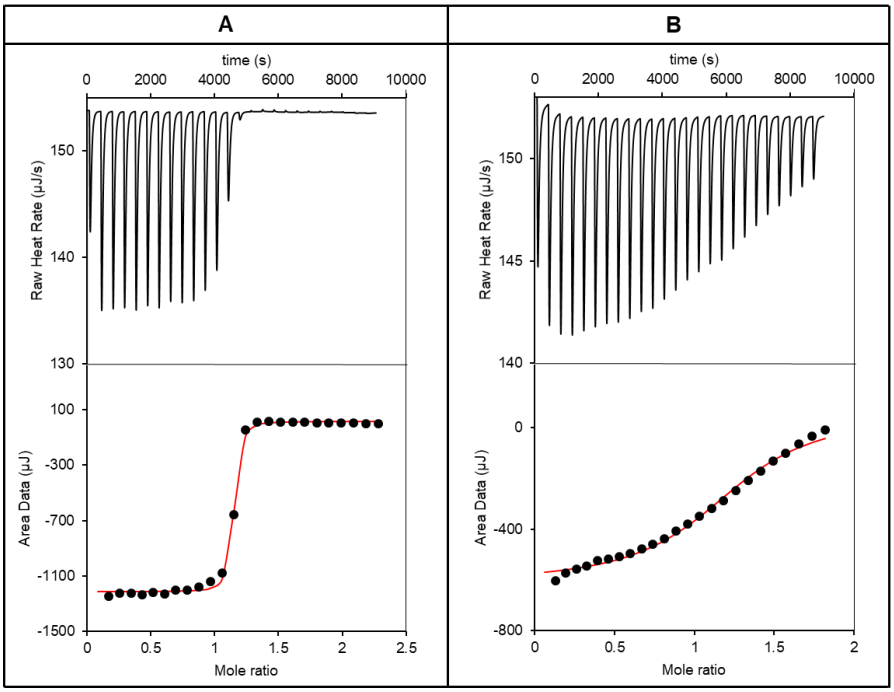

Figure 2.38 – ITC data obtained for the titration of (A) 0.3 mM CB[7] with 5 mM FGG and (B) 0.5 mM FGGNvoc with 3 mM CB[7].

The binding constant is higher for the tripeptide than for the caged analogue (**table 2.9**), which was expected taking in count previous results from UV-Vis displacement and NMR assays, and the values of the constants are in agreement with the ones obtained before. The complex formation is an exothermic process and enthalpically favourable in both cases. Contrarily, complex formation with the tripeptide is entropically unfavourable whereas with the caged peptide favourable.

Table 2.9 - Association constants and thermodynamic parameters of free/caged peptide·CB[7] complexes determined by ITC.

guest	K_{ass} (M^{-1})	ΔG (kJ/mol)	ΔH (kJ/mol)	-TΔS (kJ/mol)
FGG	5.44×10^6	-38.4	-50.6	12.1
FGGNvoc	2.99×10^4	-25.6	-21.8	-3.76

2.6.2 CB[8] complexes

ITC experiments of both free and caged biomolecules were carried out by injecting the biomolecule into the sample cell containing CB[8], due to the cucurbituril poor water solubility. In **fig. 2.39** is the titration results of tryptophan and phenylalanine. Both, fitted well to a 1:2 binding model and the resulted constant is in **table 2.10**, along with the thermodynamic parameters.

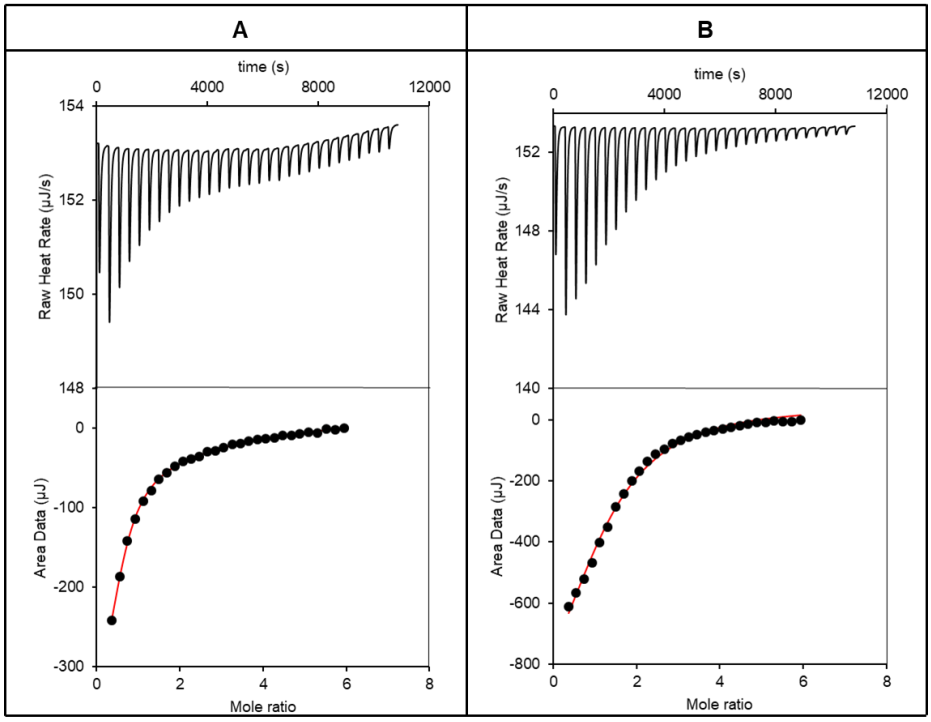

Figure 2.39 – ITC data obtained for the titration of 0.14mM CB[8] with (A) 5mM Trp and (B) 4.5 mM Phe.

2. Results and Discussion

The resulted association constants are in agreement with the previous results of displacement assays, although for tryptophan is slightly lower (previous: 1.78×10^8 M^{-2}). In both cases, the complex formation is enthalpically favourable and entropically unfavourable.

Table 2.10 - Association constants and thermodynamic parameters of amino acids·CB[8] complexes determined by ITC.

guest	K_1*K_2 (M^{-2})	ΔH1 (kJ/mol)	ΔH2 (kJ/mol)	ΔS1 (J/mol*K)	ΔS2 (J/mol*K)
Trp	4.10×10^7	-18.0	-33.7	27.9	-55.7
Phe	1.20×10^8	-48.7	-21.0	-81.0	1.74

Fig. 2.40 shows the titration results of caged tryptophan and phenylalanine. Apparently, no complex formation is observed, as expected. This finding corroborates the previous displacement results (chapter **2.3.2**).

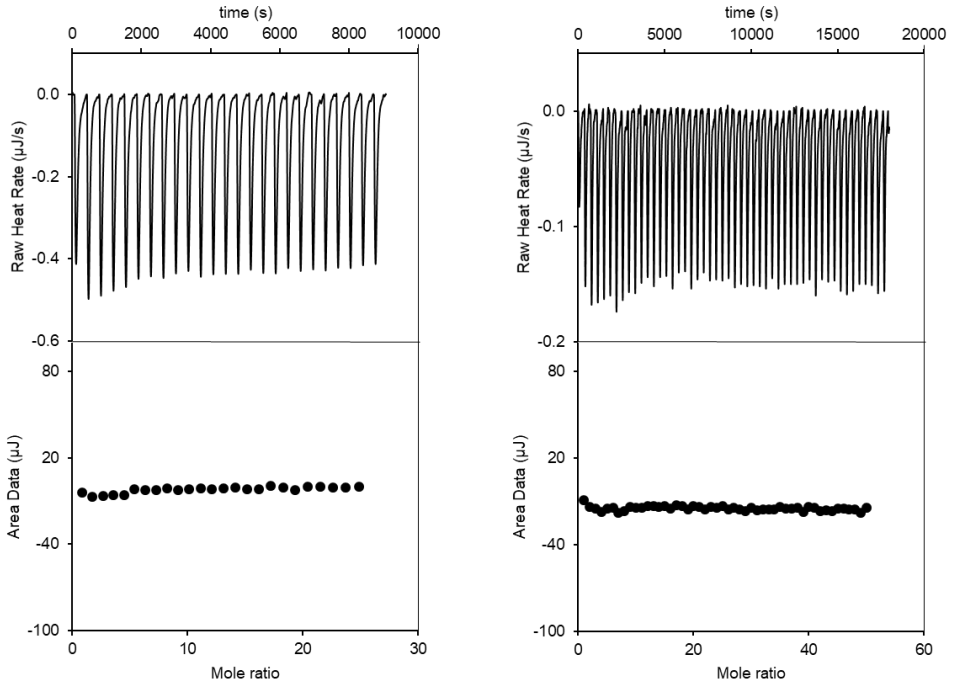

Figure 2.40 – ITC data obtained for the titration of (A) 0.14 mM CB[8] with 0.82 mM PheNvoc. (B) 0.01 mM CB[8] with 0.75 mM TrpNvoc.

Next, it was performed the titration of free and caged tripeptide and the experimental results are in **fig. 2.41**. The tripeptide complex data fitted well to a 1:2 biding model and the caged

analogue to a 1:1 binding model. These results corroborate the ones obtained by UV-Vis displacement (chapter **2.3.2**).

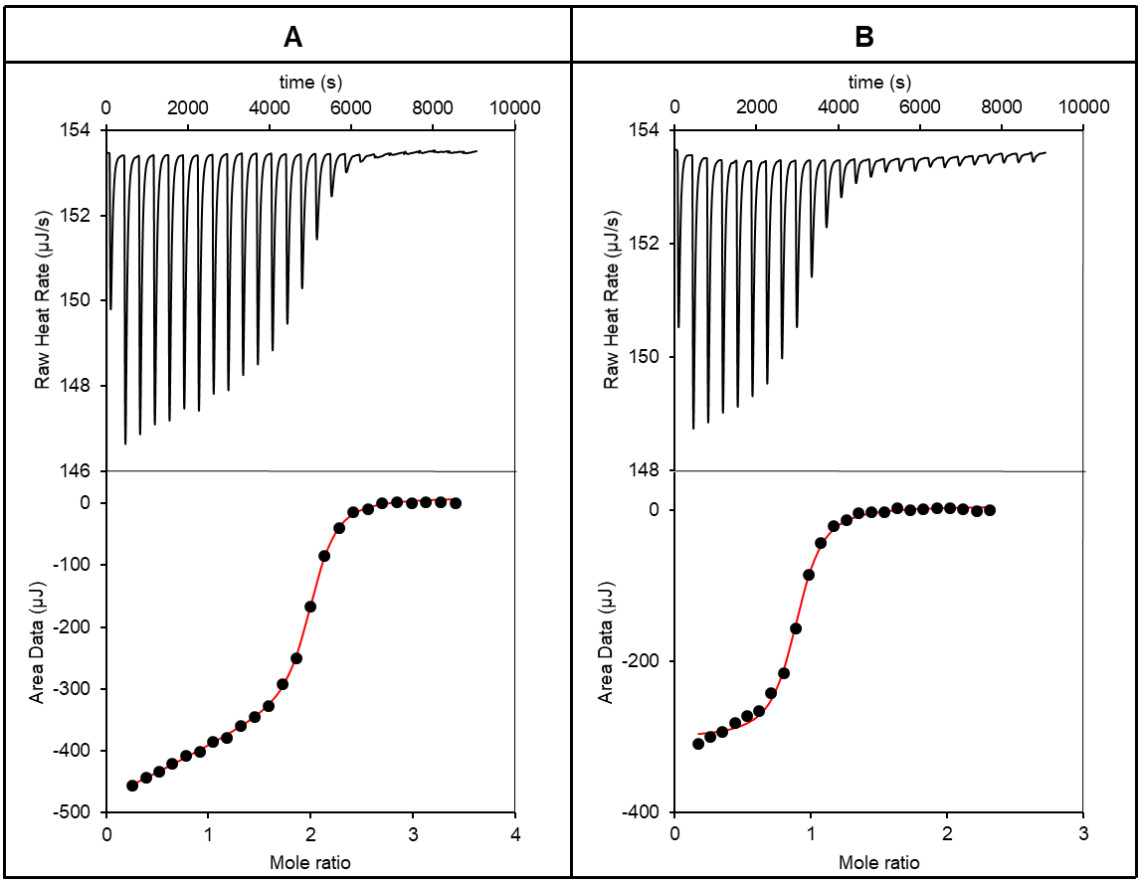

Figure 2.41 – ITC data obtained for the titration of (A) 0.14 mM CB[8] with 3.5 mM FGG and (B) 0.09 mM CB[8] with 1.52 mM of FGGNvoc.

The association constants and thermodynamic parameters are gathered in **table 2.11**. The association constants are in agreement with the ones obtained before by UV-displacement (chapter **2.3.2**). The tripeptide complex formation with CB[8] is enthalpically and entropically favourable. In caged analogue case, is also enthalpically favourable but entropically unfavourable.

Table 2.11 - Association constants and thermodynamic parameters of free/caged peptide·CB[8] complexes determined by ITC.

guest	K_{ass}	ΔH1 (kJ/mol)	ΔH2 (kJ/mol)	ΔS1 (J/mol*K)	ΔS2 (J/mol*K)
FGG	8.74×10^{11} M^{-2}	-41.0	-9.24	-20.8	80.9
		ΔG (kJ/mol)	***ΔH (kJ/mol)***	***-TΔS (kJ/mol)***	
FGGNvoc	9.75×10^{5} M^{-1}	-34.2	-41.5	7.28	

2. Results and Discussion

In **table 2.12** is gathered the association constants for each complex by different techniques for easier comparison.

Table 2.12 – Association constants of CB[n] (n= 7, 8) with free and caged molecules determined by different techniques.

COMPLEX	TITRATION WITH HOST	DISPLACEMENT	ITC	NMR
TRP·CB[7]	$2.19 \times 10^4\ M^{-1}$	$5.46 \times 10^3\ M^{-1}$	$4.00 \times 10^3\ M^{-1}$	*c.o.*
TRPNVOC·CB[7]	*n.d.*	$< 3.00 \times 10^3\ M^{-1}$	*n.c.o.*	*n.c.o.*
TYR·CB[7]	$1.88 \times 10^4\ M^{-1}$	$1.54 \times 10^5\ M^{-1}$	$1.03 \times 10^5\ M^{-1}$	*c.o.*
TYRNVOC·CB[7]	*n.d.*	$< 4.00 \times 10^3\ M^{-1}$	*n.c.o.*	*n.c.o.*
HIS·CB[7]	*n.d.*	$1.01 \times 10^3\ M^{-1}$	*n.d.*	*c.o.*
HISNVOC·CB[7]	$< 6.00 \times 10^2\ M^{-1}$	$< 1.00 \times 10^3\ M^{-1}$	*n.d.*	*c.o.*
FGG·CB[7]	*n.d.*	$3.51 \times 10^7\ M^{-1}$	$5.44 \times 10^6\ M^{-1}$	*c.o.*
FGGNVOC·CB[7]	*n.d.*	$< 6.00 \times 10^4\ M^{-1}$	$2.99 \times 10^4\ M^{-1}$	*c.o.*
TRP·CB[8]	*n.d.*	$1.78 \times 10^8\ M^{-2}$	$4.10 \times 10^7\ M^{-2}$	*n.d.*
TRPNVOC·CB[8]	*n.d.*	*n.c.o.*	*n.c.o*	*n.c.o.*
PHE·CB[8]	*n.d.*	$3.29 \times 10^8\ M^{-2}$	$1.20 \times 10^8\ M^{-2}$	*c.o.*
PHENVOC·CB[8]	*n.d.*	*n.c.o.*	*n.c.o.*	*n.d.*
FGG·CB[8]	*n.d.*	$3.79 \times 10^{11}\ M^{-2}$	$8.74 \times 10^{11}\ M^{-2}$	*c.o.*
FGGNVOC·CB[8]	$2.69 \times 10^6\ M^{-1}$	$2.94 \times 10^6\ M^{-1}$	$9.75 \times 10^5\ M^{-1}$	*c.o.*

n.d. – not determined
c.o. – complexation observed
n.c.o – no complexation observed

3 Conclusions and Future Perspectives

This work consisted in synthesizing a series of caged amino acids and a caged tripeptide to apply as photoresponsive guests in a supramolecular system based on CB[n] (n= 7, 8), where the release of cargo could be controlled with light by turning a weak competitor (caged biomolecule) into a stronger one (free biomolecule). *Trans*-chalcones were used as cargo/probes to be displaced by the photoresponsive guests in order to test the functionality of the system.

The caged biomolecules were characterized by ^{1}H-NMR and 2D NMR (^{1}H-^{1}HCOSY). Efforts to increase the reaction yields should be made for histidine and tripeptide (FFG) by changing reaction conditions (temperature or solvent, for example) and the follow workup. Also, ^{13}C-NMR and heteronuclear NMR techniques should be performed to achieve full characterization of synthesized compounds.

The association constants of *trans*-chalcones were successfully determined by UV-Vis titrations with cucurbit[n]uril (n= 7, 8) and free/caged biomolecules association constants were determined by direct UV-Vis and emission titrations, displacement assays and ITC. Moreover, to rationalize how complexes were formed NMR spectroscopy was employed. It was established that complexes of free biomolecules with CB[7] have a 1:1 host-guest stoichiometry that are stabilized by the hydrophobic effect. Complexes with CB[8] form 1:2 stoichiometry where the hydrophobic effect prevails and π- π stacking of the aromatic side chains occur within the host cavity. It was found that tyrosine and FGG caged analogues are the most promising photoresponsive guests to apply in a supramolecular system based on CB[7] since they display less affinity towards the host than the free ones. On the other hand, tryptophan and phenylalanine are the suitable photoresponsive guests to apply in a supramolecular system based on CB[8].

Photodeprotection of caged biomolecules was performed and the displacement of the probe (due to conversion of the photoresponsive guest into a strong competitor) was followed by UV-Vis absorption.

An unexpected finding was made for the pair free/caged FGG with a CB[8] based system, where the caged peptide forms a 1:1 host-guest complex (loop type), contrary to the free peptide which forms a 1:2 complex. This revealed to be promising to develop photocontrolled dimerization systems. The complex formation was characterized by UV-Vis displacement, NMR titrations, DOSY and ITC.

Future work should include pH titrations of *trans*-chalcones·CB[n]s complexes. To clarify if TCDEA$_2$MeO interacts with caged tyrosine, histidine and tryptophan more NMR studies should be performed (titration of caged amino acid into a solution with *trans*-chalcone and CB[n], for example). Another *trans*-chalcones can be applied where the association constant order of magnitude can be used to play with the formation of photoresponsive guests complexes. Furthermore, the use of fluorescent probes could be promising for imaging applications, for example, the complexed form would be quenched, and the free form would exhibit fluorescence,

and the release of the probe could be controlled by photoresponsive competitors. As a final remark, this photocontrolled released system has a significant potential as new methodology to determine photodeprotection quantum yields of caged molecules by quantification of probe molecules displaced.

4 Materials and Methods

4.1 Materials and Reagents

Solvents and Reagents for synthesis

Acetonitrile (LabChem), methanol (Sigma-Aldrich), ethyl ether (LabChem), 1,4-dioxane (LabChem), dichloromethane (LabChem), n-hexane (LabChem), ethyl acetate (LabChem), chloroform (LabChem), 4-hydroxyacetophenone (Merck, ≥ 98%), 1,4-butane sultone (Alfa Aesar, ≥ 99%), 4-(diethylamino)benzaldehyde (TCI, > 98%), 4-(diethylamino)-2-metoxybenzaldehyde (FluoroChem, 95%), L-tryptophan (Sigma-Aldrich, 99%), L-tyrosine (Sigma-Aldrich, 98%), L-histidine (Sigma-Aldrich, > 99%), L-phenylalanine (Sigma-Aldrich, 98%), Phe-Gly-Gly (Sigma-Aldrich), NVOC-Cl (Sigma-Aldrich, 97%), sodium carbonate anhydrous.

4.2 Synthesis and Structural Characterization

The NMR spectra of each compound can be consulted in the appendix.

4.2.1 Trans chalcones

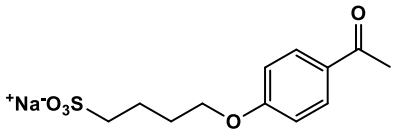

4'-(1-Sulfo-4-butyloxy)-acetophenone sodium salt (1): to a round bottom flask was added 4-hydroxyacetophenone (1.071 g; 7.886 mmol), 1,4-butanesultone (1.500 ml; 14.662 mmol) and sodium carbonate anhydrous (1.557 g; 14.698 mmol) and dissolved in 30 ml of acetonitrile. The mixture was stirred overnight and then filtered at low pressure and rinsed with methanol. The excess of solvent was eliminated by evaporation. A thin-layer chromatography (TLC) was performed, and it was observable traces of reagent. Therefore, the solid was dissolved in methanol and precipitated with ethyl ether with vigorous stirring and filtered in vacuum. To ensure the complete dryness of the final solid product it was maintained in high vacuum. It was obtained 0.923 g of product with a 40% yield.

^{1}H NMR (400 MHz, D_2O) δ (ppm) = 8.01 (d, J = 8.5 Hz, 2H), 7.10 (d, J = 8.5 Hz, 2H), 4.20 (t, J = 5.0 Hz, 2H), 3.01 (t, J = 6.7 Hz, 2H), 2.63 (s, 3H), 1.96 (m, 4H).

4. Materials and Methods

The synthesis procedure of the TCDEA and TCDEA$_2$MeO was based on Basílio et al.[47]

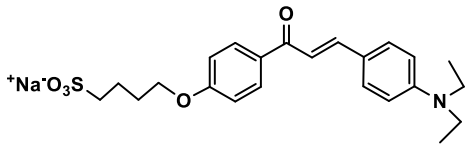

TC_DEA (2): the salt **(1)** (0.300 g; 1.020 mmol) and 4-(diethylamino)benzaldehyde (0.251 g; 1.416 mmol) were dissolved in 4 ml of methanol. The mixture was cooled in an ice bath and 0.134 ml of 40% NaOH were added while stirring. The solution was allowed to warm at room temperature and stirred at 90ºC for 2 days. A reversed phase TLC was performed (70% H_2O / 30% CH_3CN) to confirm the presence of product. 1M HCl was added so that the pH was neutralized. The solvent was removed by evaporation and the final solid dissolved in Milli-Q water and extracted with ethyl ether. The organic phase was rinsed with water and the resulting aqueous phases were mixed and concentrated by evaporation. The crude product was purified by reverse-phase (C18) column flash chromatography with a gradient elution from 100% to 70% H_2O / 30% CH_3CN. The purity of the obtained fractions was tested by reversed phase TLC and the purest were mixed and the solvent removed by evaporation. The resulting orange solid was dried in high vacuum. It was obtained 0.165 g of product with a 35.7% yield.

^{1}H NMR (400 MHz, D_2O) δ (ppm) = 7.76 (d, J = 8.2 Hz, 2H), 7.54 (d, J = 15.1 Hz, 1H), 7.26 (d, J = 8.2 Hz, 2H), 7.13 (d, J = 15.1 Hz, 1H), 6.68 (d, J = 8.0 Hz, 2H), 6.28 (d, J = 8.1 Hz, 2H), 3.64 (t, J = 5.4 Hz, 2H), 2.99 (q, J = 5.8 Hz, 4H), 2.83 (t, 2H), 1.82 – 1.55 (m, 4H), 0.82 (t, J = 6.1 Hz, 6H).

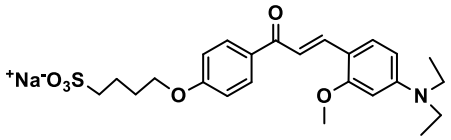

TC_DEA$_2$MeO (3): the salt **(1)** (0.147 g; 0.502 mmol) and 4-(diethylamino)-2-methoxybenzaldehyde (0.227 g; 1.096 mmol) were dissolved in 4 ml of methanol. The mixture was cooled in an ice bath and 0.250 ml of 40% NaOH were added while stirring. The solution was allowed to warm at room temperature and stirred at 60ºC for 2 days. A reversed phase TLC was performed (70% H_2O / 30% CH_3CN) to confirm the presence of product. 1M HCl was added so that the pH was neutralized. The solvent was removed by evaporation and the final solid was rinsed with ethyl ether until absence of 4-(diethylamino)-2-methoxybenzaldehyde. The remain solid was dissolved in methanol and purified by reverse-phase (C18) column flash chromatography with a gradient elution from 100% to 70% H_2O / 30% CH_3CN. The purity of the obtained fractions was tested by reversed phase TLC and the purest were mixed and the solvent removed by evaporation. The resulting orange solid was dried in high vacuum. It was obtained 0.130 g of product with a yield of 53.5%.

^{1}H NMR (400 MHz, D_2O) δ (ppm) = 7.89 (d, *J* = 15.3 Hz, 1H), 7.78 (d, *J* = 8.4 Hz, 2H), 7.38 (d, *J* = 8.8 Hz, 1H), 7.19 (d, *J* = 15.4 Hz, 1H), 6.86 (d, *J* = 8.4 Hz, 2H), 6.18 (d, *J* = 8.6 Hz, 1H), 6.06 (s, 1H), 3.92 (t, *J* = 5.0 Hz, 2H), 3.78 (s, 3H), 3.29 (q, 4H), 2.94 (t, *J* = 7.1 Hz, 2H), 1.96 – 1.73 (m, 4H), 1.09 (t, *J* = 6.9 Hz, 6H).

4.2.2 Caged amino acids and peptide

For all four amino acids (Trp, Tyr, His and Phe) and peptide (FGG), the synthetic procedure was based on the protocol reported by Peter G. Schultz et al.[28]

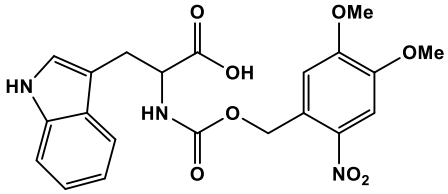

Tryptophan-Nvoc: L-tryptophan (0.101 g; 0.496 mmol) and sodium carbonate (0.055 g; 0.519 mmol) were dissolved in 8 ml of milli-Q water– solution 1. In 8 ml of 1,4-dioxane was dissolved NVOC-Cl (0.137 g; 0.496 mmol) – solution 2. Solution 2 was slowly added to solution 1 at room temperature with stirring. The progress of the reaction was followed by TLC (96% CH_2Cl_2 / 4% CH_3OH). The reactional mixture was left stirring over an hour. Then 60 ml of dichloromethane were added and with 1 M HCl the pH was set to 2. A liquid-liquid extraction was performed, and the aqueous phase was rinsed with 20 ml of dichloromethane. The organic phases were joined together and dried with sodium sulphate. The final product was concentrated by evaporation. The yellow solid obtained was recrystallized with ethyl acetate and n-hexane. It was obtained 0.128 g of product with a 58.07% yield.

^{1}H NMR (400 MHz, $CO(CD_3)_2$) δ (ppm) = 10.11 (s, 1H), 7.70 (s, 1H), 7.63 (d, *J* = 7.8 Hz, 1H), 7.39 (d, *J* = 8.1 Hz, 1H), 7.27 (s, 1H), 7.15 – 7.06 (m, 3H), 7.02 (t, *J* = 7.3 Hz, 1H), 6.75 (d, *J* = 7.8 Hz, 1H), 5.42 (dd, *J* = 15.4 Hz, 2H), 4.61 (dt, *J* = 12.7, 6.5 Hz, 1H), 3.92 (s, 3H), 3.83 (s, 3H), 3.41 (dd, *J* = 14.6, 4.4 Hz, 1H), 3.24 (dd, *J* = 14.7, 8.6 Hz, 1H).

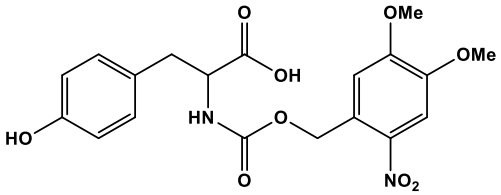

Tyrosine-Nvoc: L-tyrosine (0.078 g; 0.429 mmol) and sodium carbonate (0.163 g; 1.541 mmol) were dissolved in 8 ml of milli-Q water– solution 1. In 8 ml of 1,4-dioxane was dissolved NVOC-Cl (0.137 g; 0.498 mmol) – solution 2. The process was followed as described for

tryptophan, but due to the excess of NVOC-Cl and the presence of a second product (confirmed in TLC) a silica gel column flash chromatography was performed with a gradient elution from 90% to 70% Cl_2CH_2 / 30% CH_3OH. The purity of the obtained fractions was tested by TLC and the purest were mixed and the solvent removed by evaporation. The resulting yellow solid was dried in high vacuum. No recrystallization was performed. It was obtained 0.112 g of product with a 62.0% yield.

^{1}H NMR (400 MHz, $SO(CD_3)_2$) δ (ppm) = 7.70 (s, 1H), 7.12 (s, 1H), 7.03 (d, *J* = 8.2 Hz, 2H), 6.64 (d, *J* = 8.1 Hz, 2H), 5.33 (dd, 2H), 4.03 (q, *J* = 7.0 Hz, 1H), 3.87 (s, 6H), 2.99 (dd, *J* = 12.9, 3.3 Hz, 1H), 2.89 – 2.64 (m, 1H).

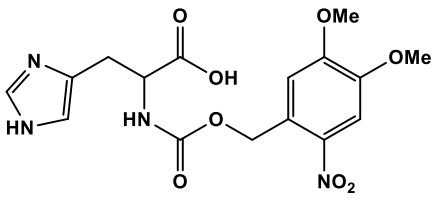

Histidine-Nvoc: L-histidine (0.080 g; 0.518 mmol) and sodium carbonate (0.064 g; 0.599 mmol) were dissolved in 8 ml of milli-Q water– solution 1. In 8 ml of 1,4-dioxane was dissolved NVOC-Cl (0.130 g; 0.472 mmol) – solution 2. The process was followed as described for tryptophan, but in the liquid-liquid extraction the aqueous phase remained yellow indicating that the product was on this phase. This was confirmed by TLC. A silica gel column flash chromatography was performed with a gradient elution from 90% to 70% Cl_2CH_2 / 30% CH_3OH, but it did not result in an effective separation of histidine caged from starting material histidine. A series of attempts of precipitation were made and it was found that at pH 7 in water the product precipitated although the water remained a little bit yellow. The precipitate was isolated and dried in high vacuum. It was obtained 0.048 g of product with a 25.8% yield.

^{1}H NMR (400 MHz, $SO(CD_3)_2$) δ (ppm) = 7.82 (d, *J* = 8.1 Hz, 1H), 7.71 (s, 1H), 7.57 (s, 1H), 7.14 (s, 1H), 6.84 (s, 1H), 5.41 – 5.29 (dd, *J* = 15.3 Hz, 2H), 4.27 – 4.21 (m, 1H), 3.89 (s, 3H), 3.87 (s, 3H), 2.97 (dd, *J* = 14.8, 4.4 Hz, 1H), 2.87 (dd, *J* = 14.8, 8.8 Hz, 1H).

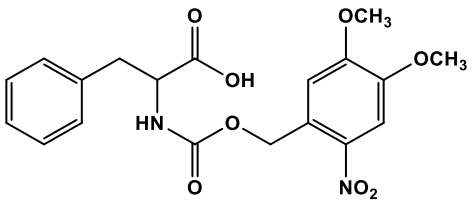

Phenylalanine-Nvoc: L-phenylalanine (0.081 g; 0.493 mmol) and sodium carbonate (0.055 g; 0.517 mmol) were dissolved in 8 ml of milli-Q water– solution 1. In 8 ml of 1,4-dioxane was dissolved NVOC-Cl (0.116 g; 0.421 mmol) – solution 2. The process was followed as

described for tryptophan. No recrystallization was performed. It was obtained 0.161 g of product with a 94.5% yield.

^{1}H NMR (400 MHz, $CO(CD_3)_2$) δ (ppm) = 7.72 (s, 1H), 7.32 (q, *J* = 7.8 Hz, 4H), 7.24 (t, *J* = 6.7 Hz, 1H), 7.15 (s, 1H), 6.86 (d, *J* = 8.3 Hz, 1H), 5.43 (dd, *J* = 15.3 Hz, 2H), 4.53 (td, *J* = 9.0, 4.7 Hz, 2H), 3.95 (s, 3H), 3.90 (s, 3H), 3.29 (dd, *J* = 14.0, 4.7 Hz, 1H), 3.05 (dd, *J* = 14.0, 9.5 Hz, 1H).

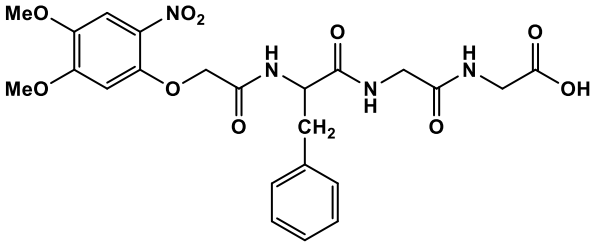

FGG-Nvoc: FGG (0.1918 g; 0.687 mmol) and sodium carbonate (0.083 g; 0.786 mmol) were dissolved in 8 ml of milli-Q water – solution 1. In 8 ml of 1,4-dioxane was dissolved NVOC-Cl (0.138 g; 0.500 mmol) – solution 2. The reaction was stirred for 1 hour at room temperature. By TLC was confirmed that the reaction was not complete, hence, the reactional mixture was stirred another hour at 60ºC. Once more, a TLC was performed, and it was confirmed the presence of product but also of NVOC-Cl and a secondary product. A silica gel flash chromatography was performed with an elution gradient of 100% to 70% chloroform / 30% MeOH. The purest fractions were mixed, and the solvent removed by evaporation. In the NMR tube was observed a precipitate that was silica gel, hence, the product was dissolved in chloroform and filtered with a paper filter. The chloroform was removed by evaporation. The resulting yellow solid was dried in high vacuum. It was obtained 0.069 g of product with a 26.7% yield.

^{1}H NMR (400 MHz, CD_3OD) δ (ppm) = 7.73 (s, 1H), 7.27 – 7.19 (m, 5H), 7.08 (s, 1H), 5.43 (dd, 2H), 4.39 – 4.35 (m, 1H), 3.95 – 3.68 (m, 10H), 3.18 (dd, *J* = 13.9, 5.8 Hz, 1H), 2.94 (dd, *J* = 13.7, 9.6 Hz, 1H).

4.3 Methodologies

UV-Visible Spectroscopy

UV-Visible spectra were acquired in a Varian Cary 100 Bio spectrophotometer at room temperature. Measurements until 220 nm were made in plastic cells and for smaller wavelengths with a quartz cell. All cells had an optical path of 1 cm.

Fluorescence Spectroscopy

Fluorescence measurements were made in a SPEX Fluorolog F111 at room temperature. Quartz cells with an optical path of 1 cm were used.

4. Materials and Methods

NMR Spectroscopy

NMR spectra were acquired on a Bruker AMX 400 instrument operating at 400.13 MHz (^{1}H).

DOSY

^{1}H NMR diffusion experiments were acquired with the stimulated echo sequence using bipolar sine gradient pulses (*ledbpgp2s*). For each experiment the pulsed gradients were applied with a power level (G) linearly incremented from 2.65 to 50.4 G cm^{-1}. The duration of the pulse field gradients (δ) applied to encode and decode the diffusion were set to 4 ms and the diffusion delay period Δ of the experiment was optimized to 150 ms. Such optimized value of Δ provided a convenient sampling of the exponential decay of the signal intensity during the diffusion experiment. A shape factor of 0.6366 (ξ) was used to correct the gradient deviation arising from the use of sine-pulsed gradients. The integral of selected ^{1}H NMR signals (*I*) were plotted against the gradient strength and the data fitted to the Stejskal and Tanner equation (where γ is the gyromagnetic ratio of the observed nucleus) to obtain the diffusion coefficient (*D*).[62]

$$I = I_0 e^{-(\gamma \xi G \delta)^2 (\Delta - \delta/3) D}$$

ITC

Isothermal titration calorimetry (ITC) measurements were performed on a Nano ITC (TA Instruments) with standard volumes. The solutions were degassed before use by stirring under vacuum.

Photochemical studies

Light-irradiation experiments were conducted with a 200 W Hg-Xe lamp using a 365 nm bandpass filter or a 280 nm cut-off filter. The photorelease was followed by UV-Vis and NMR spectroscopy. For UV-Vis experiments the sample solution was stirred with a magnetic bar in a plastic cell. For NMR experiments the tubes were exposed to light without stirring.

Spectrophotometric titrations

In a cell containing a solution of biomolecule (free or caged) was added a mixture of CB[n] with biomolecule. The titrant cell contains biomolecule with the same concentration as the titrated cell, therefore, only the CB[n] concentration is variating along the titration, which simplifies the calculations. UV-Vis spectrum was recorded in each titrated volume addition.

In displacement assays, to a cell containing a mixture of CB[n] and indicator was added a mixture of CB[n], indicator and competitor. Once again, the titrant cell contains CB[n] and indicator with the same concentration as the titrated cell.

The conditions of each experiment are described above.

Mathematical models to determine binding constants

To obtain the binding constants it's necessary to reach an equation that relates the measured signal to the total concentration of the host and guest. This equation is derived through a manipulation of equilibrium constant equations, mass balance equations, and signal-to-concentration relationships (e.g. Beer's law in case of absorption).[63]

1:1 (Host-Guest) Binding

When both the host (H) and guest (G) have only one binding site, the equilibrium equation and the binding constant (K) are given by equations (4.1) and (4.2), respectively.

$$\mathrm{H} + \mathrm{G} \leftrightharpoons \mathrm{HG} \qquad (4.1)$$

$$K = \frac{[HG]}{[H][G]} \qquad (4.2)$$

Mass balance of each compound in solution is given by equations (4.3) and (4.4).

$$[\mathrm{G}]_0 = [G] + [HG] \qquad (4.3)$$

$$[\mathrm{H}]_0 = [H] + [HG] \qquad (4.4)$$

Using equations (4.1)-(4.4) as starting point, it is possible to derive an equation based on only one unknown concentration ([G], [H] or [HG]) to which all other concentrations are related. Here is chosen [HG]. Therefore:

$$K = \frac{[HG]}{([\mathrm{H}]_0 - [HG])([\mathrm{G}]_0 - [HG])} \qquad (4.5)$$

Rearranging equation (4.5) yields a quadratic equation, which is represented by equation (4.6).

$$[HG]^2 - [HG]\left([\mathrm{H}]_0 + [G]_0 + \frac{1}{K}\right) + [\mathrm{H}]_0[G]_0 = 0 \qquad (4.6)$$

Using the quadratic formula, the value of [HG] can be obtained based on K and experimentally determined values ($[H]_0$ and $[G]_0$). By solving equations (4.3) and (4.4) it can be obtained the equilibrium concentrations of G and H.

Now, one can fit the data by relating with the spectrophotometric changes. In this case, the reporting specie is the G.

UV-Vis: $Abs_{calc} = \varepsilon^{G}[G] + \varepsilon^{HG}[HG]$ (4.7)

Emission: $I_{calc} = \frac{[G]}{[G]_0} I_G + \frac{[HG]}{[G]_0} I_{HG}$ (4.8)

The data fit was obtained recurring to solver from Excel. For absorbance fit the optimized values were K, ε^G and ε^{HG} and for emission fit were K, I_0^G and I_0^{HG}.

Indicator displacement

In an indicator displacement assay, a host is first allowed to complex with a dye (indicator, I) that possess an optical change upon binding with the host (H). The addition of a guest (G) displaces the indicator, consequently, a reversal in the absorption or emission spectrum is observable.

Displacement by 1:1 Binding

$H + I \leftrightharpoons HI \quad K_I$ (4.9)

$H + G \leftrightharpoons HG \quad K_G$ (4.10)

$K_I = \frac{[HI]}{[H][I]}$ (4.11)

$K_G = \frac{[HG]}{[H][G]}$ (4.12)

Mass balance is represented by equations (4.13)-(4.15).

$[H]_0 = [H] + [HG] + [HI]$ (4.13)

$[G]_0 = [G] + [HG]$ (4.14)

$[I]_0 = [I] + [HI]$ (4.15)

Once again, one can solve in order to the desirable specie. Defining all other concentrations in terms of [H] yields equations (4.16)-(4.18).

$[HG] = \frac{K_G[H]}{1+K_G[H]}[G]_0$ (4.16)

$[HI] = \frac{K_I[H]}{1+K_I[H]}[I]_0$ (4.17)

$[I] = \frac{[I]_0}{1+K_I[H]}$ (4.18)

Substituting equations (4.16) and (4.17) into (4.13) yields the cubic equation (4.19) that is solved most easily using Newton's iterative optimization method.[63]

$A[H]^3 + B[H]^2 + C[H] + D = 0$ (4.19)

Where

$A = K_I K_G$

$B = K_I + K_G + K_I K_G [I]_0 + K_I K_G [G]_0 - K_I K_G [H]_0$

$C = 1 + K_I [I]_0 + K_G [G]_0 - [H]_0 (K_I + K_G)$

$D = -[H]_0$

Again, one can derive a relationship to the optical data. Accordingly, equation (4.20) is derived from Beer's law.

$Abs_{calc} = \varepsilon^I [I] + \varepsilon^{HI} [HI]$ (4.20)

This time the optimized values were K_G, ε^I and ε^{HI}. The association constant of the indicator (K_I) value was fixed since it was previously determined by direct titration with the host recurring to the same mathematical principles for 1:1 binding events.

Displacement by 1:2 Binding

When the displacement of one indicator molecule occurs because two guest molecules binds to the host, besides equations (4.9)-(4.12) one must also consider other two - (4.21) and (4.22).

$\mathrm{HG} + \mathrm{G} \leftrightharpoons \mathrm{HG_2} \quad \mathrm{K_{2G}}$ (4.21)

$K_{2G} = \frac{[HG_2]}{[HG][G]}$ (4.22)

Consequently, the mass balance results in eq. (4.15) and (4.23)-(4.24).

$[H]_0 = [H] + [HI] + [HG] + [HG_2]$ (4.23)

$[G]_0 = [G] + [HG] + 2[HG_2]$ (4.24)

Following the same reasoning, eq. (4.25) and (4.26) are obtained.

$K_G K_{2G} [G]^3 + (K_G + 2K_G K_{2G} [H]_0 - K_G K_{2G} [G]_0)[G]^2 + (1 - K_G [G]_0 + K_G [H]_0)[G] +$

$K_I [I][G] - K_I [G]_0 [I] - [G]_0 = 0$ (4.25)

$K_I [I]^2 + (1 + K_1 [G] + K_1 K_2 [G]^2 - K_I [I]_0 + K_I [CB8]_0)[I] -$

$$(1 + K_1[G] + K_1K_2[G]^2)[I]_0 = 0 \quad (4.26)$$

This time a cubic equation with two incognitos ([G] and [I]) is yield. To solve this, also Newton's Method is employed, resorting to partial derivatives which turns it simpler to solve.[64]
To fit the experimental data, one must use eq. (4.20) one more time. The solver optimized values were K_1, K_2, ε^I and ε^{HI}. Once again, the K_I was already determined

5 References

1 A. Losi, K. H. Gardner and A. Möglich, *Chem. Rev.*, 2018, acs.chemrev.8b00163.

2 P. Ceroni, A. Credi and M. Venturi, *Chem. Soc. Rev.*, 2014, **43**, 4068–4083.

3 D. L. Nelson and M. M. Cox, *Lehninger Principles of Biochemistry*, Worth, 3rd edn., 2000.

4 G. C R Ellis-Davies, *Nat. Methods*, 2014, **4**, 619–628.

5 M. J. Hansen, W. A. Velema, M. M. Lerch, W. Szymanski and B. L. Feringa, *Chem. Soc. Rev.*, 2015, **44**, 3358–3377.

6 A. Gautier, C. Gauron, M. Volovitch, D. Bensimon, L. Jullien and S. Vriz, *Nat. Chem. Biol.*, 2014, **10**, 533–541.

7 W. A. Velema, W. Szymanski and B. L. Feringa, *J. Am. Chem. Soc.*, 2014, **136**, 2178–2191.

8 N. C. Fan, F. Y. Cheng, J. A. A. Ho and C. S. Yeh, *Angew. Chemie - Int. Ed.*, 2012, **51**, 8806–8810.

9 G. Mayer and A. Hechel, *Angew. Chemie - Int. Ed.*, 2006, **45**, 4900–4921.

10 P. Klan, T. Solomek, C. G. Bochet, R. Givens, M. Rubina, V. Popik, A. Kostikov and J. Wirz, *Chem. Rev.*, 2012, **113**, 119–191.

11 P. Wang, *Asian J. Org. Chem.*, 2013, **2**, 452–464.

12 R. S. Givens, P. G. Conrad II, A. L. Yousef and J.-I. Lee, *CRC handbook of Organic Photochemistry and Photobiology*, CRC Press, 2nd edn., 2003.

13 J. H. Kaplan and G. C R Ellis-Davies, *J. Org. Chem.*, 1988, **53**, 1966–1969.

14 C. M. Maragos Wang, JM, Hrabie, JA, Oppenheim, JJ, Keefer, LK, *J Med Chem*, 1993, **34**, 3242–3247.

15 S. Namiki, T. Arai and K. Fujimori, *J. Am. Chem. Soc.*, 1997, **119**, 3840–3841.

16 G. Marriott, *Biochemistry*, 1994, **33**, 9092–9097.

17 G. F. Short, M. Lodder, A. L. Laikhter, T. Arslan and S. M. Hecht, *J. Am. Chem. Soc.*, 1999, **121**, 478–479.

18 E. Arbely, J. Torres-Kolbus, A. Deiters and J. W. Chin, *J. Am. Chem. Soc.*, 2012, **134**, 11912–11915.

19 T. Measey and F. Gai, *Langmuir*, 2012, **28**, 12588–12592.

20 I. Ahmed and L. Fruk, *Mol. BioSyst.*, 2013, **9**, 565–570.

21 A. Isidro-Llobet, M. Álvarez and F. Albericio, *Chem. Rev.*, 2009, **109**, 2455–2504.

22 A. P. Pelliccioli and J. Wirz, *Photochem. Photobiol. Sci.*, 2002, **1**, 441–458.

23 G. Marriott, P. Roy and K. Jacobson, *Methods Enzymol.*, 2003, **360**, 274–288.

5. References

24 C. Chang, T. Fernandez, R. Panchal and H. Bayley, *J. Am. Chem. Soc.*, 1998, **120**, 7661–7662.

25 G. Marriott and M. Heidecker, *Biochemistry*, 1996, **35**, 3170–3174.

26 P. Barltrop, J.A., Plant, P.J., and Schofield, *J. Chem. Soc., Chem. Commun.*, 1966, 822–823.

27 M. A. Romero, N. Basílio, A. J. Moro, M. Domingues, J. A. González-Delgado, J. F. Arteaga and U. Pischel, *Chem. - A Eur. J.*, 2017, **23**, 13105–13111.

28 S. A. Robertson, J. A. Ellman and P. G. Schultz, *J. Am. Chem. Soc.*, 1991, **113**, 2722–2729.

29 A. Specht, F. Bolze, Z. Omran, J. Nicoud and M. Goeldner, *HFSP J.*, 2009, **3**, 255–264.

30 R. Göstl and S. Hecht, *Chem. - A Eur. J.*, 2015, **21**, 4422–4427.

31 P. T. Wong, S. Tang, J. Mukherjee, K. Tang, K. Gam, D. Isham, C. Murat, R. Sun, J. R. Baker and S. K. Choi, *Chem. Commun.*, 2016, **52**, 10357–10360.

32 B. Levrand, W. Fieber, J. M. Lehn and A. Herrmann, *Helv. Chim. Acta*, 2007, **90**, 2281–2314.

33 M. J. Webber and R. Langer, *Chem. Soc. Rev.*, 2017, **46**, 6600–6620.

34 K. Jain, *Drug Delivery Systems*, Humana Press, 2008.

35 G. Hettiarachchi, D. Nguyen, J. Wu, D. Lucas, D. Ma, L. Isaacs and V. Briken, *PLoS One*, 2010, **5**, 2–11.

36 C. Hou, Z. Huang, Y. Fang and J. Liu, *Org. Biomol. Chem.*, 2017, **15**, 4272–4281.

37 N. Amir and N. Werner, .

38 J. Murray, K. Kim, T. Ogoshi, W. Yao and B. C. Gibb, *Chem. Soc. Rev.*, 2017, **46**, 2479–2496.

39 K. Kim, N. Selvapalam, Y. H. Ko, K. M. Park, D. Kim and J. Kim, *Chem. Soc. Rev.*, 2007, **36**, 267–279.

40 K. I. Assaf and W. M. Nau, *Chem. Soc. Rev.*, 2015, **44**, 394–418.

41 V. Mandadapu, A. Day and A. Ghanem, *Chirality*, 2014, **26**, 712–723.

42 E. Masson, X. Ling, R. Joseph, L. Kyeremeh-Mensah and X. Lu, *Cucurbituril chemistry: a tale of supramolecular success*, 2012, vol. 2.

43 S. J. Barrow, S. Kasera, M. J. Rowland, J. Del Barrio and O. A. Scherman, *Chem. Rev.*, 2015, **115**, 12320–12406.

44 A. R. Urbach and V. Ramalingam, *Isr. J. Chem.*, 2011, **51**, 664–678.

45 L. M. Heitmann, A. B. Taylor, P. J. Hart and A. R. Urbach, *J. Am. Chem. Soc.*, 2006, **128**, 12574–12581.

46 B. B. Chavan, A. S. Gadekar, P. P. Mehta, P. K. Vawhal, A. K. Kolsure and A. R. Chabukswar, *Asian J. Biomed. Pharm. Sci. 2015*, 2016, **6**, 01-7.

5. References

47 N. Basílio, S. Gago, A. J. Parola and F. Pina, *ACS Omega*, 2017, **2**, 70–75.

48 P. Singh, A. Anand and V. Kumar, *Eur. J. Med. Chem.*, 2014, **85**, 758–777.

49 N. Basílio, V. Petrov and F. Pina, *Chempluschem*, 2015, **80**, 1779–1785.

50 N. Basílio and U. Pischel, *Chem. - A Eur. J.*, 2016, **22**, 15208–15211.

51 P. Thordarson, *Chem. Soc. Rev.*, 2011, **40**, 1305–1323.

52 P. Atkins and J. De Paula, *Atkins' Physical chemistry*, Oxford: Oxford University Press, 8th edn., 2006.

53 K. Janssens, *Section V Methods 4: Elemental Analysis*, WILEY-VCH Verlag GmbH & Co., 2003.

54 N. Jacobsen, *NMR SPECTROSCOPY EXPLAINED: Simplified Theory, Applications and Examples for Organic Chemistry and Structural Biology*, Wiley, 2007.

55 T. D. W. Claridge, *High-Resolution NMR Techniques in Organic Chemistry*, Elsevier Ltd, 3rd edn., 2016.

56 K. Hirose, *J. Incl. Phenom. Macro.*, 2001, **39**, 193–209.

57 M. R. Duff, Jr., J. Grubbs and E. E. Howell, *J. Vis. Exp.*, 2011, 2–5.

58 G. U. Nienhaus, *Protein-Ligand Interactions: Methods and Applications*, Humana Press, 2005.

59 C. Mas, Presentation ITC, http://www.isbg.fr/biophysics-characterisation/itc200/?lang=en, (accessed 31 August 2018).

60 D. S. Shin, K. N. Lee, B. W. Yoo, J. Kim, M. Kim, Y. K. Kim and Y. S. Lee, *J. Comb. Chem.*, 2010, **12**, 463–471.

61 Lecture 13 Nonlinear Systems - Newton ' s Method, http://www.ohiouniversityfaculty.com/youngt/IntNumMeth/lecture13.pdf, (accessed 17 August 2018).

62 Y. Cohen, L. Avram and L. Frish, *Angew. Chemie - Int. Ed.*, 2005, **44**, 520–554.

63 A. E. Hargrove, Z. Zhong, J. L. Sessler and E. V. Anslyn, *New J. Chem.*, 2010, **34**, 348–354.

64 Y. Wang, METHODS FOR SOLVING NONLINEAR EQUATIONS, https://www.math.purdue.edu/~wang838/notes/newton.pdf, (accessed 17 August 2018).

6 Appendix

Table 6.1 – Lester rules or Sheehan criteria.

1	The caged substrate must be soluble in the targeted media, be pure, exhibit low intrinsic activity and be stable in the media prior to and during light irradiation.
2	The photo release must be efficient, i.e., with a high *quantum yield*, Φ_{rel}. $$\Phi_{rel} = \frac{\#released\ substrate}{\#photons\ absorbed\ at\ \lambda_{irr}}$$
3	The release of caged substrate should be a primary photochemical process (i.e., occurs directly from the excited state of the cage chromophore).
4	All photoproducts should be stable in the assay media.
5	Excitation wavelengths should be longer than 300 nm and must not be absorbed by the media, photoproducts or substrate. The use of less energetic wavelengths prevents damage to biological systems.
6	A high-yielding synthetic procedure for caging the substrate is desirable.
7	To capture the incident light efficiently, the chromophore should have a reasonable absorptivity.
8	In caged substrate synthesis, the caged and the uncaged portions must be quantitative.

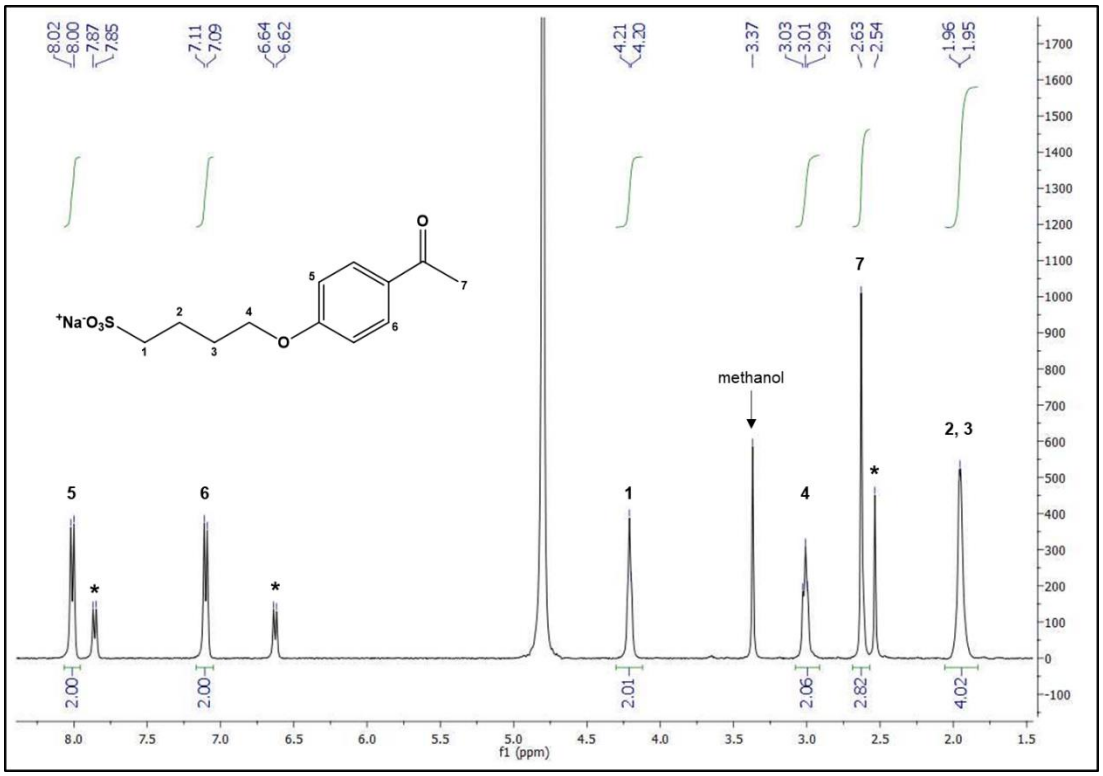

Figure 6.1 – ^{1}H-NMR spectrum of compound **1** in D_2O. Impurities are assigned with *.

6. Appendix

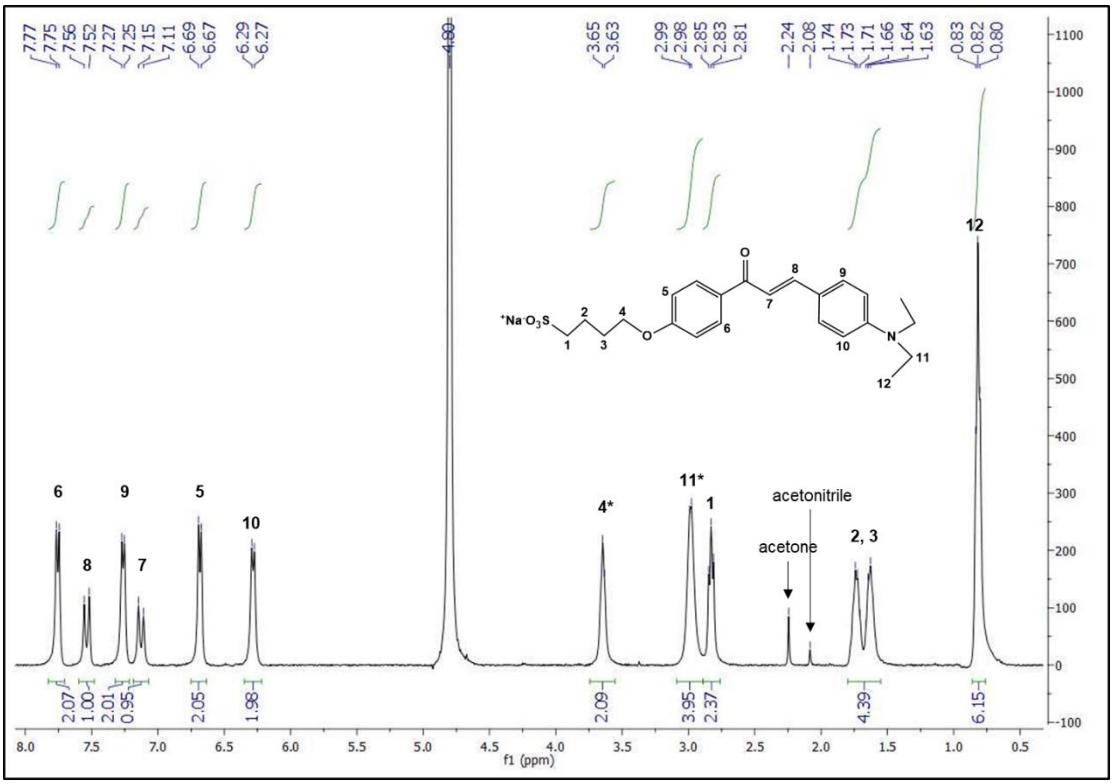

Figure 6.2 – ^{1}H-NMR spectrum of TCDEA in D_2O. Signals with * have low resolution but can be assigned from the integration.

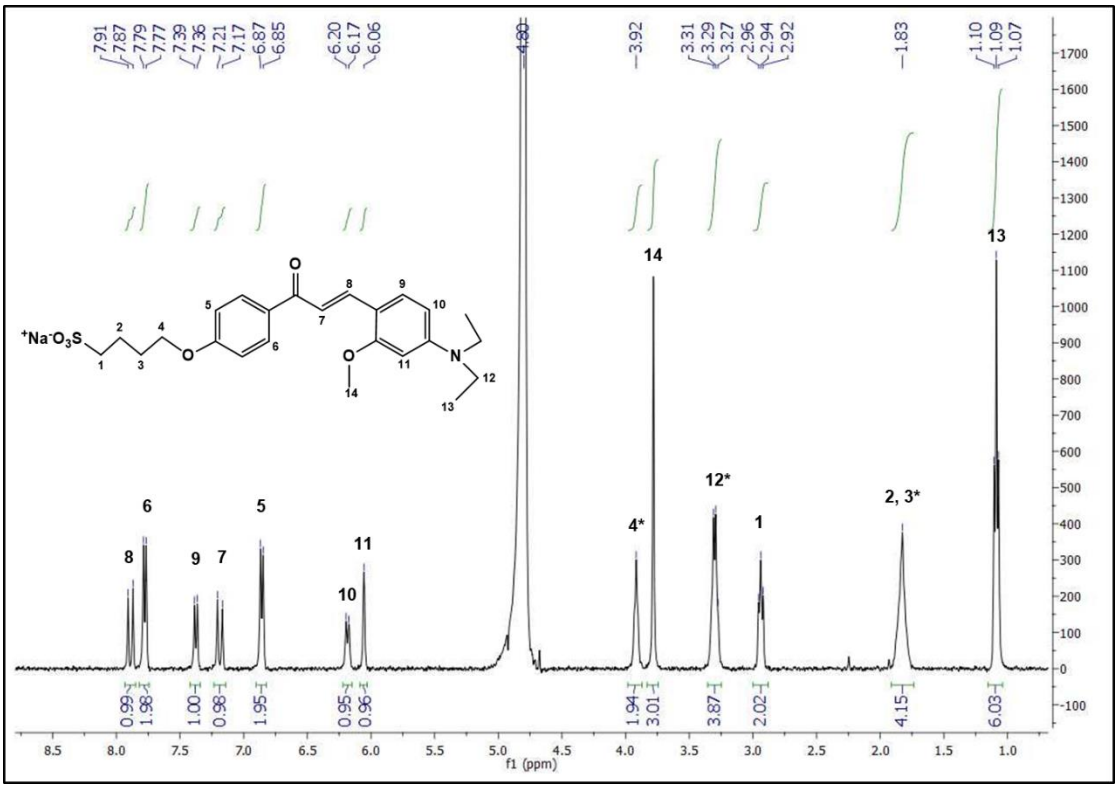

Figure 6.3 – ^{1}H-NMR spectrum of $TCDEA_2MeO$ in D_2O. Signals with * have low resolution but can be assigned from the integration.

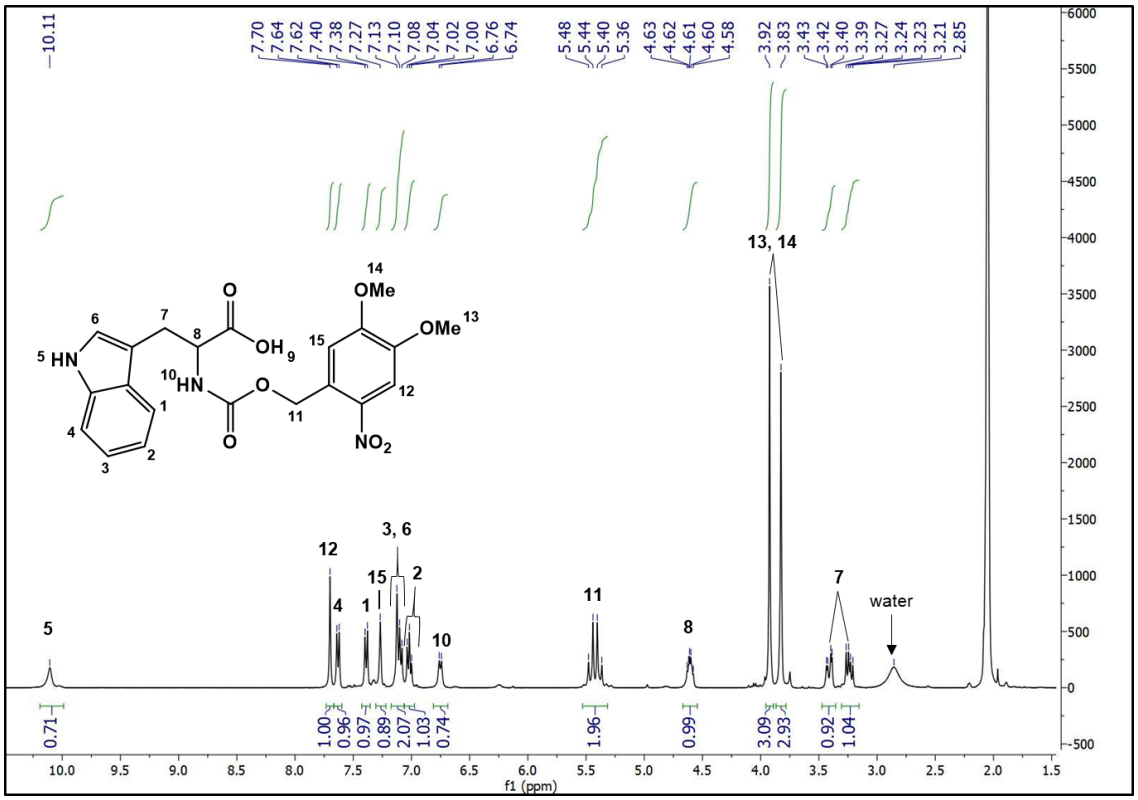

Figure 6.4 – ^{1}H-NMR spectrum of caged tryptophan in $CO(CD_3)_2$.

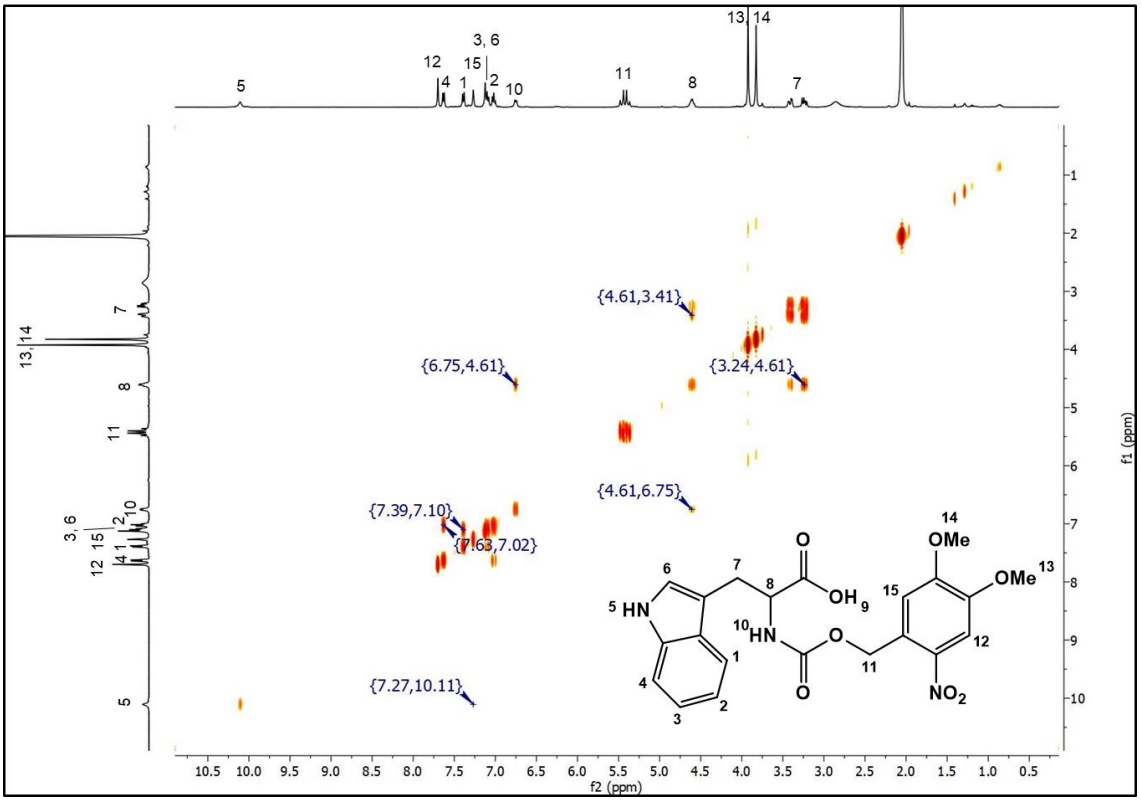

Figure 6.5 – COSY of caged tryptophan in $CO(CD_3)_2$.

6. Appendix

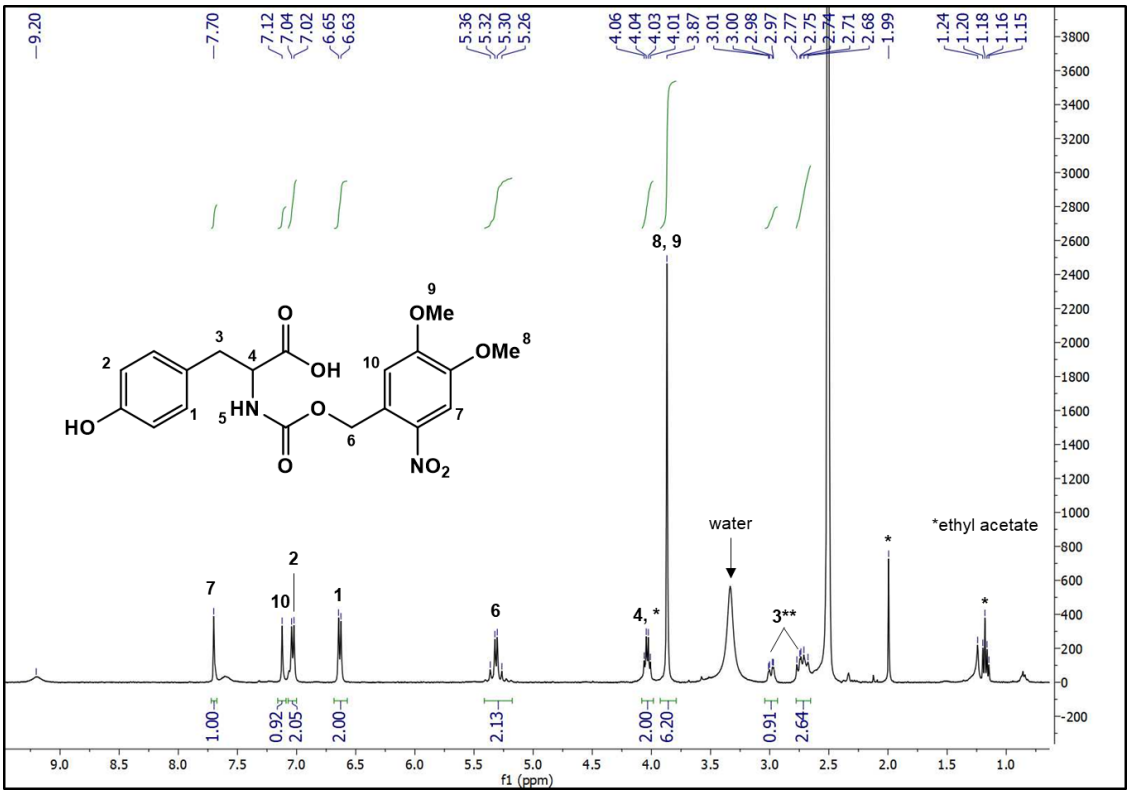

Figure 6.6 – ^{1}H-NMR spectrum of caged tyrosine in $SO(CD_3)_2$. * ethyl acetate, **the integration is higher due the proximity to the solvent peak.

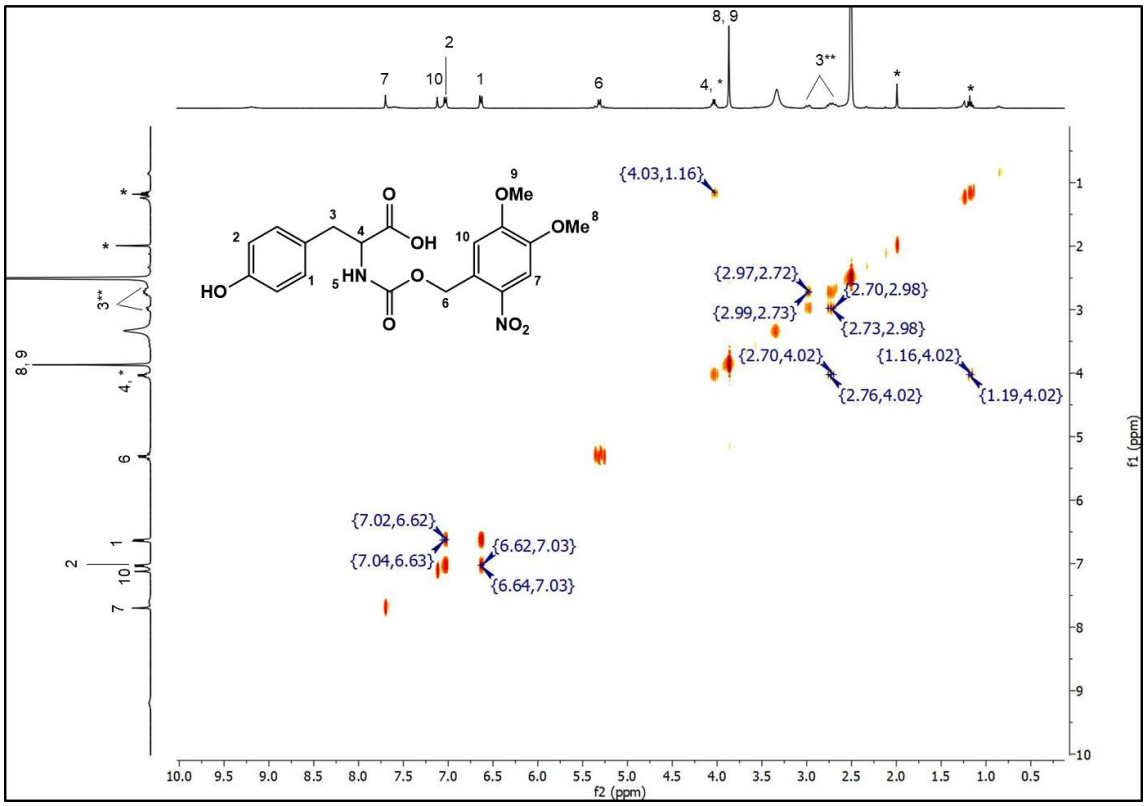

Figure 6.7 – COSY of caged tyrosine in $SO(CD_3)_2$.

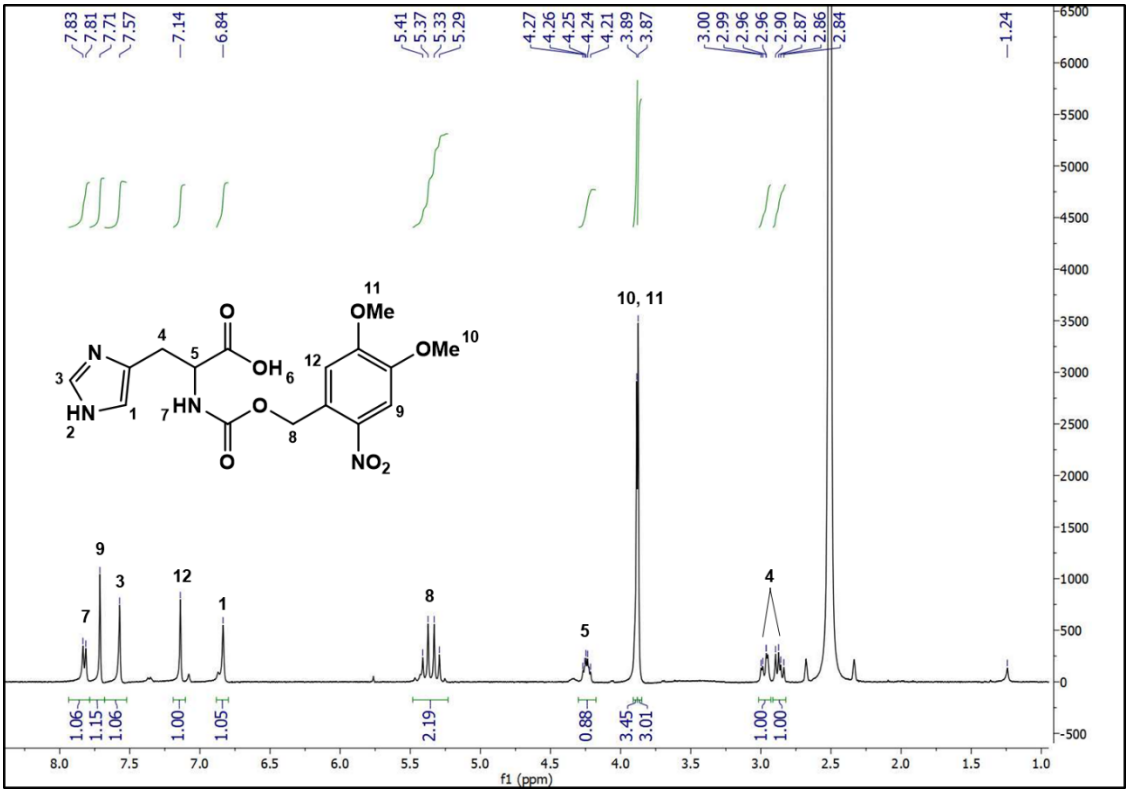

Figure 6.8 – ^{1}H-NMR spectrum of caged histidine in $SO(CD_3)_2$.

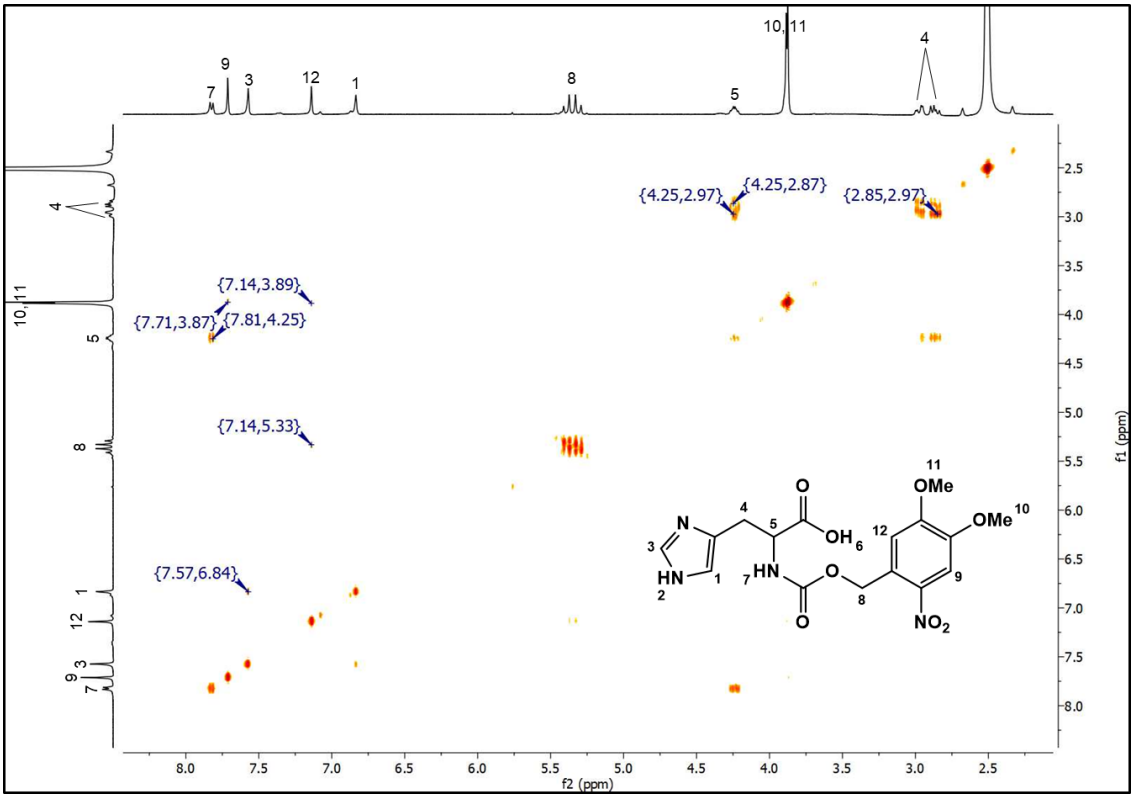

Figure 6.9 – COSY of caged histidine in $SO(CD_3)_2$.

6. Appendix

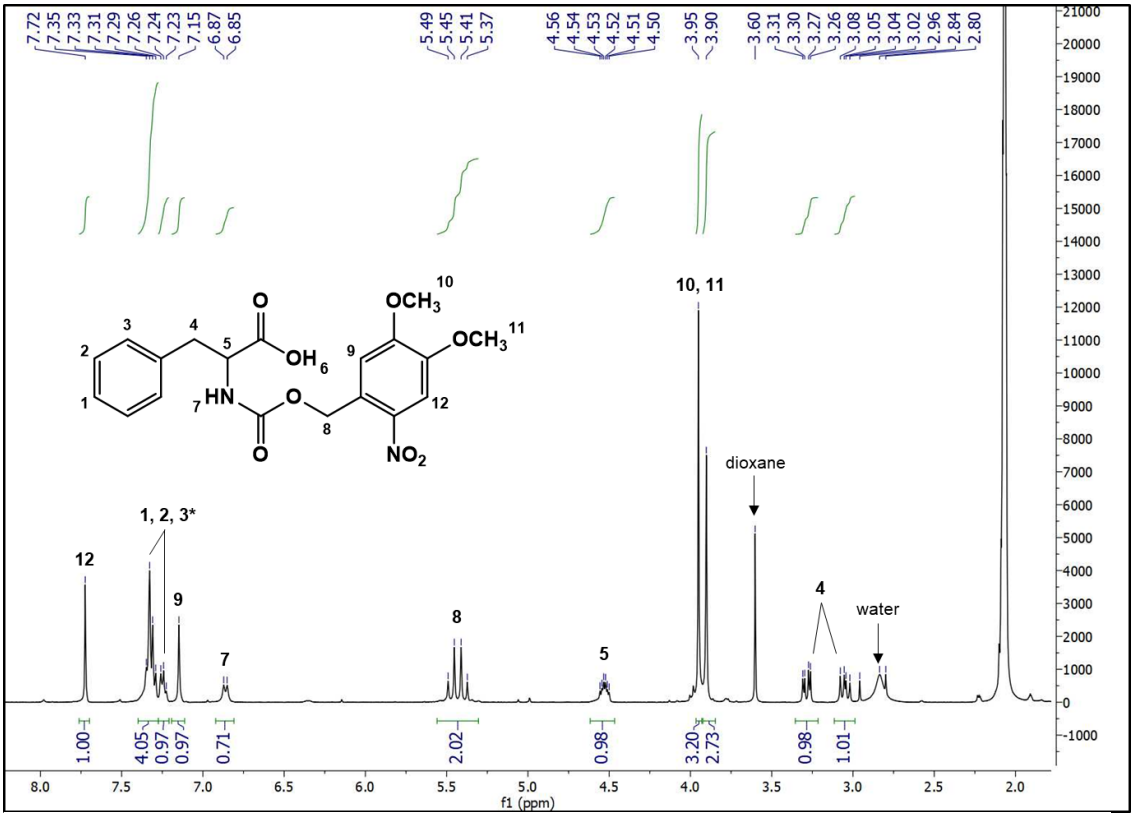

Figure 6.10 – ^{1}H-NMR spectrum of caged phenylalanine in $CO(CD_3)_2$.

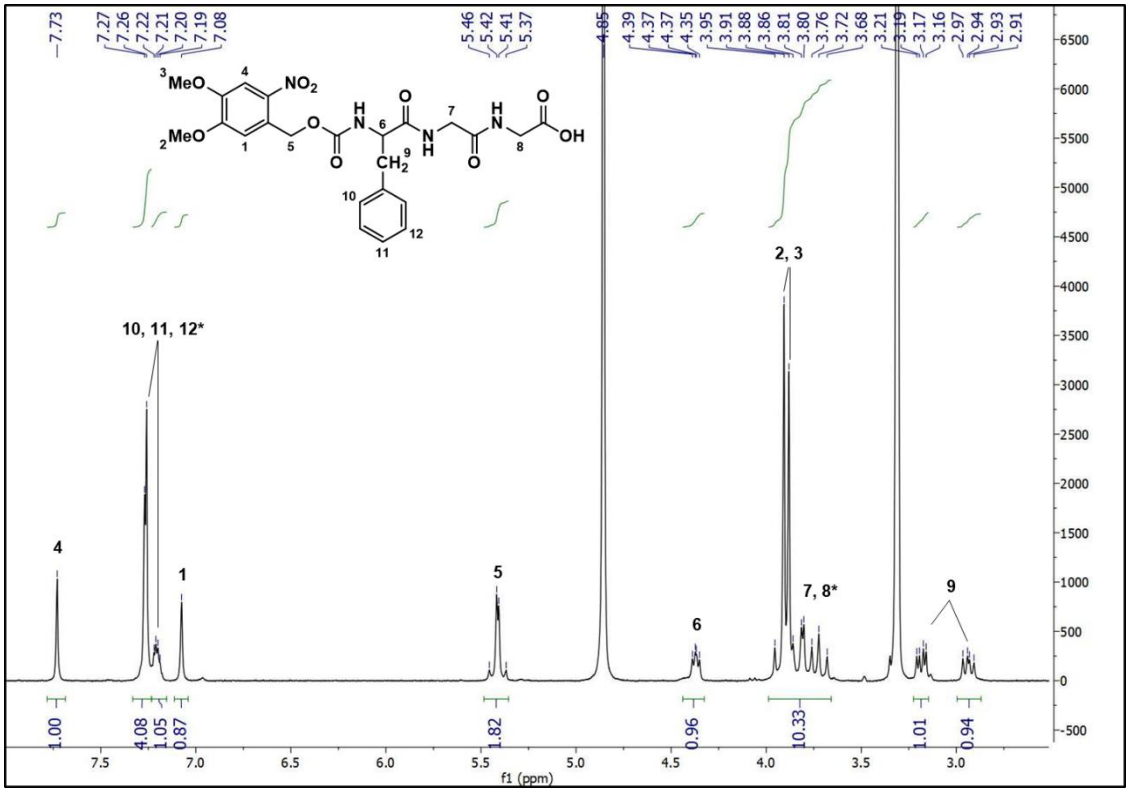

Figure 6.11 – ^{1}H-NMR spectrum of caged FGG in CD_3OD. *it was not possible to assign the type of coupling

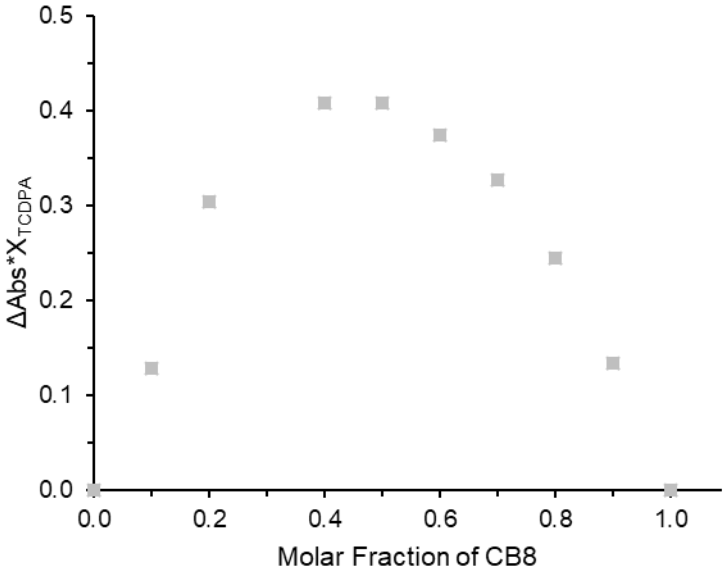

Figure 6.12 – Job Plot's of the interaction between TCDPA with CB[8], followed at 450 nm. [total] = 6.0×10^{-5} M.

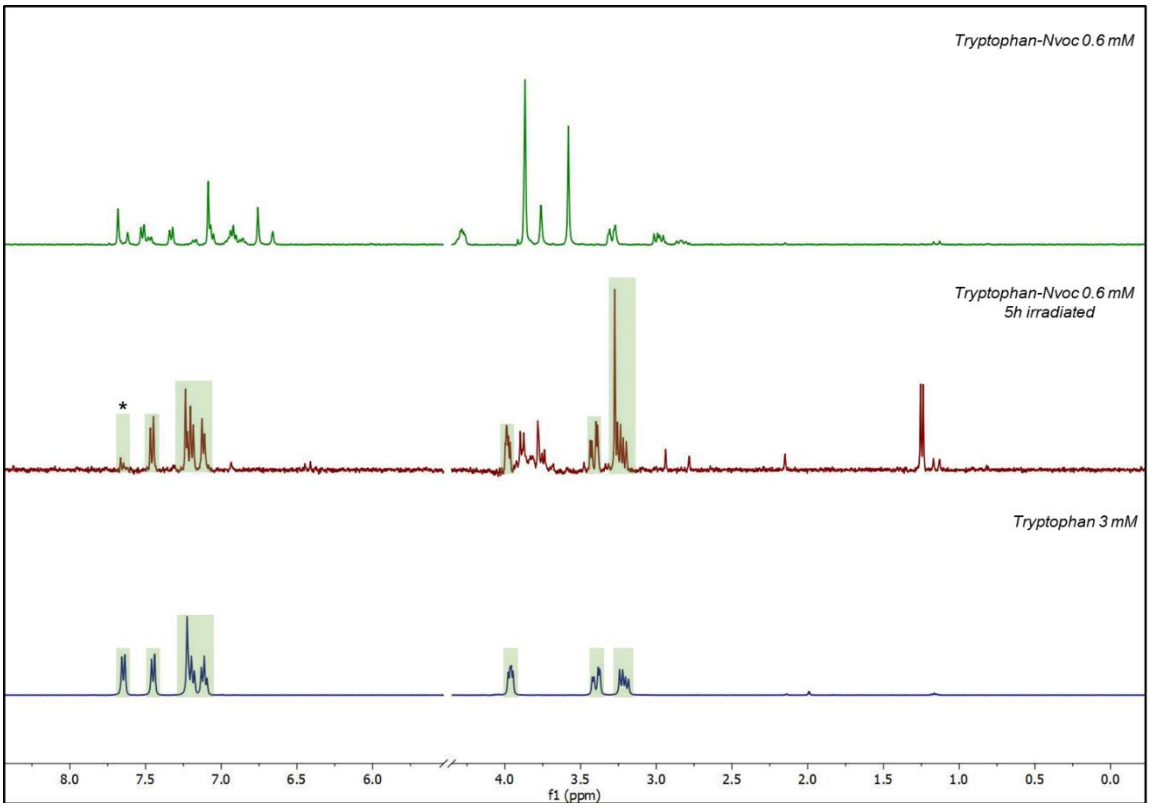

Figure 6.13 – ^{1}H-NMR spectra of TrpNvoc 0.6 mM, before (up) and after irradiation (middle), and tryptophan 3 mM (down) in D_2O. λ_{irr} = 365 nm, t_{irr} = 5h.

6. Appendix

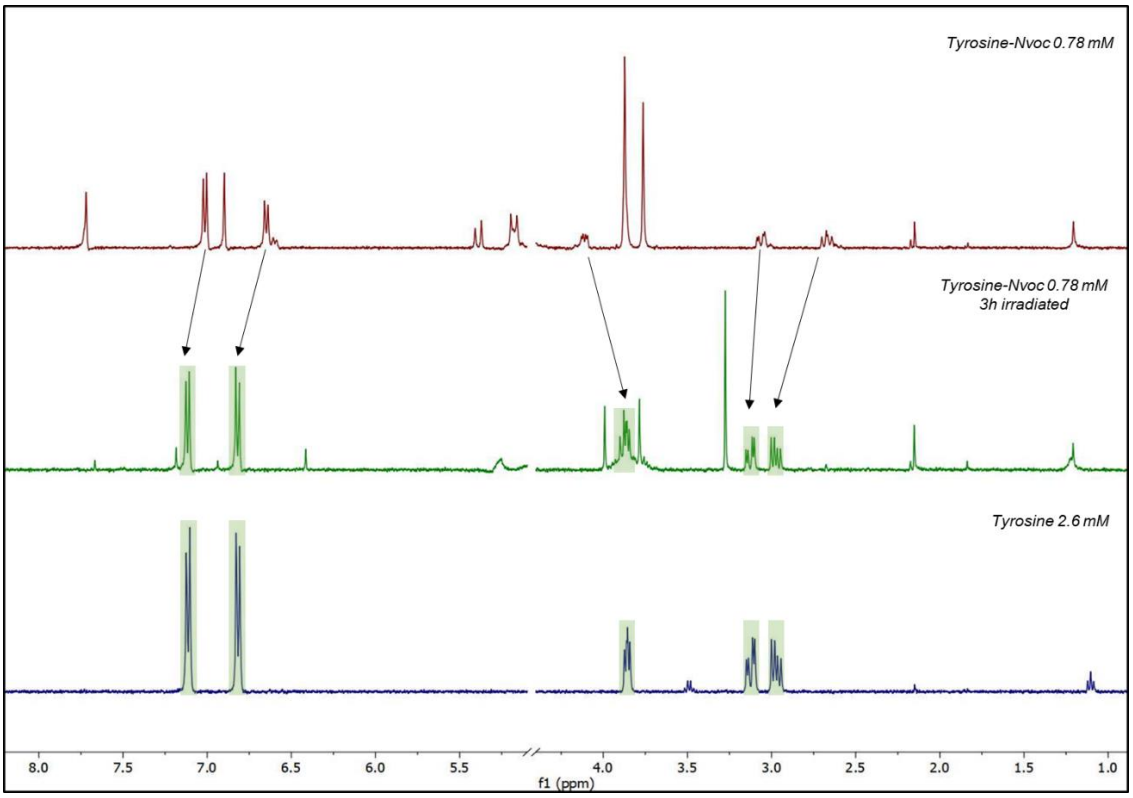

Figure 6.14 – ^{1}H-NMR spectra of TyrNvoc 0.78 mM, before (up) and after irradiation (middle), and tyrosine 2.6 mM (down) in D_2O. λ_{irr} = 365 nm, t_{irr} = 3h.

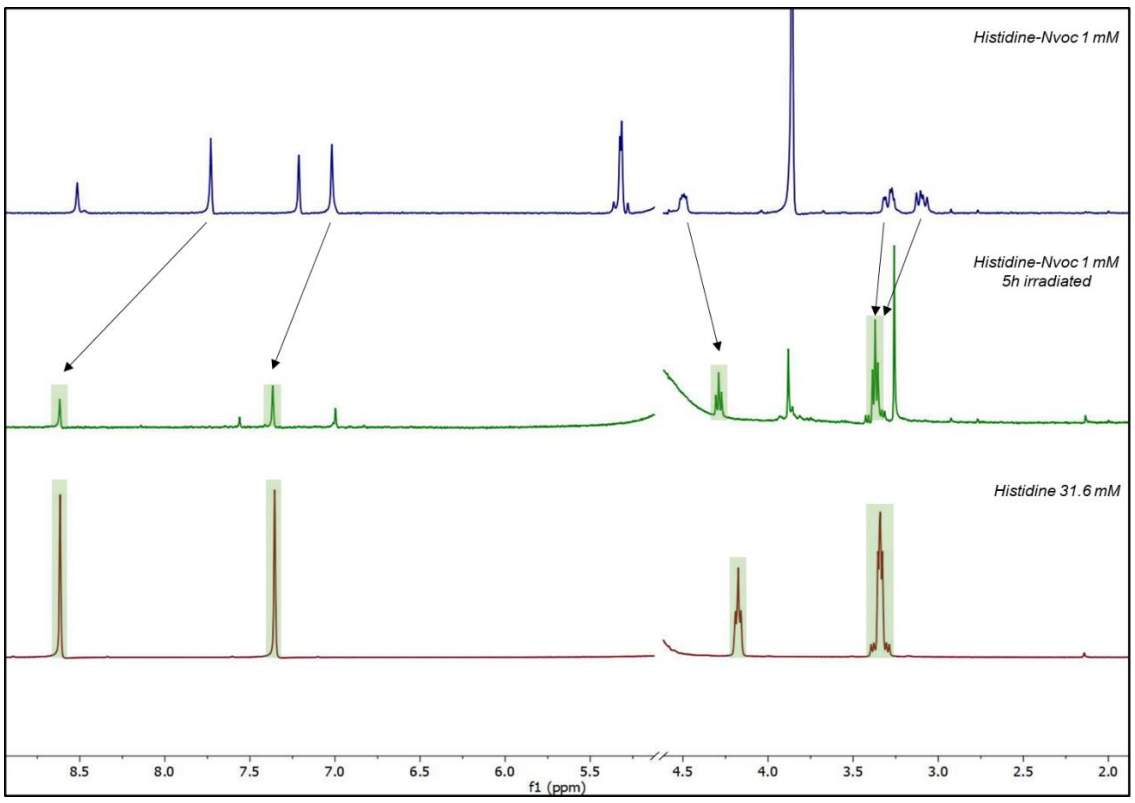

Figure 6.15 – ^{1}H-NMR spectra of HisNvoc 1 mM, before (up) and after irradiation (middle), and histidine 31.6 mM (down) in D_2O. λ_{irr} = 365 nm, t_{irr} = 5h.

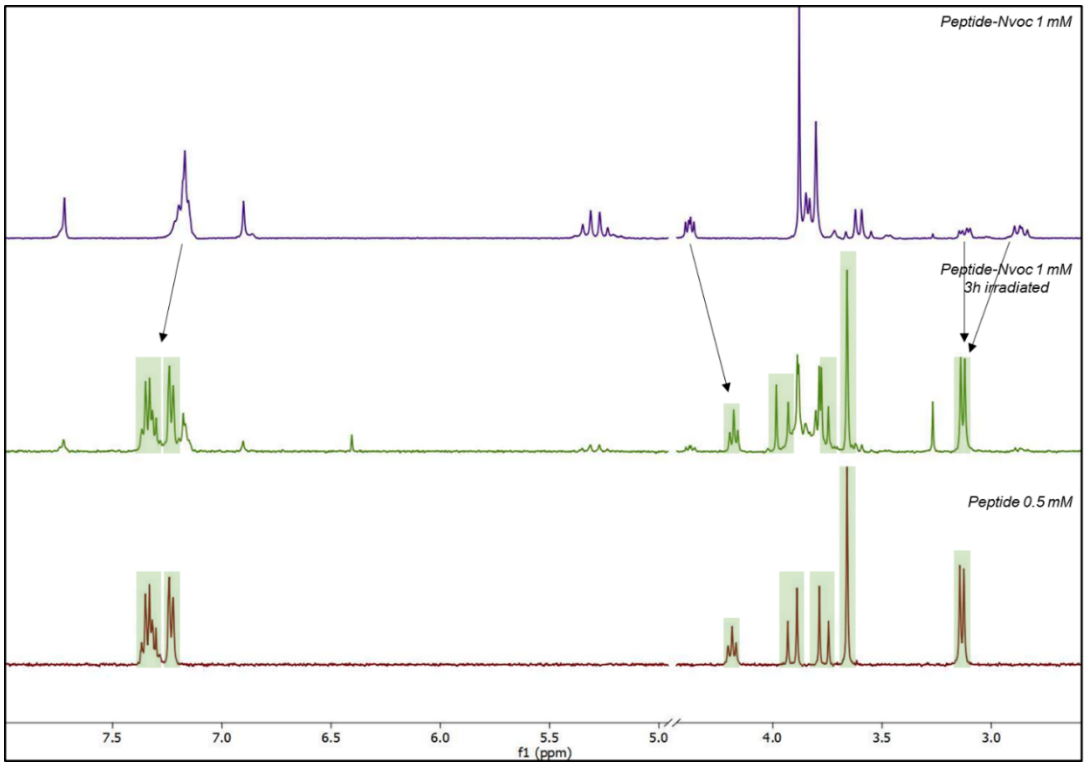

Figure 6.16 – ^{1}H-NMR spectra of FGGNvoc 1 mM, before (up) and after irradiation (middle), and FGG 0.5 mM (down) in D_2O. λ_{irr} = 365 nm, t_{irr} = 3h.

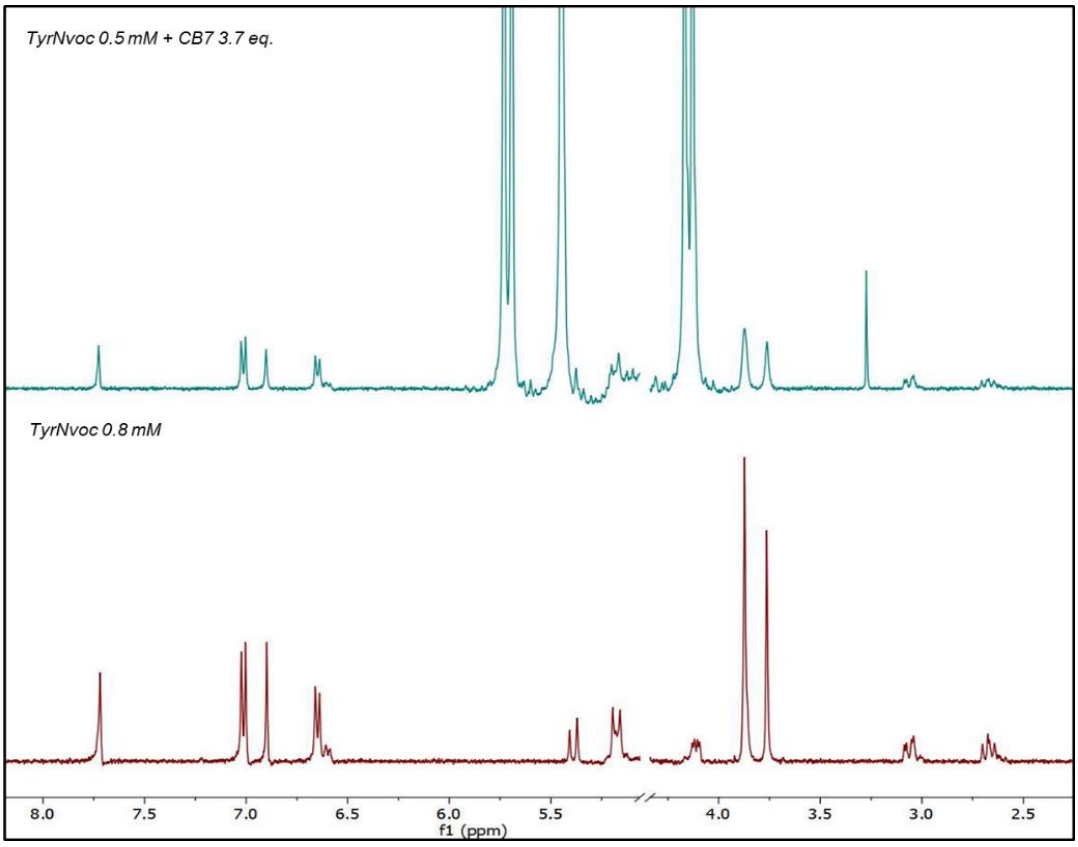

Figure 6.17 – ^{1}H-NMR spectra of TyrNvoc 0.8 mM (bottom) and TyrNvoc 0.5 mM with 3.7 eq. of CB[7] (top) in D_2O, pD 7.

6. Appendix

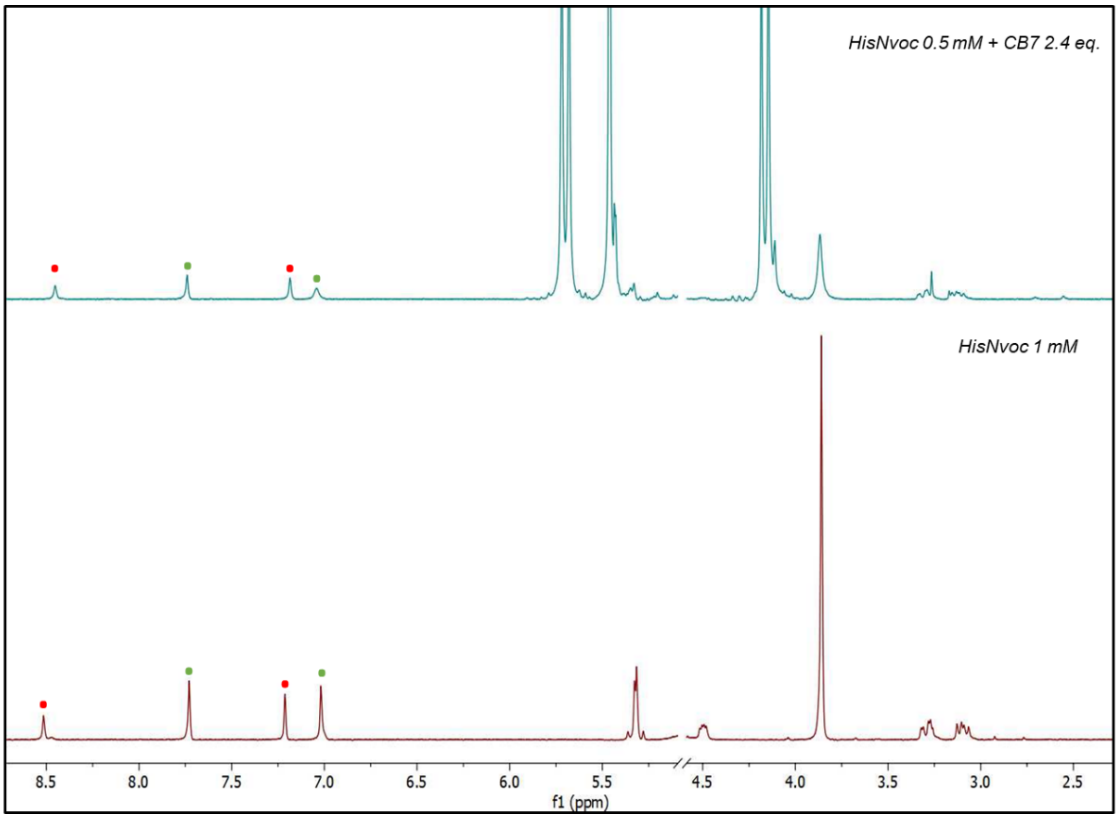

Figure 6.18 – ^{1}H-NMR spectra of HisNvoc 1 mM (bottom) and HisNvoc 0.5 mM with 2.4 eq. of CB[7] (top) in D_2O, pD 7. Red dots indicate upfield shifts and the green dots the downfield shifts.

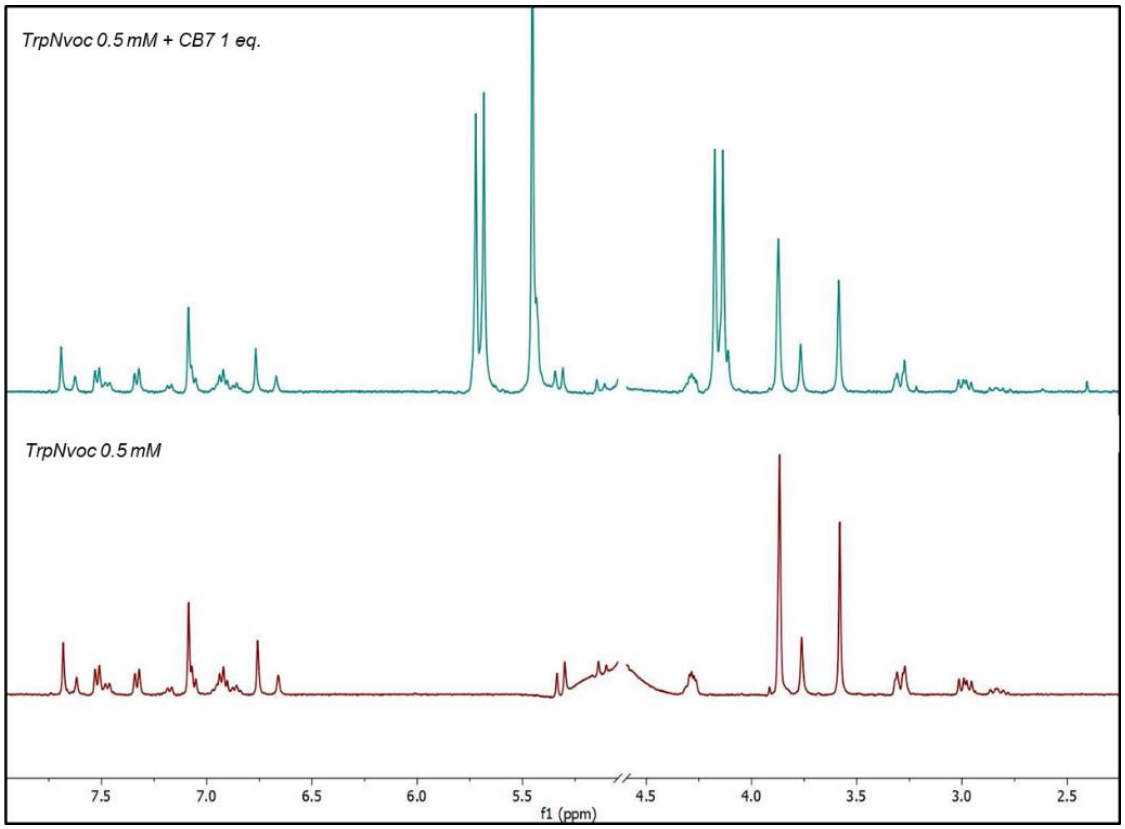

Figure 6.19 –^{1}H-NMR spectra of TrpNvoc (bottom) and TrpNvoc with 1 eq. of CB[7] (top) in D_2O, pD 7. [TrpNvoc]= 0.5 mM

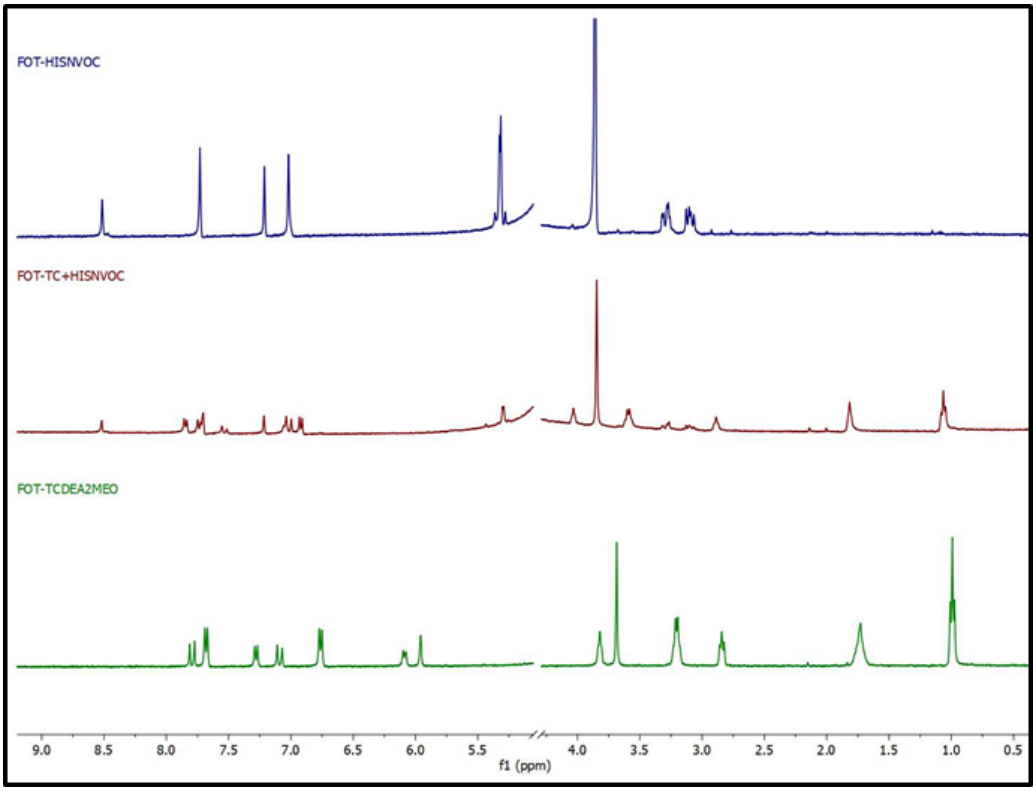

Figure 6.20 – ^{1}H-NMR spectra of 1 mM TCDEA$_2$MeO (bottom), 1 mM HisNvoc (top) and 1:1 eq. TCDEA$_2$MeO-HisNvoc (middle), in D$_2$O.

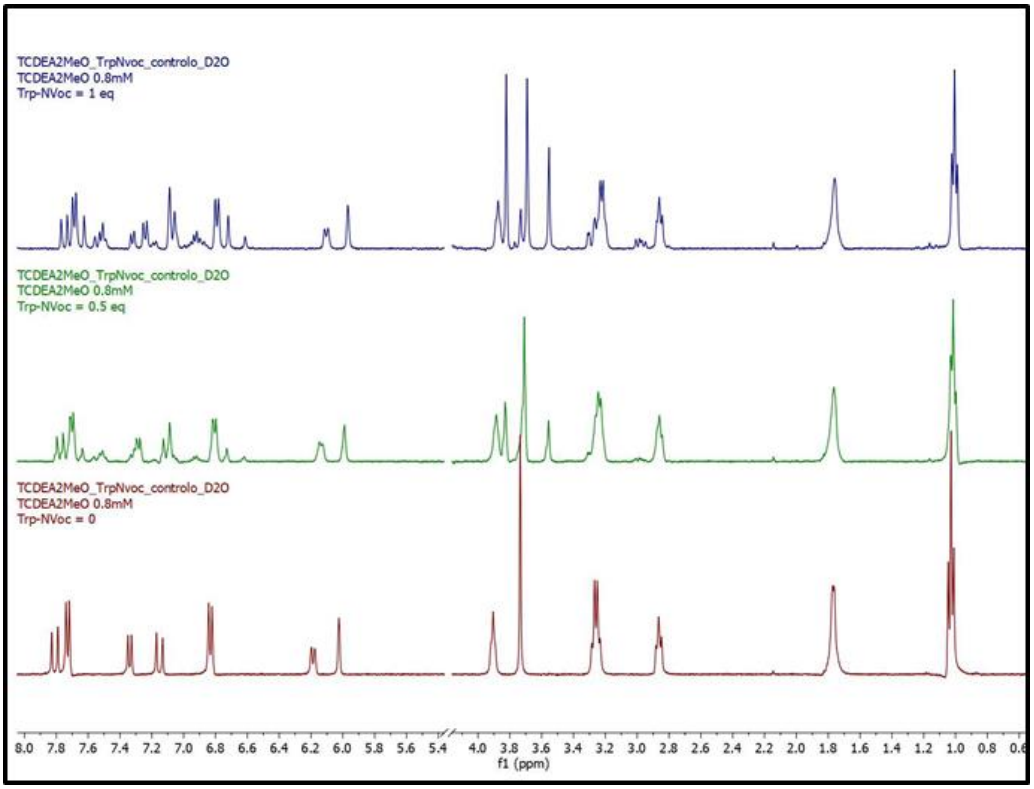

Figure 6.21 – ^{1}H-NMR titration of 0.8 mM TCDEA$_2$MeO with TrpNvoc (0-1 eq.) in D$_2$O.

6. Appendix

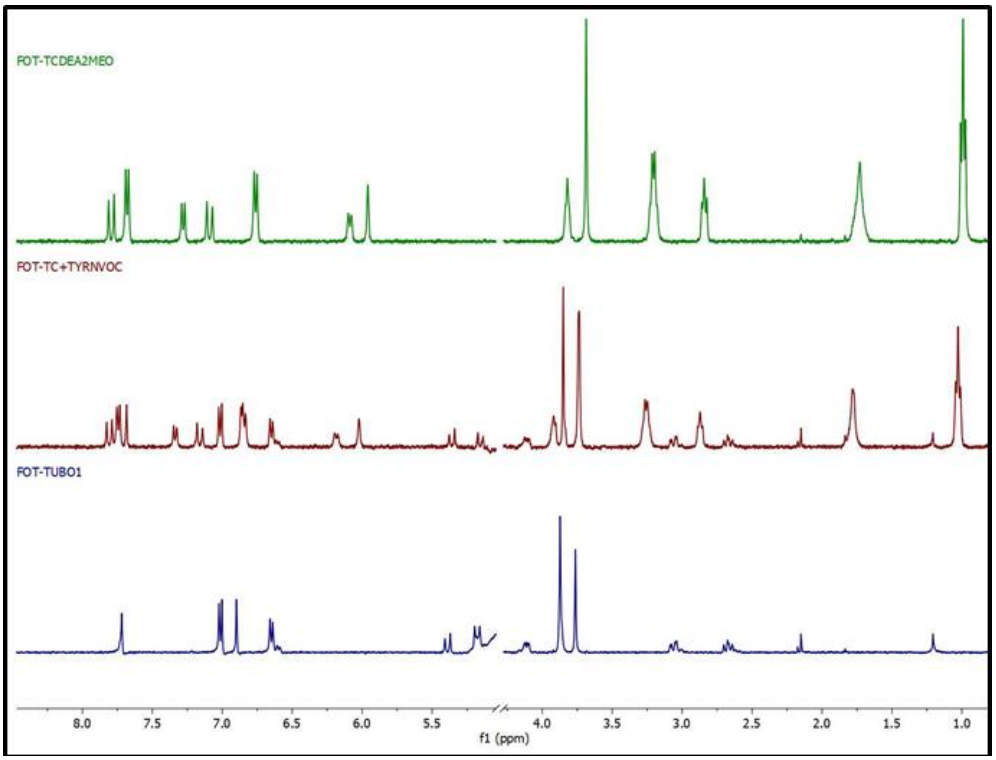

Figure 6.22 – ^{1}H-NMR spectra of 1 mM mM TCDEA$_2$MeO (top), 0.8 mM TyrNvoc (down) and 1:1 eq. TCDEA$_2$MeO-TyrNvoc (middle), in D$_2$O.

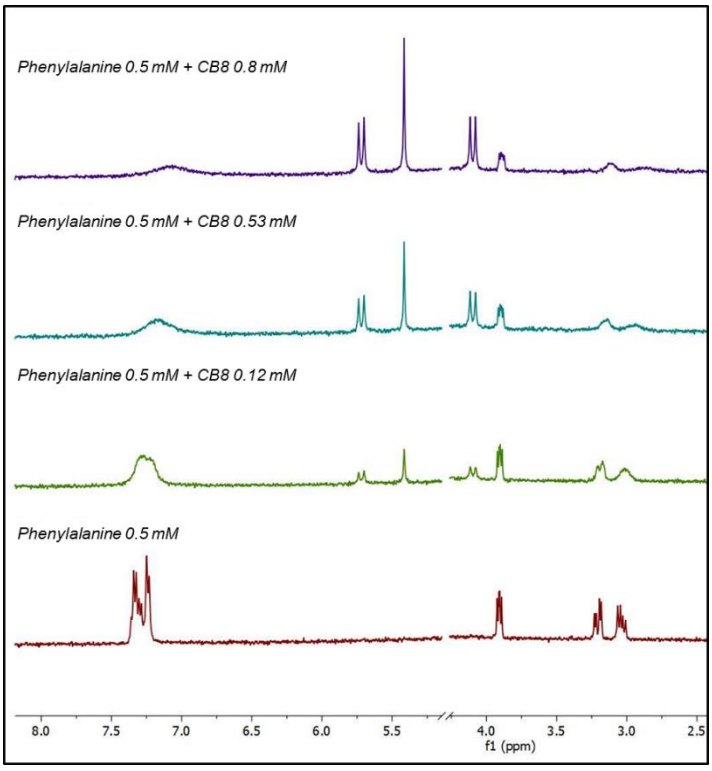

Figure 6.23 – ^{1}H-NMR titration of phenylalanine 0.5 mM (down) with CB[8] (0-0.8 mM) in D$_2$O, pD 7.

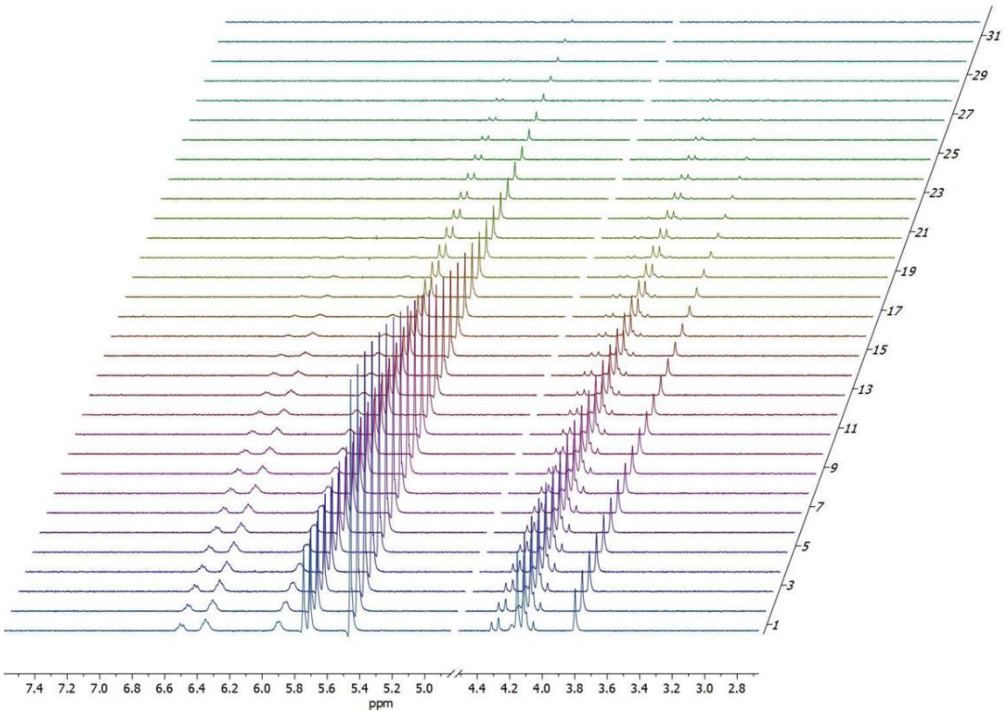

Figure 6.24 – DOSY spectra of FGG in D_2O at 298 K. [FGG] = 1 mM.and CB[8] in excess.

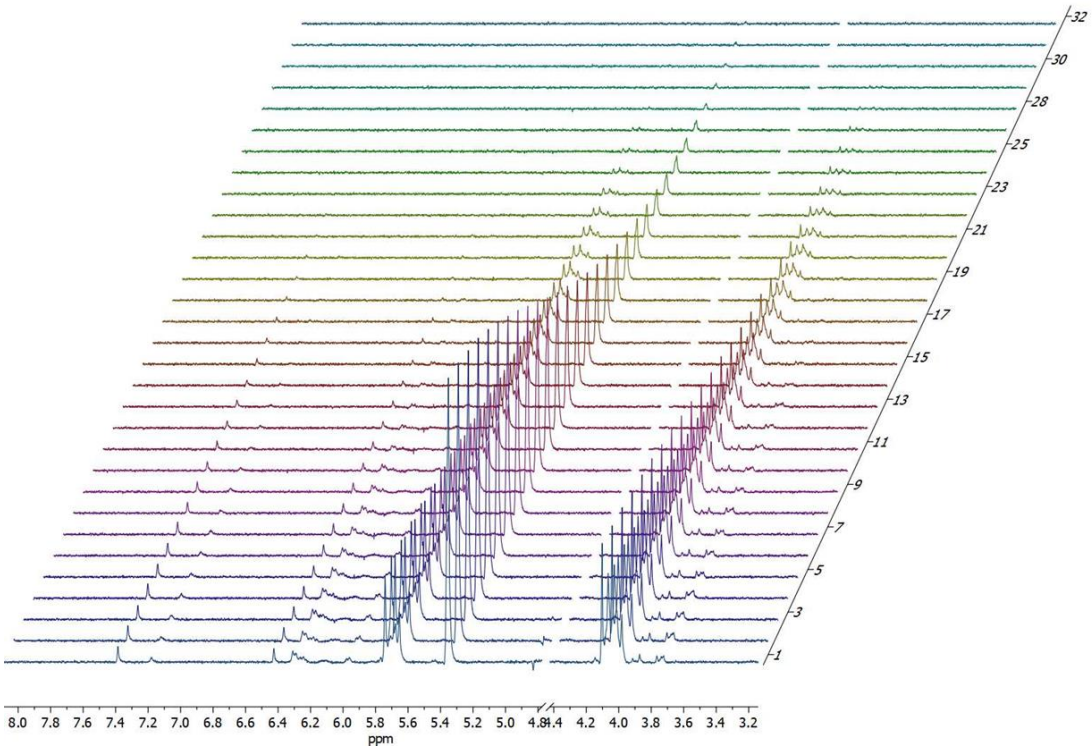

Figure 6.25 – DOSY spectra of FGGNvoc in D_2O at 298 K. [FGGNvoc] = 1 mM.and CB[8] in excess.

6. Appendix

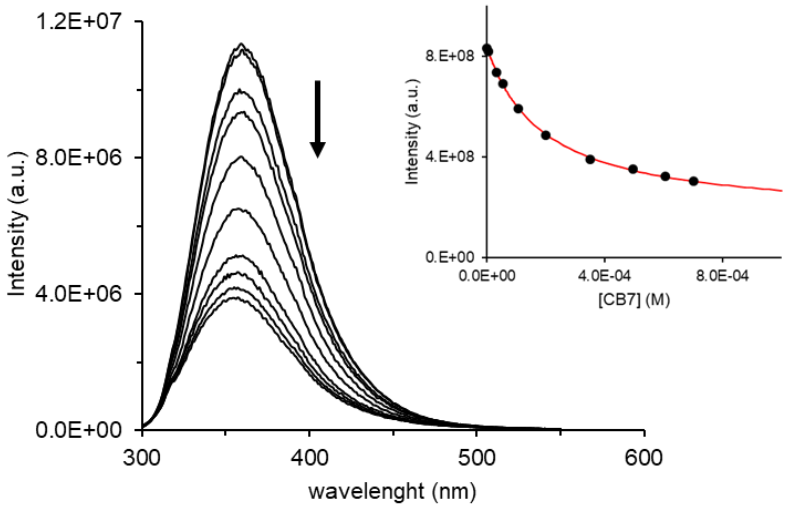

Figure 6.26 – Emission titration of 18 µM tryptophan with CB[7] (0 - 4.96 x 10^{-4} M) and data fitting in right upper corner. The black dots correspond to experimental values and the red line to a 1:1 fitting. The resulted association constant was 5.22 x 10^{3} M^{-1}. λ_{exc} = 290 nm.

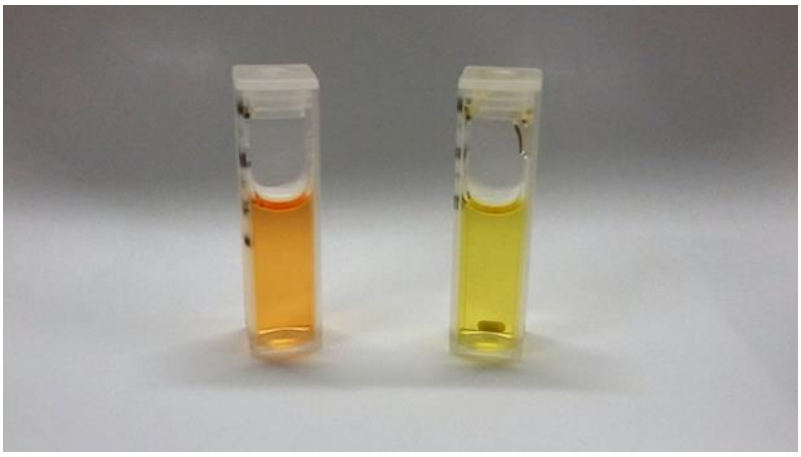

Figure 6.27 – Colour differences between control (left) and irradiated sample (right). Both cells contain 200 µM FGGNvoc, 20 µM TCDEA and 150 µM CB[7]. λ_{irr} = 366 nm, t_{irr} = 100 min. The control cell was left in the dark the same period of time that sample cell was irradiated.